Politecnico di Torino

Master of Science in Biomedical Engineering

Politecnico di Torino

Synthesis, characterization and biomimetic functionalization of thermoplastic poly(ester urethane)s

SUPERVISORS

Prof. Gianluca Ciardelli

Dr. Monica Boffito

Eng. Arianna Grivet Brancot

CANDIDATE

Alessandro Cazzolla

July 2021

Summary

Abstract

The design of biomaterials has seen a great increase in recent decades, with the specific aim to overcome the inadequacy of traditional materials in addressing the complexity of therapeutic approaches typical of tissue engineering (TE). Polymeric materials, in particular, are undergoing a significant growth in their use as biomaterials for multiple applications. Indeed, compared to metals and ceramics, polymeric biomaterials present many advantages, that include biocompatibility, biodegradability, good mechanical and physical properties and general resistance to common sterilization methods.

In this work, new thermoplastic poly(ester urethane)s, (PUs) have been designed and characterized to investigate the effects of the different chain length of the chain extender on PU physico-chemical properties. Then, surface modification through plasma treatment in the presence of acrylic acid vapor was investigated to expose carboxyl groups then exploited to graft biomolecules such as gelatin.

Poly(ester urethane)s, based on poly(ε-caprolactone) (C2000), were synthetized using 1,6-hexamethylene diisocyanate and linear aliphatic chain extenders (i.e., 1,4-butanediol, 1,8-octanediol, 1,12-dodecanediol) obtained three different PUs (BHC2000, OHC2000 and DHC2000).

PU chemical characterization was carried out using Infrared (IR) spectroscopy and Size Exclusion Chromatography (SEC). Mechanical and thermal properties were assessed by tensile tests and Differential Scanning Calorimetry, respectively. PU hydrolytic and enzymatic degradation was also evaluated between one and 8 weeks. Surface modification was performed by plasma treatment in the presence of Ar and acrylic acid vapor. -COOH exposure was evaluated through contact angle measurements and Toluidine Blue O colorimetric assay. The subsequent covalent grafting of a hydrophobic model molecule (i.e., benzylamine) and gelatin was performed exploiting carbodiimide chemistry and studied through IR and ^{1}H Nuclear Magnetic Resonance spectroscopies and colorimetric methods.

PU synthesis success was confirmed by IR spectroscopy and SEC. The three chain extenders used for the synthesis resulted in significantly different mechanical properties, thermal and degradation properties on the final PUs. In detail, the chain length of the chain extender turned out to affect the capability of hard segments to crystallize as well as PU resistance to applied tensile strength and enzyme-catalyzed hydrolysis.

In order to improve hydrophilicity a plasma treatment was carried out resulted in the exposure of a great number confirmed by a significant increase in wettability (contact angle decrease of 30-40%). The aim was to quantify the number of carboxylic groups present through TBO, and indirectly through grafting and quantification of Benzylamine, obtaining an average value of about 10^{16} units/cm^2 that however does not have repeatability.

Gelatin with three different concentration (0,1%, 0,25% and 0,5% w/v) was also successfully grafted on film surfaces, as demonstrated by IR spectroscopy; conversely, a correct quantification of benzylamine was impaired by hydrophobic absorption phenomena occurring on the surface of control samples.

In conclusion, all the designed PUs turned out to be suitable to produce TE scaffolds, with a target on long term applications and hard tissues, also using rapid prototyping techniques such as Fused Deposition Modeling. Moreover, the feasibility to easily surface functionalize them with biomolecules opens the way towards an improvement in the biocompatibility and bioactivity of PU scaffolds. Indeed, the versatility of the carbodiimide chemistry can be exploited to graft the most suitable biological cues (e.g., proteins, amino acids, peptides) for the targeted application.

Thesis Goal

In the biomedical field, referring in particular to tissue engineering, polymeric materials are having an incredible development, this due in particular to their excellent properties that includes biocompatibility, biodegradability, good mechanical and physical properties and general resistance to common sterilization methods. Moreover, synthetic polymers and especially poly(urethane)s can be ad-hoc engineered enabling the tuning of their characteristics to fit specific applications, which requirements could not be otherwise met.

Poly(ester urethane)s are usually employed as elastomeric biomaterials because of their versatile mechanical properties, processability, and good biocompatibility in different biomedical applications (i.e. cartilage tissue substitutes or guides for peripheral nerve regeneration). The purpose of tissue engineering is to restore, maintain or improve damaged tissues or whole organs, with the help of scaffolds and cells. Structurally speaking, a scaffold mimics the extracellular matrix, interacting with the surrounding environment.

In this sense, the aim of this work is the design of new thermoplastic poly(ester urethane)s, (PUs), based on poly(ε-caprolactone) diol and 1,6-hexamethylene diisocyanate. Additionally, during the synthesis different chain extenders will be added (i.e., 1,4-butanediol, 1,8-octanediol, 1,12-dodecanediol), to investigate the effects of their different chain length on the resulting PU physico-chemical properties. A chemical characterization of the materials will be thus carried out, also including degradation tests in environments with different characteristics; thermal and mechanical characterization will also be performed to evaluate the suitability of these materials to be processed through melting and printing techniques.

Since these materials are expected to be highly hydrophobic, surface modification will be necessary to improve hydrophilic and therefore make them more suitable for biomedical applications. The main feature of surface modification is that it customizes the surface characteristics of a material without changing its bulk properties. In particular, -COOH groups will be exposed by Ar plasma treatment in presence of acrylic acid vapors and then exploited to graft biomolecules, with the final aim to create a more cell-friendly surface. As a first attempt, model molecules will be grafted using carbodiimide chemistry to prove the feasibility of the process.

1. Introduction

Tissue engineering (TE) is a promising therapeutic approach that applies the principles of engineering and life sciences toward the combination of cells, biomaterials, and microenvironmental factors, aiming at creating therapeutic "strategies" to restore, maintain, or improve tissue functions[1,2]. Artificial skin and cartilage are some examples of tissue engineering applications approved by the Food and Drug Administration (FDA). Tissue engineering technologies are often paired with the wider field of regenerative medicine, which is constantly evolving and aims to focus on cures instead of treatments for complex, often chronic, diseases.

However, given the complexity of these therapeutic approaches, traditional materials are often inadequate to answer their demands. For this reason, over the last decades the development of biomaterials has increased continuously: many materials are used for the design of scaffolds, including metals and ceramics. Polymeric materials, anyway, have become increasingly common, due to their versatile mechanical properties, high porosity with very small pore size, biodegradation, and good biocompatibility[3,4].

1.1. Polymers

Polymers are used in multiple applications. In 2018, the annual plastic production has been estimated to be about 359 million tons[5]. Moreover, the annual plastics' production growth is about 4-5%[6]. According to this estimation (**Figure 1**)[7], the total amount of

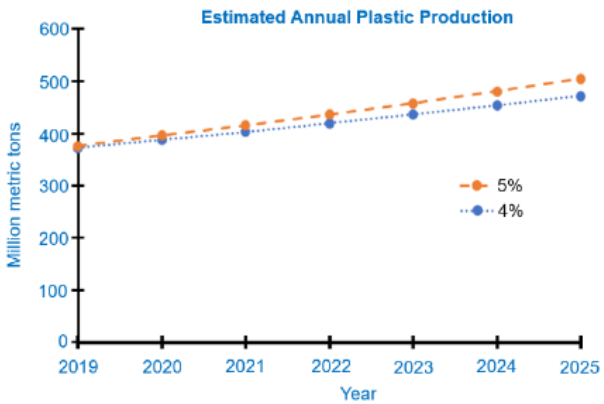

Figure 1: *Estimation of the annual million tons plastic production growth from 2019 to 2025*

polymers produced would pass from approximately 505 million tons in 2025 to 1000 million tons/year in 2039. It has also been observed that among the various polymers, the most economically important are poly(urethane)s (PUs), poly(ethylene) (PE), poly(amide) (PA), poly(ethylene terephthalate) (PET), poly(styrene) (PS), poly(vinyl chloride) (PVC), and poly(propylene) (PP). In **Figure 2**, the annual global production of these polymers for 2016 is shown[8].

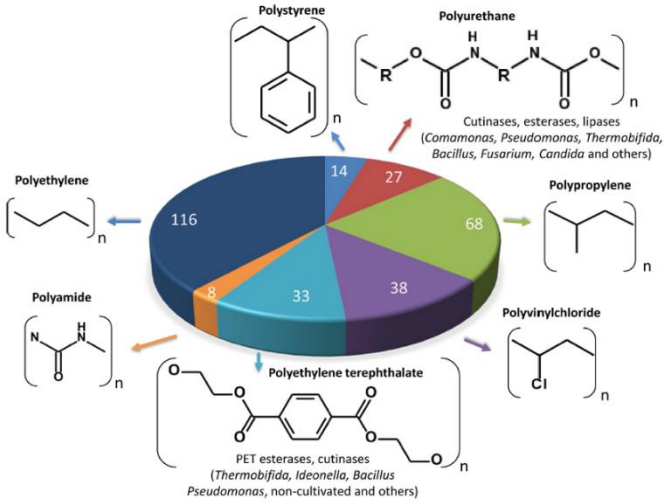

Figure 2: *Annual global production for the most common polymers in 2016*

Regarding the biomedical field, over the years the production, and therefore investment in this market, is constantly increasing. In 2019, the market size reached a value of 106.5 billion dollars[9], with an estimated production growth of +15% in 2025. The main reason for this growth is found in the use of these materials in tissue engineering applications[10]. **Figure 3**[9] shows an example of this increase in terms of USD billion in the UK.

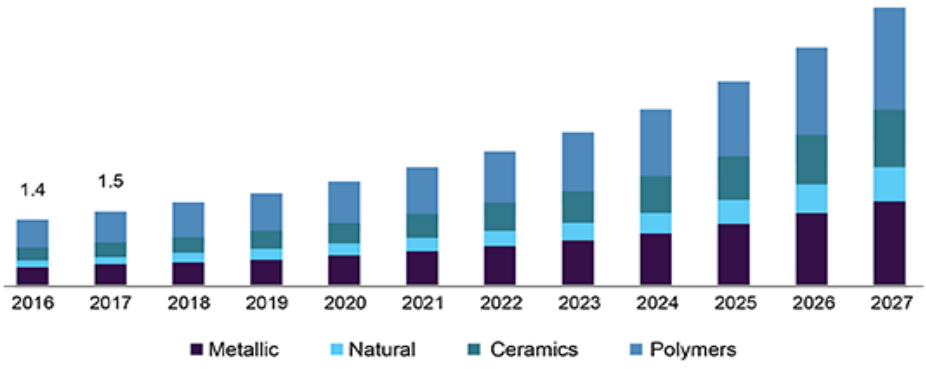

Figure 3*: Estimation of UK biomaterials market size between 2016 and 2027.*

Compared to metals and ceramics, the use of polymers in the field of biomaterials presents many advantages. These include biocompatibility, better degradability, sterilizability, good mechanical and physical properties. Moreover, in most cases they are easier to process with various manufacturing techniques[11]. However, mechanical properties usually restrict their use to applications where load-bearing is limited. In addition, control over bioresorbability is often limited[12]. Regarding biomedical applications, polymers of both synthetic and natural origin have been extensively investigated[13,14].

1.1.1. Natural Polymers

Natural polymeric materials such as proteins (especially gelatin) or polysaccharides (alginate, chitosan) have become a potential source for the manufacturing of scaffolds for TE[15,16]. Their main advantages reside in their inherent bioactivity, including the ability to stimulate cell proliferation, migration and adhesion and their nontoxicity to native healthy tissues[17].

These materials create an ideal environment for cells because they mimic the native extracellular matrix (ECM)[18] and the presence of bio-functional molecules plays pivotal roles in many biomedical processes[19]. However, these polymers also present significant disadvantages that strongly limit their use, especially regarding their poor mechanical properties[20]. The processing performance is also generally poor, the degradation rate is difficult to control, and a great batch-to-batch variability within production and purification processes (different molecular weight, charge, polydispersity of the polymers structure) typically occurs[1,21,22].

1.1.2. Synthetic Polymers

Compared to polymers of natural origin, in general synthetic polymers possess more versatility, more predictable properties and batch-to-batch uniformity. They can be divided into inert and biodegradable polymers and their design can be varied according to the specific applications[20].

Inert polymers are difficult to degrade within the human body and remain almost stable without substantial changes. They have excellent mechanical properties and do not cause side effects because they do not produce waste products that can be toxic to our body[23].

Biodegradable polymers, on the other hand, are materials that undergo significant structural changes (mainly reduction of molecular weight), caused by a degradation that depends on the environment in which they are located and exposure time. They need to be biocompatible and their starting mechanical properties are usually good; however, they can vary over time due to the loss of material and result in increased brittleness[17]. While using biodegradable polymers, it is necessary to pay attention to side effects, because the waste products produced during degradation could be toxic[24]. It has been demonstrated that the most commonly used synthetic polymers, such as polyurethanes, degrade into components that can be metabolized by the body[25–27].

The formulation of synthetic biological substitutes for tissue engineering applications could overcome many of the shortcomings associated with the use of natural biopolymers alone [28–31]. Both natural and synthetic materials present drawbacks. A possible way to address this issue is the surface modification of synthetic polymers with natural components, to obtain a hybrid material[32,33] able to fit different TE applications[34,35]. This combination is considered to be an effective way to achieve the desired biological activity while maintaining adequate mechanical properties and biostability: a better therapeutic effect can thus be obtained, as demonstrated by various studies[26,34–36].

1.2. Classification of polymers

1.2.1. Polymerization method

A traditional approach to classify polymers is based on the way the polymer chain is formed.

For the addition-type polymerization, also known as chain polymerization, all monomers can react with each other; as a consequence, dimers, trimers and then longer chains are progressively formed during the process. Three steps are required:

1. *Initiation*: a free-radical catalyst reacts with a double-bonded carbon monomer; in this way, a reactive compound is formed from which the polymer chain can start

2. *Propagation*: a repetitive operation that permits different activated monomers to bond and form the actual polymer chain. This reaction is thermodynamically favored because the reaction between monomers globally diminishes the system's energy
3. *Termination*: there are three possible termination methods

3.1. *Combination*: when two reactive chains bond together **(Figure 4)**[37]:

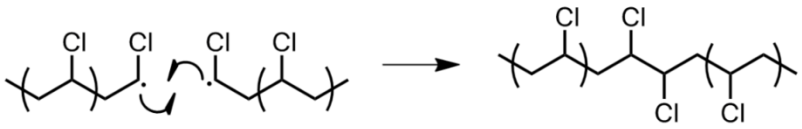

Figure 4: *PVC termination by combination*

3.2. *Radical Disproportionation:* one hydrogen atom passes from one end of a chain to a reactive one, creating two polymers, one with a terminal unsaturated group and the other with a terminal saturated group **(Figure 5)**[37]:

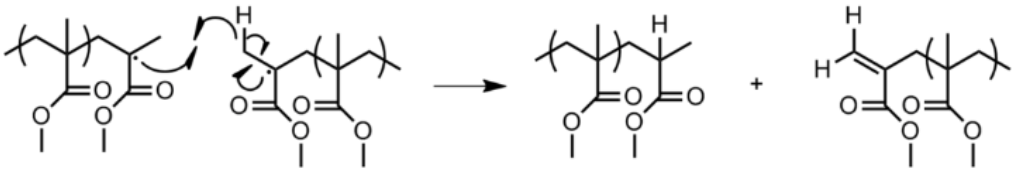

Figure 5: *Poly(methyl methacrylate) termination by disproportionation*

3.3. *Chain Transfer:* the activity of a growing polymer chain is transferred to another molecule. There are several types of this mechanisms, these are some examples:

3.3.1. *To solvent* **(Figure 6)**[37]:

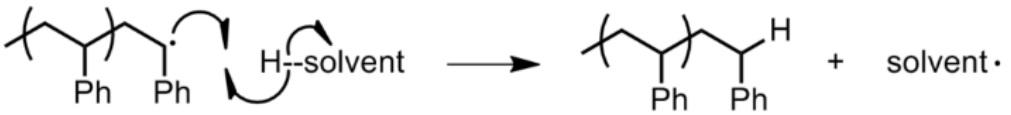

Figure 6: *Chain transfer from a polymer to solvent*

3.3.2. *To monomer* **(Figure 7)**[37]

Figure 7: *Chain transfer from a polymer to monomer*

The second method is the condensation-type or step-growth polymerization. In this case, monomers are classically di- or tri-functional and different steps are required to obtain the final polymer. In the first step, a single reaction is responsible for the generation of a prepolymer, then a propagation reaction allows the formation of the final structure. Typically, this method produces polymers of lower molecular weight and requires higher temperatures compared to addition-type polymerization. Poly(caprolactone), poly(caprolactam)s and poly(urethane)s are all produced through condensation processes.

1.2.2. Monomer composition

Another possible way to classify polymers is based on the nature of monomers. In general, a polymer can be formed by only one type of monomer (homopolymer) or by different monomers (heteropolymers).

For homopolymers, four different structures are possible, as reported in **Figure 8**[38]:

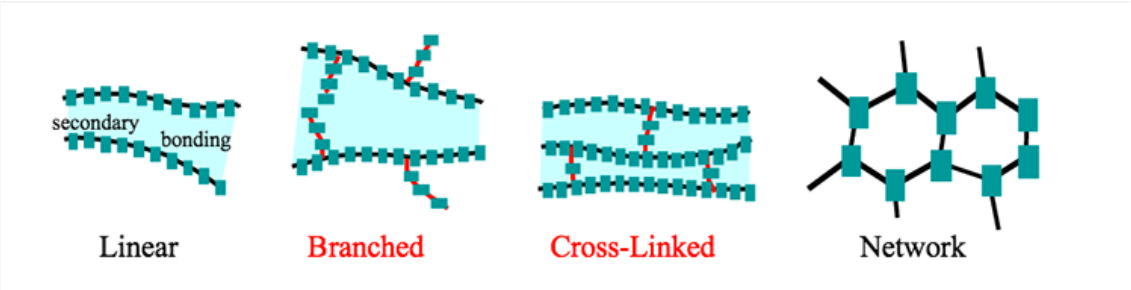

Figure 8: *Homopolymer different structures*

- ***Linear:*** formed by long chains held together by Van der Waals or hydrogen bonding. Heat easily breaks these bonds, so the material can be remolded.
- ***Branched:*** linear polymers with the addition of shorter chains hanging from the principal backbone.
- ***Crosslinked:*** different polymer chains are linked by covalent bonding, forming a more stable structure.
- ***Networked:*** chains are linked in multiple ways to form complex, three-dimensional networks.

For heteropolymers, that are commonly called copolymers, two or more monomers are used to obtain the final structures. In **Figure 9**[39], an example of how two different monomers can alternate in the final polymer structure is shown: for linear chains, an alternating, random or block structure is possible, while a homopolymeric backbone with side chains composed by different monomers is also possible.

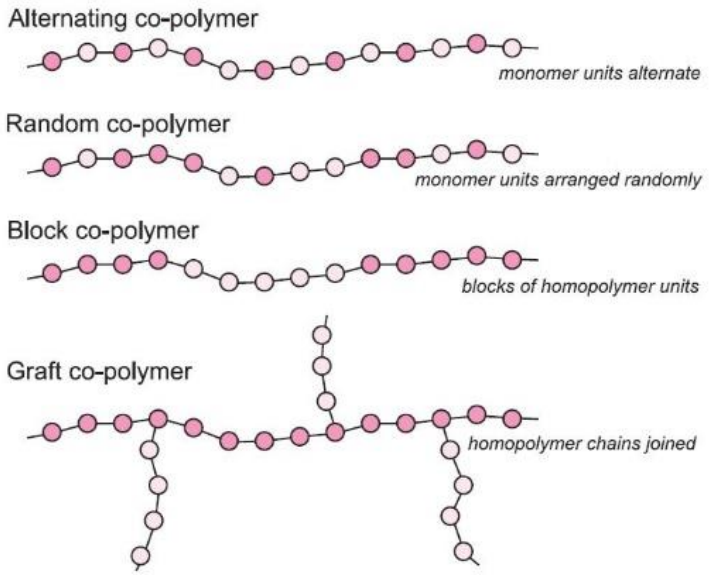

Figure 9: *Structures of different types of co-polymers*

1.2.3 Physical structure

Another classification can be made based on the physical microstructure of the polymer, especially linked to how the chains are inter-bonded. These characteristics reflect mostly on the processability of the polymer and on its final mechanical properties.

- *Thermoplastic polymers:* individual chains are held together by weak forces (Van der Waals or hydrogen bonds). Consequentially, when heated the chains can move freely and therefore these materials can be easily molded and processed multiple times.
- *Thermosets:* these materials are characterized by a set three-dimensional structure, due to covalent bonds between the chains. They can be molded by heat and pressure, but they cannot be processed a second time without losing their properties.
- *Elastomers:* amorphous and elastic solids. These materials are characterized by coiled chains that are able to stretch under solicitation, but also to recover their original shape once the stress is released.

1.2.4. Steric Structure

A final classification of polymers can be done by examining their steric structure, which is possible only for polymers with side chains. These polymers can be divided into two classes: stereoregular polymers, which have a recurring pattern in terms of stereochemistry, and atactic polymers, with no regular structure.

A typical example to represent these differences can be found with poly(propene), which monomer chemical structure is shown in **Figure 10**.

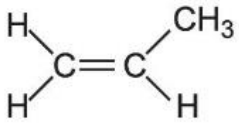

Figure 10: *Chemical structure of propene*

The two double-bonded carbon atoms are asymmetric. When polymerized, the resulting poly(propene) can form three basic chain structures, dependent on the position of the methyl groups in the side chain. Two are stereoregular (isotactic and syndiotactic) and the third does not have a regular structure and is termed atactic (**Figure 11**)[39].

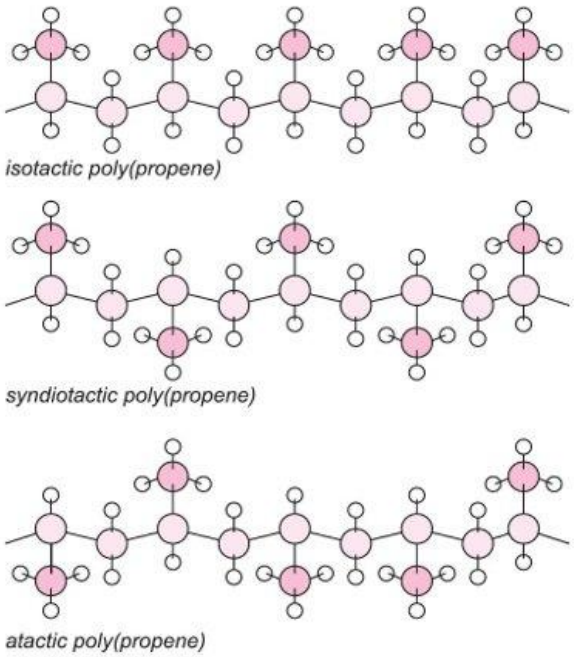

Figure 11: *Molecular structures of poly(propene)*

2. Poly(ester)s

Poly(ester)s are generally considered attractive starting materials for TE scaffold production. Usually, these materials possess good processability and can be manufactured into different shapes with the morphological features required by the final use[40,41]. Although all poly(ester)s may undergo degradation, aliphatic poly(ester)s with relatively short chain lengths are preferred because they possess suitable degradation profiles for biomedical applications[40].

Table 1[42] reports the main aliphatic poly(ester)s used for biomedical applications. Polyesters' synthesis can be achieved through several methods, including polycondensation, ring-opening polymerization, melt esterification and others[40,41].

Polymer	Acronym	Chemical structures
Poly(glycolic acid) or poly(glycolide)	PGA	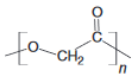
Poly(lactic acid) or poly(lactide)	PLA	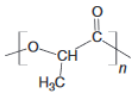
Poly(4-hydroxybutyrate)	4PHB	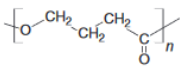
Poly(3-hydroxy butyrate) or poly(hydroxy butyrate)	PHB	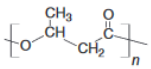
Poly(para-dioxanone)	PDO	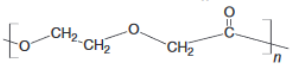
Poly(beta-malic acid)	PMLA	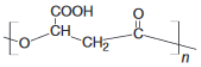
Poly(valerolactone)	PVL	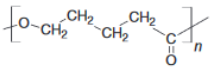
Poly(hydroxy valerate)	PHV	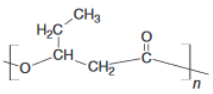
Poly(ε-caprolactone)	PCL	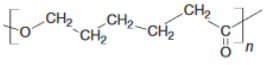
Poly(ethylene succinate)	PES	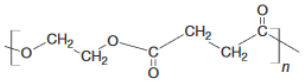
Poly(ε-decalactone)	PDL	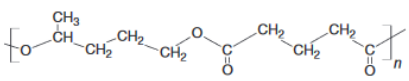

Table 1: *The most common poly(ester)s used for biomedical applications.*

2.1. Poly(ε-caprolactone)

Poly(ε-caprolactone), PCL, is a biocompatible, biodegradable and bioresorbable poly(ester). Its aliphatic ester linkages belong to the poly-α-hydroxy acid group; hence, this material shows a thermoplastic behavior. PCL presents a glass transition temperature of −60 °C and a low melting point ranging from 59° to 64 °C; it is therefore easier to manufact and manipulate than other biodegradable polymers, also because of its better viscoelastic properties. PCL was first synthesized during the 1930s by ring-opening polymerization of the cyclic monomer of ε-caprolactone[43,44], catalyzed by metal alkoxides, metal carboxylates or others at high temperature (> 120 °C)[45,46]. The same result can be obtained by polycondensation of 6-hydroxyhexanoic acid. This technique produces a lower quality product but has the significant advantage of not requiring metal-based catalysts, that are toxic and difficult to remove during the purification step. The two synthetic pathways of PCL are shown in **Figure 12**[47,48].

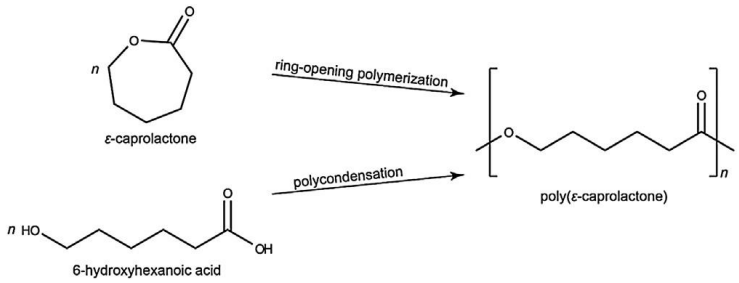

***Figure 12**: Two methods to synthesize poly(ε-caprolactone)*

If particular properties are required, PCL can be also used to create copolymers, for example with poly(lactic acid) (PLA), or polyhydroxibutyrate (PHB)[47,49–51]. PCL is biocompatible, biodegradable and bioresorbable.

The degradation time of polycaprolactone depends on its molecular weight, degree of crystallinity and morphology[52]. The process starts from the amorphous phases and then involves the crystalline domains[53]. Degradation occurs following chemical or enzymatic pathways, but random chain scission has been described as the dominant driver, and can proceed through both acid- and base-catalyzed ester hydrolysis[54,55].

2.1.2 PCL for biomedical application

PCL, thanks to its unique properties, is extensively used in different biomedical applications. For example, it can be used to produce drug delivery carriers, thanks to its slow degradation rate and its hydrophobic nature, that its compatible with a wide range of drugs.

It can also be employed in 3D printing[43,56], especially for bone tissue engineering applications. Biodegradable PCL films are also excellent materials when the purpose is to create patches or an active surface for dental, skin and vascular applications.

In the literature, there are also examples of PCL use for clinical applications, as in the case of Chaturvedi et al., that developed a delivery system for periodontal infections using electrospun PCL nanofibers[57].

2.2. Poly(urethane)s

Poly(urethane)s (PUs) are one of the classes of polymers most used nowadays in many aspects of modern life, such as biodegradable packaging, electronics and automotive. Their employment is widespread also in the medical field, especially thanks to their easily tailorable physical and chemical properties and possible biocompatibility[58,59].

2.2.1. Chemical composition and synthesis

Polyurethanes are a family of copolymers which repetitive units are characterized by the presence of the urethane linkage[60]. The reaction requires an isocyanate and a hydroxyl group that react as shown in **Figure 13**[61] (amide-ester of carbonic acid[62]):

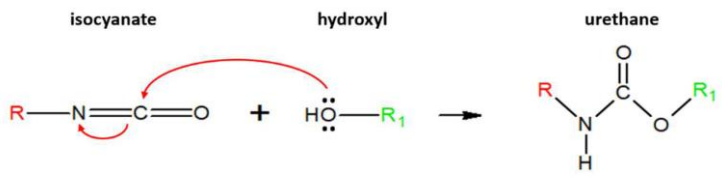

Figure 13: *Urehtane linkage reaction from an isocyanate and a hydroxyl group*

Variations in the R group and substitutions of the amide hydrogen produce multiple urethanes. A bifunctional diisocyanate and a polyol with -OH terminal groups are required to synthesize linear chain polyurethanes. Multifunctional polyols or isocyanates can also be used to introduce branches along the main polymer chain[63]. The synthesis can be conducted in one or more steps, even if multiple steps are preferred to maintain better control over the chemistry of the reaction. The most common synthesis method is known as the prepolymer method (**Figure 14**)[61]. In the first step, the macrodiol will react with a double quantity of the diisocyanate, forming a diisocyanate-terminated prepolymer that already presents urethane bonds. This prepolymer, however, does not have a sufficient molecular weight; hence, chain extenders are used to link the prepolymers until the desired molecular weight is reached, forming a poly(urethane) (if the extender is a diol) or a poly(urethane urea) (if the extender is a diamine).

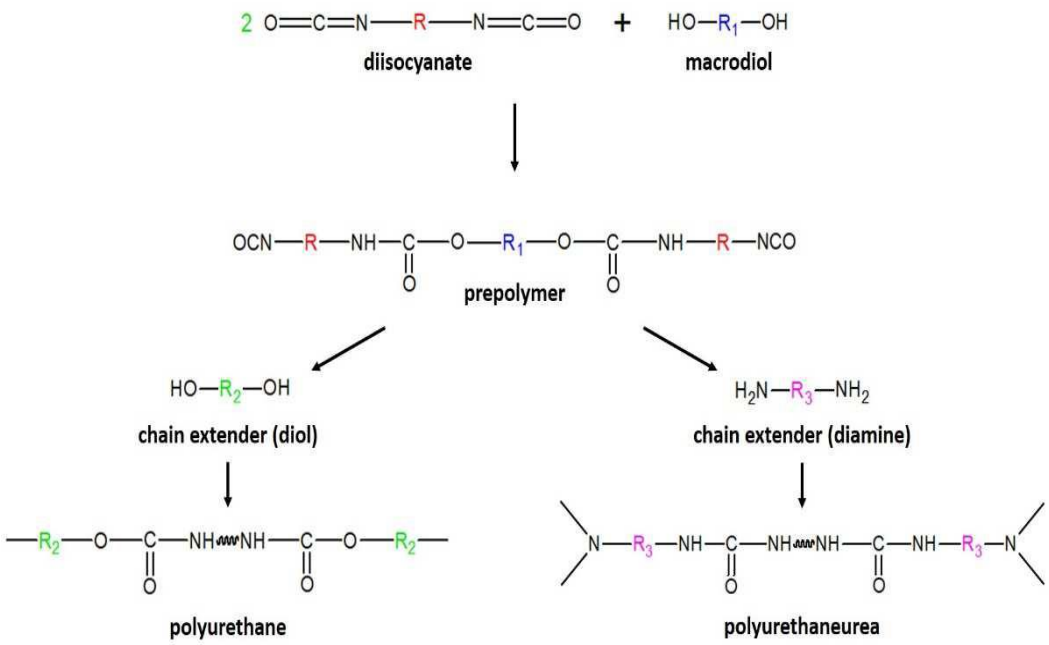

Figure 14: *Multistep prepolymer method to synthesize poly(urethane)s/poly(urethane urea)s*

A general formula for a linear PU is reported in **Figure 15**, where *n* is the number of repetitions and *R2* is a hydrocarbon chain. *R* represents a hydrocarbon containing the -OH group.

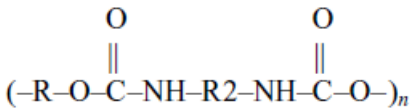

Figure 15: *General formula for linear PU*

PUs represent a very versatile polymer class, since it is possible to combine different monomers, to create a final material with the desired properties[58,64]. The three main components required to synthesize a PU are a diisocyanate, a polyol, and a chain extender, which is usually either another smaller diol or a diamine[65]. **Figure 16**[66] shows how molecular weight affects the physical properties of poly(urethane).

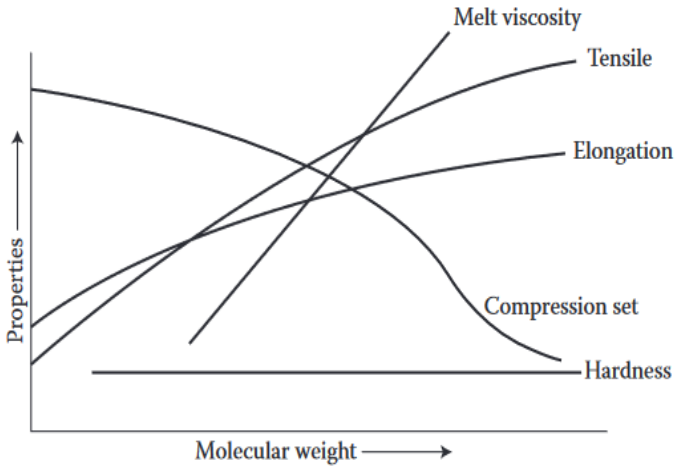

Figure 16*: Effect of molecular weight on PU properties*

2.2.2. Diisocyanate

Isocyanates are isocyanic acid derivatives in which groups, for example alkyl or aryl, are directly connected to the fraction N=C=O by the nitrogen atom. They can be both aromatic and aliphatic, but the aromatic ones are generally more reactive than the aliphatic ones due to the presence of the aromatic ring[67]. For biomedical applications,

however, the use of aromatic isocyanates is almost completely avoided since the 1980s[63,68], due to the toxicity of the degradation products[63].

To synthesize poly(urethane)s, an isocyanate with two functionalities per molecule (diisocyanate) is generally used. The double functionality allows to bind molecules on both sides, thus forming a linear chain as shown previously in **Figure 15**. If there are more than two functionalities, side branching will also occur[69]. Some example of common diisocyanates used in the biomedical field are shown in **Table 2**[61,69].

Chemical name	*Structure*
1,6-Diisocyanatohexane (HDI)	
1,4-Diisocyanatobutane (BDI)	
Isophorone diisocyanate (IPDI)	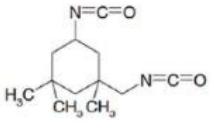
Dicyclohexylmethane diisocyanate (H12MDI)	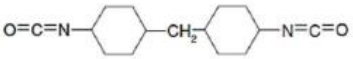
Lysine methyl ester diisocyanate (LDI)	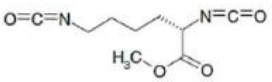
4,4′-Diphenylmethane diisocyanate (MDI)	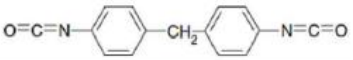

Table 2: *The most common diisocyanates used for biomedical applications*

2.2.3. Polyol

Polyols, the most prominent reaction partners of isocyanates, are reactive substances containing at least two hydroxyl groups attached to a single molecule. Polyols are telechelic and their molecular weight determines if they are liquid or solid at room temperature[60].

The physico-chemical properties of polyols have a profound effect on the properties of the resulting poly(urethane). The final PU often reflects at least in part the characteristics of the starting polyols, especially regarding chemical and mechanical properties[70].

Polyether- or polyester-based polyols are the most used for biomedical purposes; however, some examples of polycarbonates are also reported. Some example of commonly used polyols for poly(urethane) synthesis are shown in **Table 3**[61,69].

Chemical name	*Structure*
Poly(ethylene oxide) (PEO)	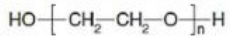
Poly(propylene oxide) (PPO)	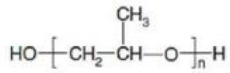
Poly(ε-caprolactone) (PCL)	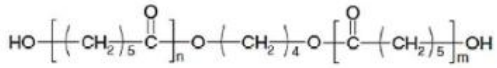
Poly(D,L-lactide)	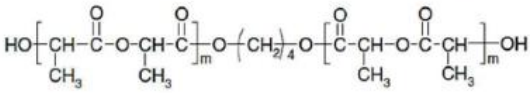
Poly(glycolide)	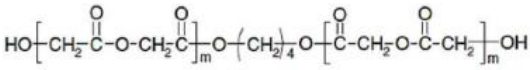

Table 3: *The most common polyols used for biomedical applications*

2.2.4. Chain Extender

The first step of PU synthesis produces a prepolymer that generally presents low molecular weight and unsatisfactory mechanical properties, similar to a soft gum rubber[60]. Chain extenders are small molecules (usually in the range of 40–300 Da), hydroxyl- or amine-terminated, used for improving the properties of the final products[71].

This component is considered to be a chain extender when two functionalities are present, otherwise it is defined as a cross-linker. The increased intermolecular interaction or bonding (covalent or hydrogen bonds) within the structure given by the chain extender contributes to the hard phase present in the PU structure[72] (**Figure 16**).

A reaction between a polyamine and an isocyanate produces a poly(urea). Amine-containing chain extenders generally react quickly with isocyanate functionalities but can be more difficult to process and may also impart an odor to the resultant polymeric product. A reaction between a polyol and an isocyanate produces a poly(urethane).

Hydroxyl-terminated chain extenders are frequently slower to react and may require the use of catalysts to achieve a sufficiently fast reaction. They generally produce more flexible materials; however it is possible to increase the final product strength using aromatic or cyclic polyols[69,63].

Some example of possible chain extenders are shown in **Table 4**[61,69].

Chain Extenders

Trival Name	Chemical Name	Structure
1,4 BD	1,4-Butanediol	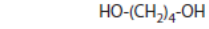
CHDM	1,4-Cyclohexandedimethanol	
Glycerine	1,2,3-Propanetriol	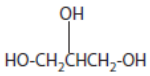
1,6 HD	1,6-Hexanediol	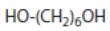
HQEE	Hydroquinone di (B hydroxyethyl ether)	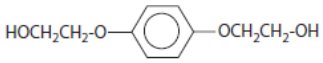
MPD	2-methyl-1, 3 propanediol	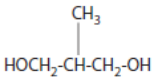
Quadrol	*N,N,N',N'* tetrakis (2-hydroxythyl) ethyl diamine	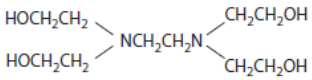
Sorbitol	D-glucitol	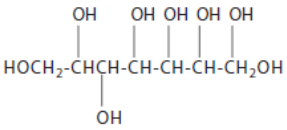
TMP	Trimethylolpropane	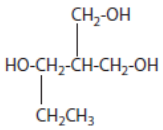

Table 4: *The most common chain extenders used for biomedical applications*

2.3. Poly(urethane) properties

2.3.1. Structure

Intermolecular order describes a geometrical relationship between polymer chains and their organization in the bulk material. There are three different states of intermolecular order: crystalline, amorphous and segmented (**Figure 17**)[66]:

- *Amorphous*: the polymer chains are arranged randomly and without a precise order.
- *Crystalline*: the polymer chains are organized into specific position in a tightly packed repeating regular structure.
- *Segmented*: co-presence of the two previous situations.

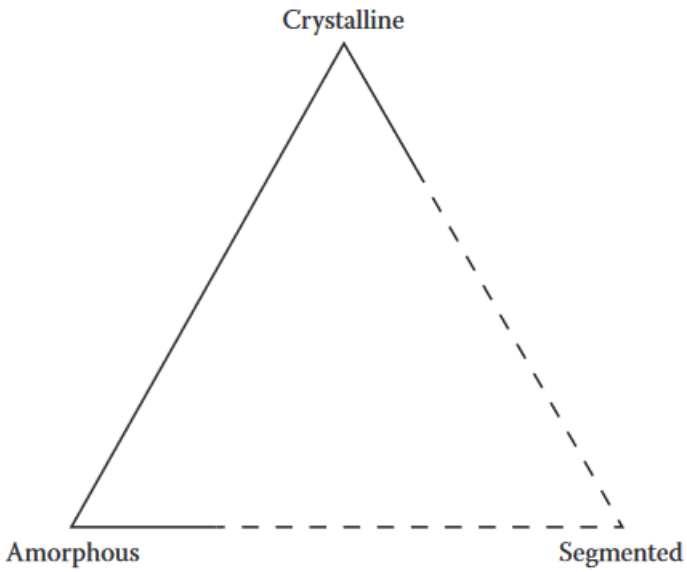

Figure 17: *Polymer's states of intermolecular order*

PUs form a two-phase structure where a "hard" semicrystalline segment, derived from the contributions of the diisocyanate and chain extender components, separates to create discrete domains in a matrix of "soft" segment, which is in turn composed by the macrodiol[66].

The hard segments act as bridges between the polymeric chains and as reinforcing filler particles for the soft segment matrix. In this case, the interchain attractive forces between

different hard segments are superior than those present in the soft ones, due to a higher concentration of polar groups, that can increase the possibility of hydrogen bonding. For this reason, hard segments significantly affect the PU mechanical properties and are also important for biocompatibility[66].

Hydrogen bonding occurs between individual hard blocks, creating a three-dimensional structure as shown in **Figure 18**[73]; however, the morphology is unstable and is also strongly dependent on the thermal history of the poly(urethane)[60].

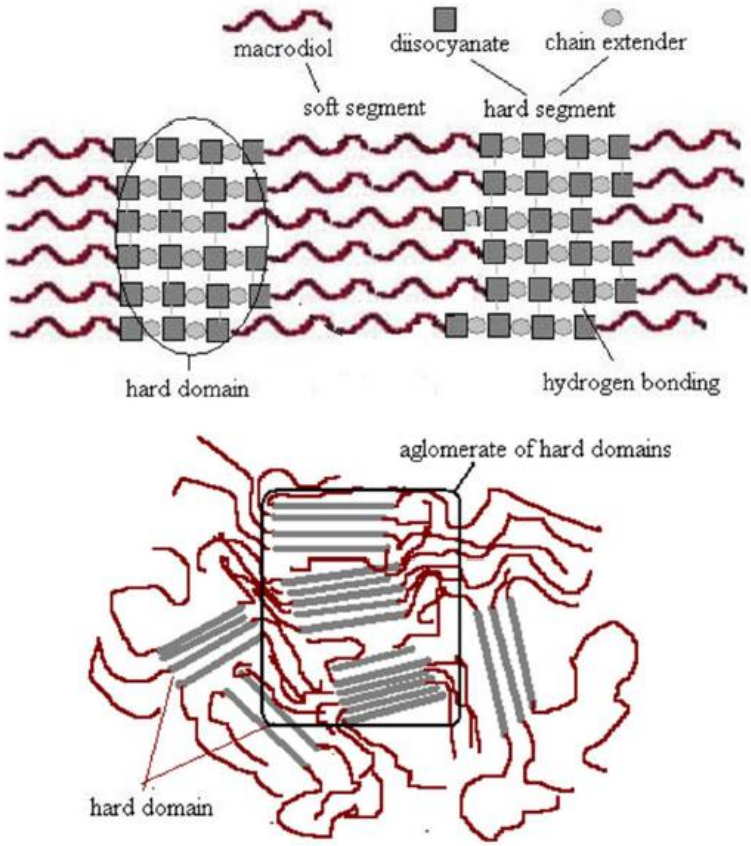

Figure 18: *Three-dimensional structure created by hydrogen bonding between individual PU hard blocks*

2.3.2. Mechanical Properties

The mechanical properties of polymers generally depend on several factors, including temperature. Polymers are viscoelastic materials, meaning that they exhibit both the behavior of a viscous fluid and an elastic solid, with a strong dependance of their properties from time and temperature. For PUs, soft domains provide the material with

elasticity due to their rubber-like behavior, since their glass transition temperature is usually below 0 °C. The hard segments instead provide the material with resistance under stress, due to the presence of the hydrogen bonds between the chains[61]. Thus, the crystallinity and cross-linking degree play an important role in controlling the PU mechanical properties, but molecular weight is also a relevant factor.

Compared to other materials, polymers generally present a relatively high molecular weight: when lower, polymers are easier to process, but when higher it gives better end-use properties[74,75]. As previously mentioned, an increase in molecular weight leads to an increase in the mechanical strength, Young modulus and extensibility. This is particularly true with thermoplastic polymers, as it is the case with segmented poly(urethane)s presenting alternating hard and soft blocks. The tensile strength is variable in the tens of MPa and the elongation can in some cases reach 800%[60].

As for thermoset poly(urethane)s, the presence of cross-linking between poly(urethane) molecules produces a restriction of molecular mobility. At low degree of cross-linking, the chains are still free to move and there is only a slight loss of flexibility and impoverishment in strength and creep resistance. As the degree of cross-linking increases, Young modulus raises, and the extensibility greatly decreases. At high cross-linking levels, PU chains can be totally immobilized and the material becomes a rigid thermoset[75].

2.3.3. Biocompatibility

In vitro and *in vivo* biocompatibility studies have been performed on various poly(urethane)s for a wide range of applications, focused on the cellular, enzymatic, and tissue responses to the material[69,76].

In vitro testing procedures, using different cell culture techniques, are a fundamental part of any material evaluation. Rough materials and devices based on poly(urethane)s have yield good results from this point of view[77,78]. Direct contact assays using fibroblasts or endothelial cells are also frequently used for the determination of the cellular response toward biomaterials and for cytotoxicity tests. Endothelial cells seem to have a good proliferation rate when seeded on PUs, while fibroblasts have shown poor adhesion properties on poly(urethane) foams[69].

In vivo studies have also been performed to evaluate the response of the organism, with subcutaneous, intramuscular or intraperitoneal implants[60]. Another important aspect to consider is protein absorption. The composition of the adsorbed protein layer is strongly dependent on the structure and composition of the polymers[79,80]. It has been found that a reduced plasma protein absorption on poly(urethane) surfaces can reduce thrombogenicity and bacterial adhesion[81,82].

2.3.4. Biodegradability

PUs have been traditionally used in long term medical devices due to their excellent mechanical properties and an acceptable hemocompatibility. However, these materials were soon found to lack the suitable resistance to degradation. The main reason of this behavior is that living tissues are a complex and very aggressive environment and even when the degradation of these polymers can be simulated by *in vitro* experiments, after *in vivo* usage results can be significantly different[83,60].

Biodegradable PUs typically undergo hydrolytic or enzymatic degradation *in vivo*, with a release of non-toxic degradation products[61]. The hydrolization of the ester bond both *in vitro* and *in vivo* yields the formation of α-hydroxy acids products and urethane or urea fragments with terminal acid groups[84,85]. By selecting the correct polyol, it is possible to control the degradation rate[86], since amorphous and hydrophilic soft segments degrade more rapidly than semicrystalline ones[69]. Finally, a chain extender recognizable by an enzyme can be included into the PU structure to further control the degradation.

Another phenomenon to which polyesters are subjected to is called environmental stress cracking (ESC), which involves crack formation and propagation in devices produced with these materials and is believed to be caused by residual surface stress[69]. The presence of enzymes also contributes to the biodegradation of poly(urethane)s in the physiological environment.

2.4. Poly(ester urethane)s

Poly(ester urethane)s are usually employed as elastomeric biomaterials because of their versatile mechanical properties, processability, and good biocompatibility in different biomedical applications. Some examples are:

- Shape-memory polymers (SMPs), that are systems able to remember and recover their permanent shape after deformation under a certain stimulus[87].
- Drug delivery systems, that allow a controlled release of medication such as epirubicin[88].
- Tissue engineering, e.g., for cartilage tissue substitutes[89] or guides for peripheral nerve regeneration[90].

One of the peculiar characteristics of poly(ester urethane)s concerns their degradation. Hydrolytic biodegradation can occur by various processes, but at rates much slower than those that would be expected from a material designed for biodegradation[91]. These degradation rates can be accelerated to levels relevant for tissue engineering applications by introducing hydrolytically labile segments into the polymer backbone, such as polyester soft segments (e.g., poly(lactide)s, poly(caprolactone)) and their copolymers[92–94]. The biodegradability in this case depends mainly on their chemical structure and especially on the hydrolizable ester bond in the main chain, which is also susceptible to enzymatic activity[95,96]. It is also important to mention that their degradation products are not toxic, since they are substances normally found in the body (e.g., lactic acid for PLA).

3. Scaffolds for tissue engineering

The purpose of tissue engineering, as mentioned above, is to restore, maintain or improve damaged tissues or whole organs, with the help of scaffolds and cells[97–99]. Structurally speaking, a scaffold mimics the extracellular matrix, interacting with the surrounding environment. The pores present in the structure allow cell adhesion and proliferation[100,101], which are also aided by growth factors and other elements incorporated into the scaffold itself[102]. The main features required in a scaffold are biocompatibility, non-cytotoxicity, but also easy processability. Depending on the final goal, the scaffold must present proper mechanical properties, which also depend on the forming material used, and its biodegradable/biostable properties. The most common materials are metals, ceramics, and polymers.

Metallic scaffolds are important for bone tissue engineering because of their osteoinductivty; however they are non-biodegradable[103–105]. Ceramics scaffolds present limited processability and low biodegradability and are rigid materials, unsuitable for many types of tissues[106]. Polymeric scaffolds, on the other hand, are the most versatile, with an optimal processability and tunable degradation rate, mechanical properties and wettability; this makes them a great choice for skin, cardiac and neural tissue regeneration and others[106]. Nevertheless, as already mentioned, it is always important to consider the impact of waste products, as they must not be toxic to the environment and must be readily disposed of[98]. Producing a scaffold with a single biomaterial is not usually enough to obtain satisfying results.

To improve its properties, several methods can be used. One possibility is to use block copolymers, that permit to optimize the ratio between hydrophilic and hydrophobic domains and thus obtain a greater or lower wettability[107]. Another example could be the tuning of cross-linking density to stabilize pore geometry during process[108,109]. Finally, one of the most popular strategies in this sense is surface modification (for example with a plasma treatment) to improve cell adhesion and proliferation[98]. There are many topological formulations for scaffolds, such as films, sponges, meshes, fibers, and foams. To give the right properties to a scaffold the choice of a specific fabrication method is critical since it determines both bulk and surface properties. Two main groups of techniques can be identified: conventional and non conventional[98].

3.1. Conventional Fabrication Methodologies

Conventional scaffold fabrication techniques are defined as "processes by which scaffolds with a continuous, uninterrupted pore structure can be made, but which lack any long-range channeling microarchitecture"[110,111]. In **Figure 19**[95], a scheme of the main conventional techniques is reported. In **Figure 20**[98], these techniques are explained more thoroughly, including the various necessary steps.

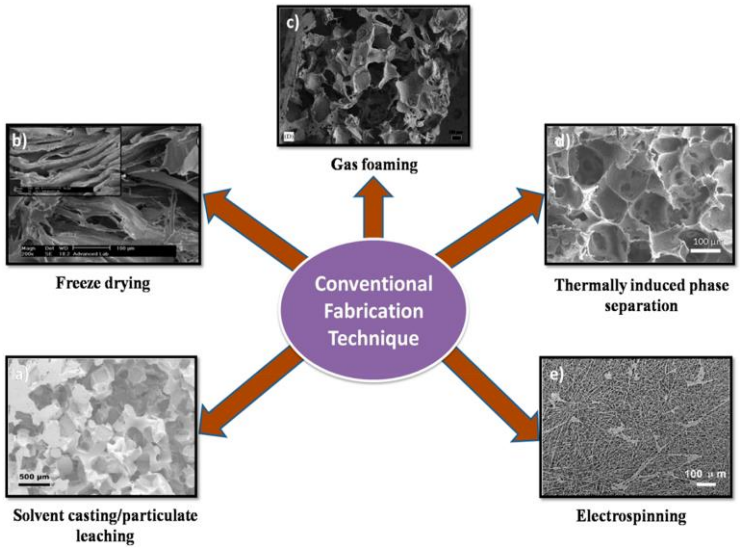

***Figure 19**: Conventional scaffold fabrication techniques for polymers*

3.1.1. Solvent Casting and Particulate Leaching

This method requires a two-step procedure (**Figure 20A)**:

1. *Solvent Casting:* a solution of a polymer prepared in a selected solvent is firstly casted in a mold. The formation of a solid product can then happen in two possible ways[114]: evaporation of the solvent (in an appropriate amount of time) or absorption of the solvent by the mold membrane. In this second case, the solvent can be extracted from the membrane and reused for other applications[115,116].

2. *Particulate Leaching:* Porogenic agents of various types can be used in this phase, such as salts, polymeric microspheres, etc., to give porosity to the scaffold. The porogens are mixed with the polymer matrix and properly dispersed, then the mixture

is treated with a compound that serves as a solvent for the porogenic agent but not for the polymer, so that the main structure is preserved[98].

The density and size of the pores obtained can be controlled, because it depends on how much agent is used and its nature. However, this technique does not permit to control the interconnection between the formed pores.

3.1.2. Freeze-Drying

This technique is also known as lyophilization[117] (**Fig. 20B**). As in the previous method, a polymeric solution is poured into a mold to fit the desired shape. Afterward, the system is exposed to a low temperature that allows it to solidify; then pores are created through sublimation under vacuum of the crystals formed by the frozen solvent.

The pore size mainly depends on the solution pH and freezing rate (°C/min) of the scaffold. A unidirectional solidification can facilitate a homogeneous and well-ordered pore size and distribution. A washing step is not required in this case.

3.1.3. Gas Foaming

The gas foaming (**Fig. 20C**) is a non-solvent technique performed at room temperature[118,119]. High-pressure carbon dioxide gas is infused into the polymeric matrix, permitting to achieve high porosity. Polymer density declines for longer time of exposure until a porous polymeric scaffold is formed[115]. Pressure is the only parameter to tune the porosity and no control on the interconnection of pores is possible. It is also important to verify that carbon dioxide is not reactive to the polymer used to form the scaffold.

3.1.4. Thermally Induced Phase Separation

The thermally induced phase separation technique, (TIPS, **Fig. 20D**) is based on temperature variations that induce the phase separation of a polymer solution into two phases, one with low polymer concentration and the other with high polymer concentration[120,121].

Two types of phase separation mechanisms are known: solid–liquid or liquid–liquid phase separations[122]. In both techniques, a homogeneous solution is formed by melt-blending the polymer with a high-boiling, low molecular weight liquid or solid diluent[123,124]. The solution is then cast into the desired shape. A conversion via the removal of thermal energy takes place, with formation of two-phase separated domains composed of a polymer-rich phase (high concentration) and a polymer-lean phase (low concentration)[120]. In the liquid–liquid de-mixing method, on the other hand, the polymer solution is cooled at a temperature lower than the solvent melting point, to induce a thermodynamic instability that promotes phase separation[120].The diluent is then removed (typically by solvent extraction) to produce a microporous structure[98,120].

3.1.5. Electrospinning

Electrospinning (**Fig. 20E**) is a common and versatile technique in tissue engineering, since it enables an easy production of polymer fibers with constant diameters (from 3 nm to more than 5 μm) and optimal mechanical properties[117,121,125]. The electrospinning setup basically consists of three parts: a high power voltage source, a syringe with a nozzle, and a metallic collector[98]. A high voltage (10–20 kV) is applied between the syringe's nozzle and the metallic collector. The polymeric solution is ejected from the nozzle and attracted by the collector when the applied potential will reach a force that exceeds the surface tension of the liquid[120]. Before reaching the collector, the solvent evaporates, and a dry fiber is deposited[98,120]. Electrospinning can be also conducted starting from a polymer melt to eliminate the risk of inadequate solvent evaporation[120]. The collector can be stationary or rotating, depending on the desired fiber arrangement (random or aligned)[120,126]. It is possible to modulate the fiber characteristics by modifying three classes of parameters: solution properties (viscosity, conductivity, molecular weight, surface tension, dipole moment and dielectric constant), controlled variables (flow rate, electrical field, nozzle–collector distance, nozzle design, collector shape and composition), and ambient parameters (temperature, humidity, air velocity)[120].

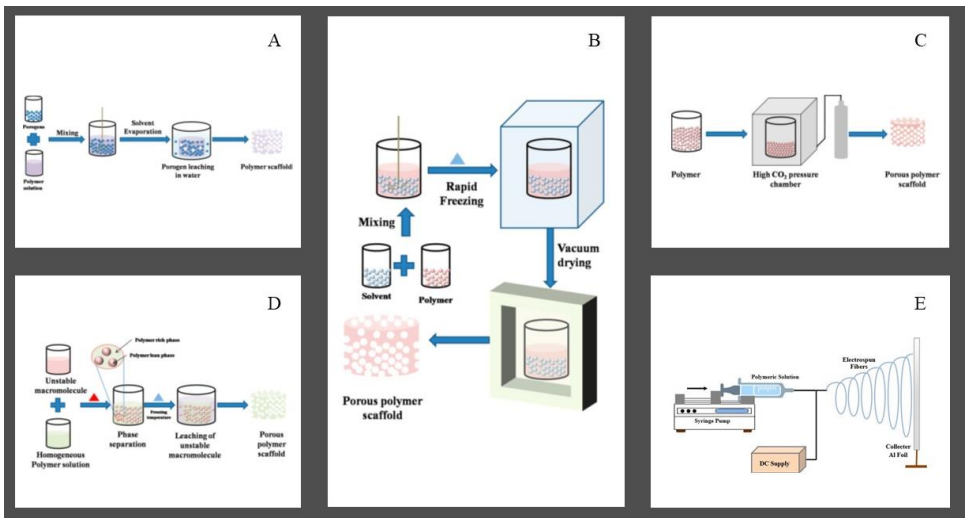

Figure 20: *Step by step conventional scaffold fabrication techniques*

3.2. Non-Conventional Fabrication Methodologies

These techniques have been introduced to overcome some of the limitations of the methods previous presented, such as the use of porogens, limited size of the produced scaffolds and poor reproducibility. On the other hand, non-conventional methods present numerous advantages, such as versatility and flexibility. Ultimately, they permit a better control of the external shape and internal morphology of the scaffold, since all parameters are controlled via computer, thus allowing for a better tuning of the final structure's properties[127–129].

3.2.1. 3D printing

3D printing techniques, also known as rapid prototyping (RP), are computer-aided fabrication methods that allow the rapid production of complex three dimensional structures[120,129,130]. Scaffold structure is designed and virtually divided into several slices; then, the fabrication is conducted layer-by-layer starting from the bottom[120,131–133] (**Figure 21**)[98].

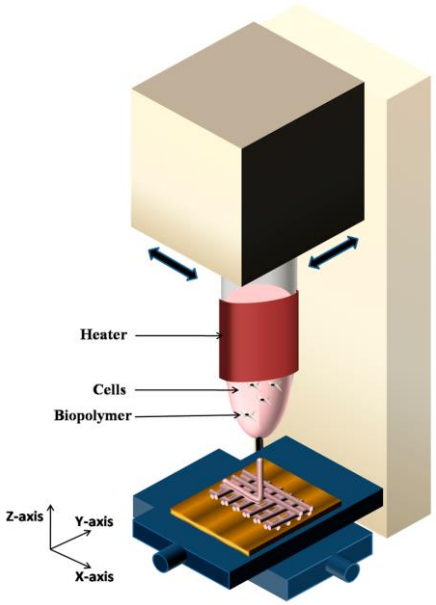

Figure 21: *3D printing technique*

There are six different families of techniques that are part of 3D printing[98]:

- *Fused Deposition Modeling* (FDM): the molten material is extruded through the machine nozzle.
- *Stereolithography* (SLA): this technique uses a laser to transform a liquid resin into a hardened plastic (photo-polymerization).
- *Selective Laser Sintering* (SLS): it uses a high-power laser to melt small particles of polymer powder.
- *Selective Laser Melting* (SLM): it makes metal parts from a bed of molten metal powder using a high-power laser.
- *Polyjet Printing:* it jets photopolymer curable liquid layers onto a build tray.
- *Bioprinting*: digital fabrication of living constructs encapsulating cells, and biomolecules into a scaffold.

The main limit of these techniques lies in their resolution, that is determined by the jet/laser size (200–500 μm depending on the technique), making the fabrication of scaffolds with fine microstructures difficult[127,129].

3.2.2. 4D Printing

4D printing generally refers to 3D printed objects that are able to modify their structure thanks to an external energy input, such as temperature, light, or other environmental stimuli. 4D printing is thus referred to as 3D printing transforming over time; hence, the main difference between these two classes is the time dependance[134,135]. The input material used in 4D printing is defined "smart" and usually can be either a hydrogel or a shape memory polymer. Thanks to their thermo-mechanical properties, these materials can change their shape and even properties in particular conditions, thus differentiating from the common rigid 3D printing materials[136,137]. This method is used in the biomedical field for example for tissue engineering and drug delivery. In the first case it can be used to create a network of blood vessels within a scaffold: multiple types of cells can be patterned in a hydrogel through a 4D printing system that can lead to vascularization. In case of drug administration, 4D bioprinting allows to spatially control the distribution of components that can encapsulate and release drugs or cells[138]. The main differences between 3D and 4D printing are summarized in **Figure 22**[137].

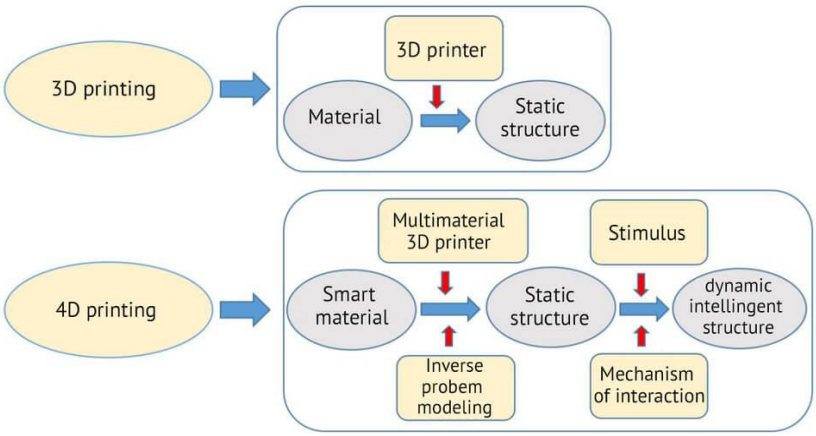

Figure 22: *Main differences between 3D and 4D printing*

3.3. Surface Modification

The biological response to implanted materials and devices is largely controlled by chemistry and surface morphology. In this regard, modification of polymer surfaces is of extraordinary importance to develop materials that can maximize their performance in specific applications[139]. The main feature of surface modification is that it customizes the surface characteristics of a material without changing its bulk properties[140,141]. Surface properties have a fundamental impact on material interaction with cells, because they determine how much the material will be performant in mimicking the native ECM[141–143]. The surface chemical structure, which involves the presence of groups that could start a reaction in biological systems, morphology, that represents the distribution of hydrophilic/hydrophobic and crystalline/amorphous phases, and topography of the surface[140] are the most important characteristics to consider. Cellular responses, including adhesion[142,144], morphology[145], and migration, have been shown to be influenced by surface chemistry[145].

Surface modification can be performed using biological, chemical or physical methods. Examples of chemical modifications include radiation grafting of monomers[146], coating with inorganic additives, plasma treatment[147,148] and biological molecule immobilization[149]. On the other hand, physical modifications of the substrate impact cell-material interactions by altering the interface, while maintaining the bulk material properties, such as biocompatibility and hardness. Physical characteristics of the substrate, like the chemicals ones, affect cellular adhesion, spreading, migration, proliferation, and morphology[150,151]. Physical alterations are typically accomplished through the addition of topographical features and by tuning the stiffness of the substrate[146].

3.3.1. Plasma treatment

Plasma surface modification (PSM) is a versatile technique that can be effectively applied for different materials, including polymers, requiring improved biointerfacial compatibility[152]. Plasma treatment can be divided into two main categories, thermal and non-thermal. However, thermal plasmas cannot be used for the surface treatment of polymers because of their high gas temperature. Non-thermal plasmas do not cause any

thermal damage to the surface of heat sensitive materials, but their use still needs to be controlled since chemical and physical modifications in bulk are still possible[153]. When the surface of a scaffold is exposed to a plasma generated in inert atmosphere (such as helium (He) or argon (Ar)), an environment consisting of electrons, radicals, ions, and excited molecules is created[154,155]. These active plasma species bombard the scaffold surface and transfer their energy through elastic and inelastic collisions; this induces chemical and/or physical changes of that surface[156,157]. This process, known as plasma treatment (or etching) creates a surface rich in highly reactive free radicals, that could be used for subsequent modification with other molecules[158,159]. Plasma is able to interact with the topmost layer of the surface in a depth of a few nanometers[155,160,161].

Subsequent modifications can be done directly using plasma, for example by polymerizing a monomer over the treated scaffold surface. The goal is to produce a thin interface film with the desired chemical properties, like good cell adhesion, to favor the scaffold interaction with the biological environment. Among the various groups that can be exposed depending on the gas and monomer used during treatment, carboxylic acid groups are the most common in the biomedical field, due to their ability to support adhesion and cell proliferation[65]. A possible way to obtain this result is the reaction of a pre-treated surface, rich in radical groups, with acrylic acid (**Figure 23**)[162].

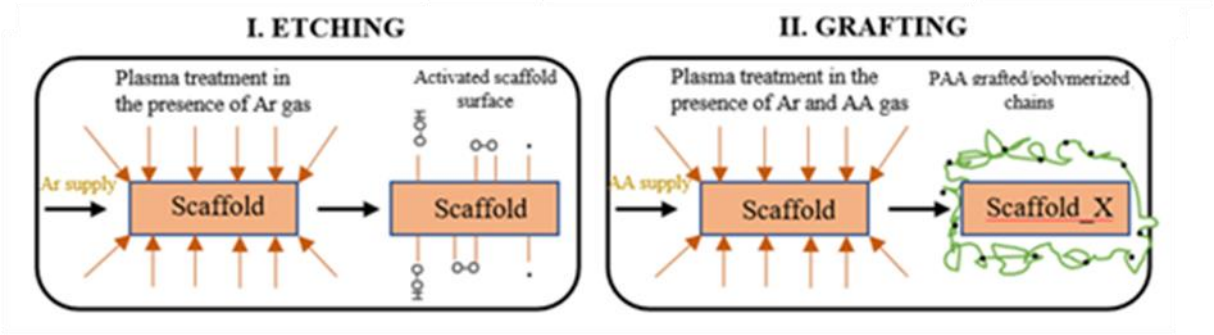

Figure 23: *Two steps plasma surface modification*

The monomer can also be firstly adsorbed by the substrate, and then subjected to the plasma treatment. In this way, surface radicals will be created in the monomer layer and the substrate surface, resulting in a cross-linked polymer top-layer. This process is called plasma syn-irradiation[153]. In **Figure 24**[153], the above mentioned techniques are outlined.

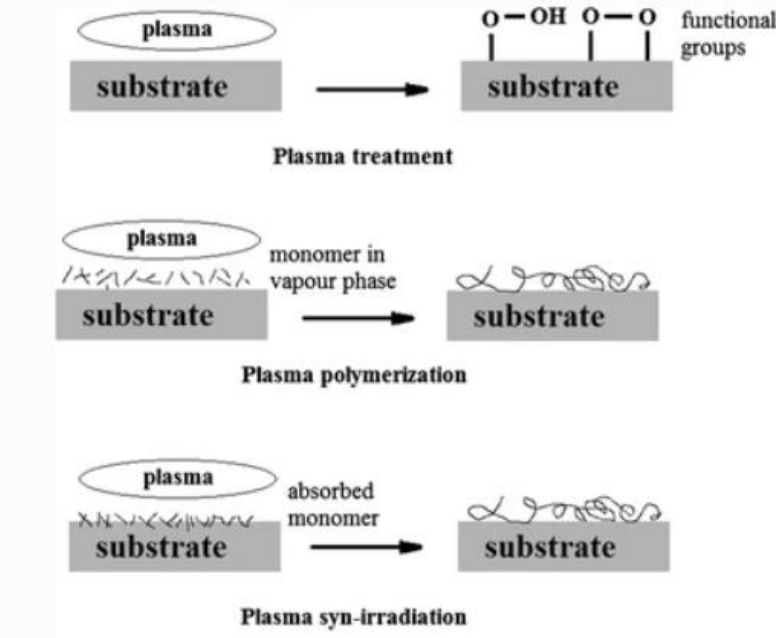

***Figure 24**: Three different plasma techniques*

Plasma based processes, compared to the other surface modification treatments, offer great advantages[163]. Indeed, they can occur at low temperatures and permit to avoid the use of wet chemicals and organic solvents which residues can be difficult to eliminate and can be toxic one the construct is placed within the body. Moreover, the variety and versatility of modifications that can be performed with this method is significant. The main changes regard surface roughness, hydrophilicity/hydrophobicity and molecular weight, thereby regulating crucial biocompatible parameters such as protein adsorption[164], cell adhesion and proliferation[165], and bacterial attachment[155,166].

3.3.2. Grafting of biomolecules

To achieve the final goal, scaffold surfaces often need a specific modification to graft different kinds of biomolecules, for example targeting molecules, particular proteins or antibodies complementary to receptors highly expressed on the desired target tissues[167,168]. The combination of polymeric materials with, for instance, dendrimers, liposomes, inorganic nanoparticles (INPs) or even other polymers leads to the formation of hybrid materials with properties that otherwise cannot be achieved[167]. Grafting on a substrate is often a multi-step process, where the surface must be first modified to ensure appropriate interactions and sufficient bonding sites for the grafted biomolecules. There

are various degrees of surface activation, like plasma treatment. The amount of molecules bound to the modified surface depends not only on the chemical pre-treatment but also on the type of biomolecules[169].

In case of polymer surface grafting, the process is divided into two steps: surface activation and graft polymerization. Surface activation process is needed to create reactive sites on the substrate surface that can generate further grafting processes[170]. The grafting methods are divided into two classes, i.e., "grafting-to" and "grafting-from" processes. In "grafting-to" method, preformed polymer chains carrying reactive groups are covalently bounded to the surface. The "grafting-from" method utilizes the active species existing on the material surfaces to initiate the polymerization of monomers from the surface toward the outside bulk phase[170].

3.3.2.1 Carbodiimide chemistry

As mentioned above, plasma modified scaffold surfaces present reactive groups that can be available for further modification processes. Considering for example carboxylic acid groups, many methods can be used for the grafting of biomolecules, but one of the most common techniques involves the carbodiimide chemistry[171]. Carbodiimides are a unique class of reactive organic compounds having the heterocumulene structure as shown in **Figure 25**.

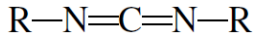

***Figure 25**: Structure of a carbodiimide*

They are widely used to mediate the attachment of biomarkers to polypeptides, since they can be used as carboxyl activating agents for the creation of amide bonds with primary amines[172]. Moreover, carbodiimides work in a way similar to what happens in the internal environment of the human body. For example, Collagen I, the most abundant ECM protein component, is stabilized *in vivo* by an enzyme modification that leads to crosslinking; carbodiimide chemistry presents a very similar mechanism[173]. The most common methods in which carbodiimide chemistry is employed involves the crosslinking of 1-ethyl-3-(3-dimethylaminopropyl-carbodiimide hydrochloride, (EDC) in presence of N-hydroxy-succinimide, (NHS)[144]. In summary, there is a reaction between EDC and a

carboxylic acid group to form an active intermediate called O-acylisourea (that is not very stable) as shown in **Figure 26**[174].

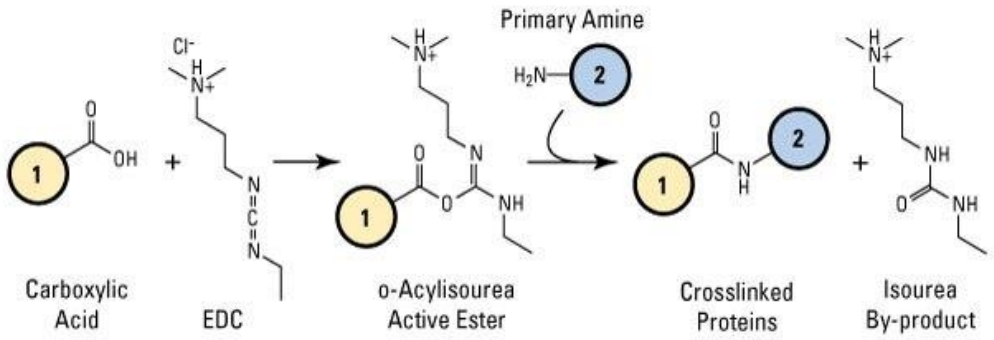

Figure 26: *EDC reaction chemistry with a primary amine*

This intermediate will combine with a primary amine to form an amide bond and release an EDC by-product and the reaction is most efficient in acidic (pH 4.5) conditions[174].
To make the intermediate more stable, a coupling with N-hydroxysuccinimide (NHS) or its water-soluble analog (Sulfo-NHS) is often included in the protocols **(Figure 27)**[174], which also improves its effectiveness[174].

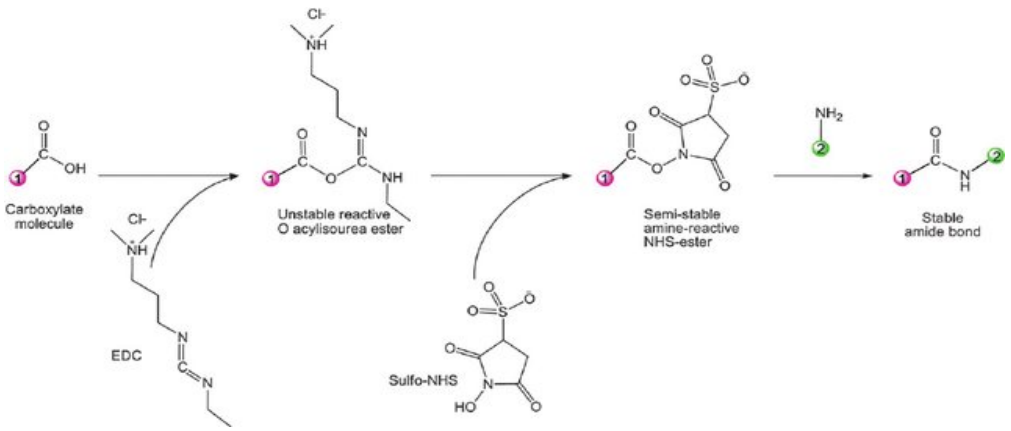

Figure 27: *EDC/NHS carbodiimide reaction scheme*

By modifying the crosslinking regime, it is also possible to control the mechanical properties and the degradation kinetics of the scaffold[175]. One of the reasons for using this type of crosslinking is that it stabilizes a 3D structure, with well-defined pore geometry[176,177] and percolation diameters[178] for optimal internal interconnection that allows a favorable cell migration[173].

4. Materials and methods

4.1 Poly(urethane)s synthesis

4.1.1. Synthesis reagents

PCL diol (M_n = 2000 Da) was purchased from Polysciences, Germany. 1,6-diisocyanatohexane (HDI), the catalyst dibutyltin dilaurate (DBTDL) and the chain extenders 1,4-butanediol, 1,8-octanediol, 1,12-dodecanediol were all purchased from Merck (Italy). PCL was dried under vacuum at 100 °C for 8h, then kept under vacuum at 30 °C before use. The chain extenders were also dried under vacuum at room temperature. 1,6-diisocyanatohexane (HDI) was distilled under vacuum before use. 1,2-dichloroethane was dried over activated molecular sieves and under inert atmosphere overnight. The required glassware for the synthesis was dried at atmospheric pressure and 120 °C. All solvents were purchased from Carlo Erba (Italy).

4.1.2. Poly(urethane)s nomenclature

The nomenclature used for the synthesized poly(urethane)s (PUs) is based on the components that form the polymer chains. The first letter indicates the chain extender, the second identifies the diisocyanate, HDI in all cases, and the last letter and numbers refer to the polyol, which for all PUs is PCL diol (M_n = 2000 Da), indicated with C2000. Therefore, the PUs in this work are named as followed:

- PU obtained from C2000, HDI and 1,4-butanediol (B): ***BHC2000***
- PU obtained from C2000, HDI and 1,8-octanediol (O): ***OHC2000***
- PU obtained from C2000, HDI and 1,12-dodecanediol (D): ***DHC2000***

4.1.3. Synthesis procedure

The PUs were all synthesized through a two steps procedure in inert atmosphere (nitrogen). 1,2-dichloroethane (DCE) was used as solvent in anhydrous conditions.
The first step involved for all PUs the reaction of C2000, dissolved at 40% w/v in DCE, with HDI (molar ratio C2000:HDI 1:2), to obtain a prepolymer. The reaction was conducted for 75 min at 80 °C in the presence of DBTDL at a concentration of 0.1% w/w with respect to C2000. In the second step, the extension of the prepolymer was performed with one of the afore mentioned chain extenders: these agents were added to the prepolymer solution after dissolution in DCE at 3% w/v (molar ratio C2000:chain extender 1:1). Both 1,8-octanediol and 1,12-dodecanediol required heating to solubilize completely in DCE and were added to the synthesis flask before lowering the temperature. The second part of the reaction was then conducted at room temperature for 20 h and stopped with methanol (6 ml of methanol for every 16 g of produced PU considering a 100% reaction yield).

Finally, the PUs were collected by precipitation in petroleum ether (4:1 v/v with respect to the total DCE reaction volume) and finally purified by dissolution at 35% w/v in DCE, followed by precipitation in methanol (5:1 v/v with respect to the DCE used in the re-solubilization phase). The PUs were thus collected by filtration through a Buchner funnel and dried overnight at room temperature.

4.2. Poly(urethane) characterization

4.2.1 Attenuated Total Reflectance Fourier Transform Infrared (ATR-FTIR) spectroscopy

Attenuated Total Reflectance Fourier Transform Infrared spectra of the three PUs were obtained with a Perkin Elmer Spectrum 100, equipped with an ATR accessory (UATR KRS5) with diamond crystal. The tests were performed at room temperature, in the spectral range 4000-600 cm^{-1}, with a resolution of 4 cm^{-1}. Each spectrum was derived from 32 scans and analyzed using the Perkin Elmer Spectrum Software.

4.2.2 Size Exclusion Chromatography (SEC)

For this analysis, *N,N*-dimethylformamide (DMF, HPLC grade, Carlo Erba, Italy) added with LiBr (0.1% w/v, Sigma Aldrich, Italy) was used as mobile phase at 0.4 mL/min. The analyses were all performed with an Agilent Technologies 1200 Series, USA instrument carrying a Refractive Index Detector (RID) and two columns (Waters Styragel HR1 and HR4) equilibrated at 55 °C. 2 mg/mL concentrated PU samples were prepared and filtered (0.45 μm poly(tetrafluoroethylene) syringe filter) before analysis. A calibration curve based on poly(methyl methacrylate) (PMMA) standards (Peak Molecular Weight (M_p) within the range 1102-22300 Da) was used to estimate the Molecular Weight of the tested PUs (Number Average Molecular Weight, M_n – Weight Average Molecular Weight, M_w). The following equations were used:

$$M_n = \frac{\sum n_i \cdot M_i}{\sum n_i} \quad ; \quad M_w = \frac{\sum n_i \cdot {M_i}^2}{\sum n_i \cdot M_i}$$

The polydispersity index (D) was also evaluated as the measure of the uniformity of the molecular weight distribution of a given polymer. Its value is always ≥1 and is calculated as:

$$D = \frac{M_w}{M_n}$$

4.2.3. PUs film preparation through solvent casting

To produce PUs films useful for further characterizations and for the optimization of the surface modification processes, the chosen material was dissolved at a concentration of 10% w/v in chloroform. The solution was then poured in a Petri dish and left to evaporate overnight at room temperature.

4.2.4 Mechanical characterization

Tensile tests are used to study the behavior of materials subjected to a given load. The applied force (F) and sample elongation (ΔL) are measured during the test. Material properties are represented in terms of *stress* (force per unit area, σ) and *strain* (percent change in length, ε). To obtain stress, the force measurements are divided by the sample's

area ($\sigma = F/A$). Strain measurements are obtained by dividing the change in length by the initial length of the sample ($\varepsilon = \Delta L/L$). The samples have the classic shape of a dog bone as shown in **Figure 28**. The mechanical properties of PU films were measured using a tensile tester (Instron, model 3365; Norwood, MA, USA) equipped with a 10 N f.s. load cell. All the tested samples had the same useful initial length (15 mm) and width (5 mm); the thickness varied and was measured through a caliper (*Digital caliper 0-200nm - RUPAC).*

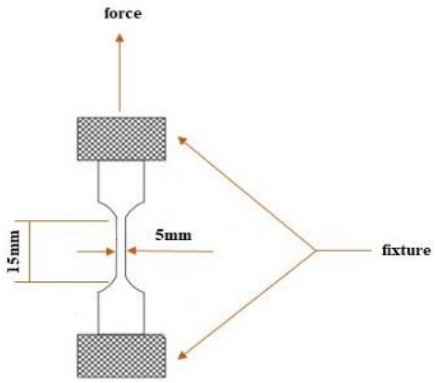

***Figure 28**: Preparation of samples, dog bone shape*

Elastic modulus (E), ultimate tensile stress (UTS) and strain at UTS were derived from stress –strain curves. The elastic modulus was determined as the slope of the curve in the initial elastic region (strain <1%). All analyses were performed in the dried state at room temperature.

4.2.5 Thermal characterization

A differential scanning calorimetry (SII DSC 7020 EXSTAR, Seiko, equipped with a liquid nitrogen cooling system) was used to perform the thermal characterization of the PU samples.

Each sample (5-10 mg) was inserted in an aluminum capsule with a lid (not hermetic closure) before analysis. The characterization included two heatings and one cooling cycles as follows: heated from 20 °C to 200 °C at 10 °C min^{-1} (first heating), isothermally controlled at 200 °C for 3 min, cooled to −60 °C at 30 °C min^{-1} (first cooling), isothermally controlled at −60 °C for 3 min and reheated (second heating) from −60 °C

to 200 °C at 10 °C min^{-1} under nitrogen. Melting temperature (T_m) was measured as the melting peak temperature, while by linearly integrating the endothermic melting peak the melting enthalpy (ΔH_m) can be obtained. The glass transition temperature (Tg) was measured as the midpoint temperature of the transition step. The crystallization temperature (T_c) was measured as the crystallization peak temperature, while integrating linearly the exothermic crystallization peak it is possible to get the crystallization enthalpy (ΔH_c)[179]. The percentage of crystallization of PCL for all three Pus has been calculated on the second heating cycle with the following formula:

$$C\ \% = \frac{\Delta H_m \cdot 100}{w \cdot \Delta H_m^{\circ}}$$

where ΔH_m integration peak, w = PCL weight fraction and ΔH_m° = 135.44 J/g.

4.2.6 Degradation Tests

Degradative tests were performed on the three different PUs, using square shape samples (1 cm x 1cm). Sample in a weight range between 20-25 mg were chosen for all three PU families, so that comparable results could be obtained. Two types of degradative tests were conducted. For the first one, enzymatic degradation was evaluated by incubating the samples in a solution containing lipase from Pseudomonas cepacia (Merck, Italy) at a concentration of 0.5 mg/mL. On the other hand, a hydrolytic degradation test was performed by incubating samples in a Phosphate Buffered Saline (PBS, pH 7.4) solution. During both tests, all samples were kept at 37 °C in an incubator (IF 75 Incubator, Memmert).

For each time point evaluated in the two tests (7d, 10d, 2w, 3w, 4w, 6w, 8w), five samples for each PU were weighed (W_i) before the test, placed in Bijou vials and covered with an amount of degradative solution proportional to their weight, considering as reference 1 ml of solution for 25 mg of PU. The degradative solution was changed twice a week.

At the predefined time point, the samples were taken from the incubator, freeze dried (Martin Christ ALPHA 2-4 LSC) and weighed again ($W_{freeze\ dried}$). Degradation was then evaluated as the weight loss compared to the initial weight.

$$Sample\ Degradation\ (\%) = \frac{W_i - W_{freeze\ dried}}{W_i} \cdot 100$$

To assess also how the degradation process influences the PU molecular weight, one sample for each time point was also analyzed through SEC as previously described. Molecular weight, polydispersity index and molecular weight profiles were compared to those of pristine PU films. A statistical analysis, One-Way ANOVA Calculator, Including Tukey HSD, has been calculated and the resulting p-values have been converted has shown in **Table 5**:

Symbol	Meaning
ns	$p > 0.05$
*	$p \leq 0.05$
**	$p \leq 0.01$
***	$p \leq 0.001$
****	$p \leq 0.0001$

Table 5: *p value format*

4.3. Surface modification

All tests were performed on the three different PUs, using square shape samples (1 cm x 1cm).

4.3.1. Plasma treatment

Plasma treatments were performed to expose carboxylic acid groups over the PU films surfaces using a plasma reactor (Diener electronic, Ebhausen, Germany) equipped with a floor electrode. The samples were prepared as for the degradation tests; then, they were subjected to a two-step functionalization procedure: (i) surface activation (etching) through argon (Ar) plasma to create free radicals on film surface, and (ii) plasma treatment in the presence of acrylic acid (AA) vapor for the polymerization/grafting of poly(acrylic acid) on the polymeric surface and consequent exposure of carboxylic acid groups. To maximize the amount of exposed functional groups, plasma process has been standardized in terms of Ar gas supply (50 sccm gas flow during both steps). After 10 minutes of Ar supply in the chamber, the activation phase was performed at direct power supply (50 W) for 5 min, while keeping the Ar gas flow constant. The reactor was then

purged with AA vapor at 50 µL/min for 60 min, while maintaining the same Ar flow. After that, the treatment was performed for 10 min at 200 W alternated power supply (9 Hz, Pulse ON 10 ms, Pulse OFF 990 ms, Duty Cycle 0.01, mean power applied 22 W)[162]. Samples were then extracted, washed with distilled water and dried under the fume hood.

4.3.2 ATR-FTIR spectroscopy

Attenuated Total Reflectance Fourier Transform Infrared spectroscopy analyses were performed as previously described in paragraph 4.2.1, to verify the correct surface modification with plasma. Spectra obtained from functionalized samples were compared with those taken from untreated samples.

4.3.3 SEC

Size Exclusion Chromatography analyses were performed as previously described in paragraph 4.2.2, to verify that samples have not deteriorated after plasma treatment. Results obtained from functionalized samples were compared with those taken from untreated samples.

4.3.4 Toluidine Blue O (TBO) colorimetric assay

Toluidine blue O (**Figure 29**[179]) is a cationic dye commonly employed for colorimetric assays in the biomedical field, for example as a marker to detect premalignant or malignant lesions or for staining chromosomes in plant or animal tissues[180]. When in basic environment, it can bind carboxyl groups in a 1:1 ratio through ionic interactions, since at high pH it is in its deprotonated form[179].

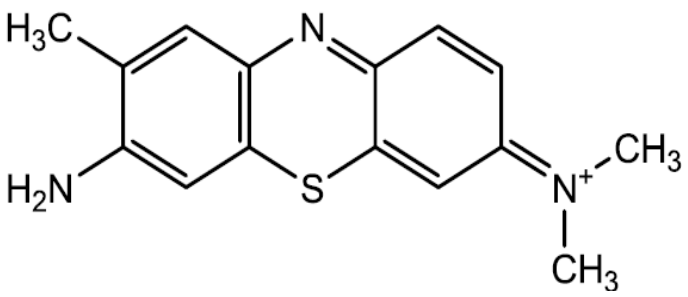

Figure 29: *Toluidine blue O molecule*

For this reason, it was used in this work to quantify the number of -COOH groups exposed on the surface of plasma treated samples

Samples both treated and untreated with plasma as previously described were immersed in 5 ml of TBO solution in double distilled water (ddH2O, 500 µmol/L, pH 10). After 18 h incubation, samples were rinsed and placed for 1 h in 5 mL of a 50:50 acetic acid:ddH2O solution, to unbound the TBO molecules from the carboxylic acid groups and permit quantification. The absorbance of the resulting solutions was measured between 400 nm – 700 nm using an UV/Vis spectrophotometer (Lambda 25, Perkin Elmer, Waltham, MA, USA) and the reference peak considered was at 632 nm. The final concentration of TBO and therefore of carboxylic acid groups was derived using a calibration curve based on standard solutions (20-1 µmol/L) prepared by dissolving TBO in a 50:50 acetic acid:ddH2O solution.

4.3.5 Contact Angle Measurements

Contact angle, θ (theta), quantitatively measures the wetting of a solid when a liquid is in contact with it. It geometrically represents the angle that forms at the three-phase boundary where the liquid phase (usually water), solid (the material), and gas (air) intersect and where forces are being exerted (as indicated in **Figure 30**[180]).

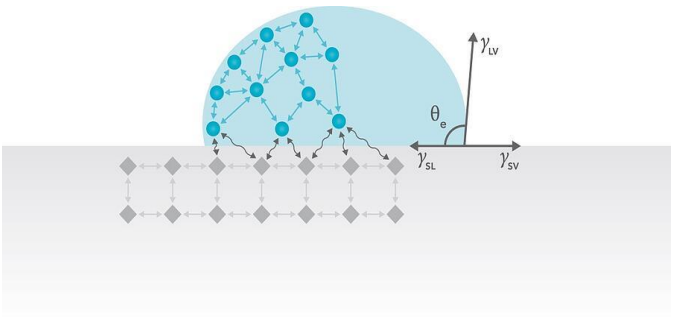

Figure 30: *Geometrical representation of contact angle*

Contact angles can be divided into static, dynamic and roughness corrected contact angle. Static contact angles are measured when the droplet is placed on the surface and the three-phase boundary is fixed. The static measurement of the contact angle is based on the Young equation:

$$\gamma_{LV} \cos\theta = \gamma_{SV} - \gamma_{SL}$$

which assumes that the interfacing forces are thermodynamically stable.

To assess the wettability of the PUs, contact angle measurements were performed using a Drop Shape Analyzer (Kruss, Germany). The polymers were dissolved in chloroform (CF) at 15% w/v concentration and casted over glass sample holders. The measurement was repeated on 3 samples (plasma treated and untreated) and 3 drops where deposited on each of them. Contact angle values (reported as average ± standard deviation) were obtained by analyzing the pictures with the KRÜSS ADVANCE 1.11.0.15801 Software. The reported data represent the mean angle between right and left contact angles detected for each drop.

4.4 Grafting of biomolecules

After plasma treatment, the grafting of biomolecules over the samples surface was carried out as a proof of concept of the feasibility to surface modify PUs. For the purposes of this work, benzylamine (BA) and gelatin were used. The grafting was performed through carbodiimide chemistry, mediated by EDC and NHS, to covalently bond the exposed carboxylic acid groups on the samples surface and the amino groups present in the two biomolecules. Due to the similarity of the three PUs and generally comparable properties, the further optimization of the surface modification process was conducted only on BHC2000 as a proof of concept. No significant differences are expected to be found with the other two polymers.

4.4.1. Benzylamine grafting

An aqueous solution containing 3.3 mg/mL of 1-ethyl-3-(3-dimethylaminopropyl-carbodiimide hydrochloride, (EDC, Merck, Italy) and 2 mg/mL of N-hydroxy-succinimide (NHS, Merck, Italy) was prepared and its pH was adjusted to 5. Samples prepared as previously mentioned and plasma treated were immersed in 5 mL of this solution and the reaction was carried out at 3 °C under magnetic stirring for 3 h. Untreated samples were also examined as control. The samples were then washed in a known volume of water at pH 5 (5 mL) to eliminate unreacted EDC/NHS residues and transferred to a BA solution in ddH_2O (4 µL/mL, pH 12). The reaction was then carried out for 24 h

under magnetic stirring at room temperature. Finally, the samples were washed in water and dried under the fume hood.

4.4.1.2. UV-Vis spectroscopy

The quantification of the BA grafted on the PU samples was carried out by an indirect method. After the samples were taken from the BA solutions used during the grafting procedure, 1 ml of these same solutions was analyzed using an UV/Vis spectrophotometer (Lambda 25, Perkin Elmer, Waltham, MA, USA), considering the absorbance relative to the main BA peak at 260 nm. The amount of unbound molecule in the solution was estimated using a calibration curve obtained from standard solutions of BA in water (0.4% v/v – 0.04% v/v).

4.4.1.3. ATR-FTIR

Attenuated Total Reflectance Fourier Transform Infrared spectroscopy analyses were performed as previously described to verify the success of the BA grafting. Beside the samples treated as explained above, spectra of the pristine and only plasma treated PUs film were taken as comparison.

4.4.1.4 Proton Nuclear Magnetic Resonance Spectroscopy (^{1}H NMR)

Proton nuclear magnetic resonance (^{1}H NMR) spectroscopy can be used to obtain information about the structure of molecules in a non-invasive manner.

^{1}H NMR spectra of BA, BHC2000, BHC2000 plasma treated (control) and BHC2000 grafted with BA were obtained through solubilization of 10 mg of sample in 750 µl of anhydrous deuterated dimethyl sulfoxide (DMSO-d6, 99.8% D with 0.03% TMS, Merck, Italy). Tests were performed with an Avance III Bruker spectrometer equipped with a 11.75 T superconductor magnet (500 MHz 1H Larmor frequency). The spectra were obtained by the average of 12 runs, with 10s of relaxation time and the signals were referenced to tetramethylsilane (TMS) at 0 ppm. The reference peak is given by dimethyl sulfoxide (DMSO) at 2.5 ppm; for BA quantification, the BA peak at 3.7 ppm was chosen in a region without PU signals.

4.4.2. Gelatin grafting

To graft gelatin on the PUs surface, a procedure similar to the one performed for BA was carried out. Incubation in the EDC/NHS solution and first washing were performed in the same way. After that, samples were inserted in aqueous gelatin solutions at different concentrations (0.1% w/v, 0.25% w/v and 0.5% w/v, pH 10) and then incubated for 24h at 37 °C (IF 75 Incubator, Memmert) to avoid gelation of the protein. Finally, samples were washed and dried as previously described.

4.4.2.1. ATR-FTIR

Attenuated Total Reflectance Fourier Transform Infrared spectroscopy analyses were performed, as previously described in paragraph 4.2.1, to verify the success of the gelatin grafting. Beside the samples treated as explained above, spectra of the pristine and only plasma treated PUs film were taken as comparison.

4.4.2.2. Bicinchoninic acid assay (BCA)

The bicinchoninic acid assay (BCA assay, Sigma Aldrich, Italy), is a biochemical assay used for determining the total concentration of protein in a solution. Determination of the total protein concentration is based on a change in color of the sample solution from green to violet in proportion to the protein concentration, which can then be measured using colorimetric techniques. Absorbance at 562 nm was evaluated with a plate reader (Multimode Plate Reader VIC- TOR X3, PerkinElmer). The quantification method was indirect as for BA quantification, since the incubation solutions were diluted (usually 1:10), analyzed and compared to gelatin solutions at the starting concentration (0.1%, 0.25% and 0.5% w/v, respectively). A calibration curve was also obtained from standard gelatin solutions (concentration within 0.002 and 0.2 mg/ml).

5. Results

5.1 Poly(urethane) chemical characterization

5.1.1 Attenuated Total Reflectance Fourier Transform Infrared spectroscopy

PU synthesis was verified by Attenuated Total Reflectance Fourier Transform Infrared (ATR-FTIR) spectroscopy. **Figure 31** shows the ATR-FTIR spectra obtained for the three synthesized poly(urethane)s and for the macrodiol C2000.

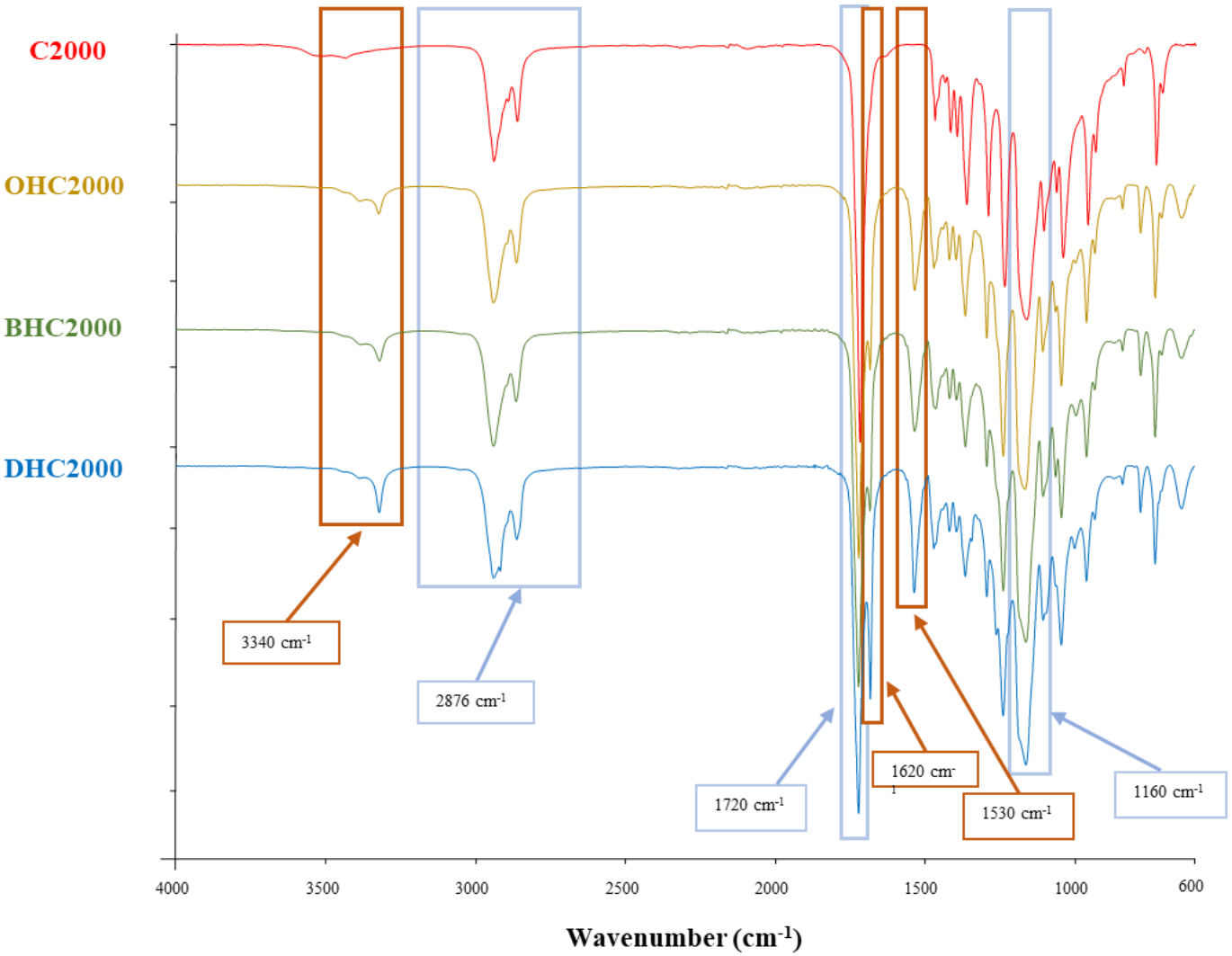

Figure 31: *ATR-FTIR spectra of the three poly(urethane)s and C2000*

C2000 spectrum shows two characteristic peaks at 2876 cm^{-1} (CH_2 stretching vibrations) and 1160 cm^{-1} (CH_2 rocking and C-O-C stretching vibrations), caused by the repeated -(O-CH_2-CH_2)- units of PCL in the macrodiol. Another distinctive peak is present at 1720 cm^{-1} which is due to the stretching vibration of the carbonyl (-C=O) of PCL. In the case of PUs, an additional peak due to the C=O (amide I) of urethane domains was observable in the region between 1620-1640 cm^{-1}. In addition, the peak at 1530 cm^{-1}, not present in C2000, represents the N-H bending vibrations (amide II), indicating the presence of the urethane linkages and thus the success of the synthesis. The urethane and amide groups also showed an absorption peak at 3340 cm^{-1}, ascribed to N-H stretching[179].

5.1.2 Size Exclusion Chromatography (SEC)

Size Exclusion Chromatography was conducted to study the distribution of the molecular weights of the three PUs.

Figure 32 shows the molecular weight profiles of all the synthesized PUs. Values of number average molecular weight (M_n), weight average molecular weight (M_w) and Polydispersity Index (D) of each PU are reported in **Table 6**.

All three PUs showed a M_n between 20 and 30 kDa and a M_w between 30 and 40 kDa. Thus, the polydispersity index was always comprised between 1.4-1.5, which is a typical value for this type of materials[181].

By comparing the molecular weight profiles of the three PUs (**Figure 33**), it is even more evident that no great differences in the chain length distributions and values can be detected.

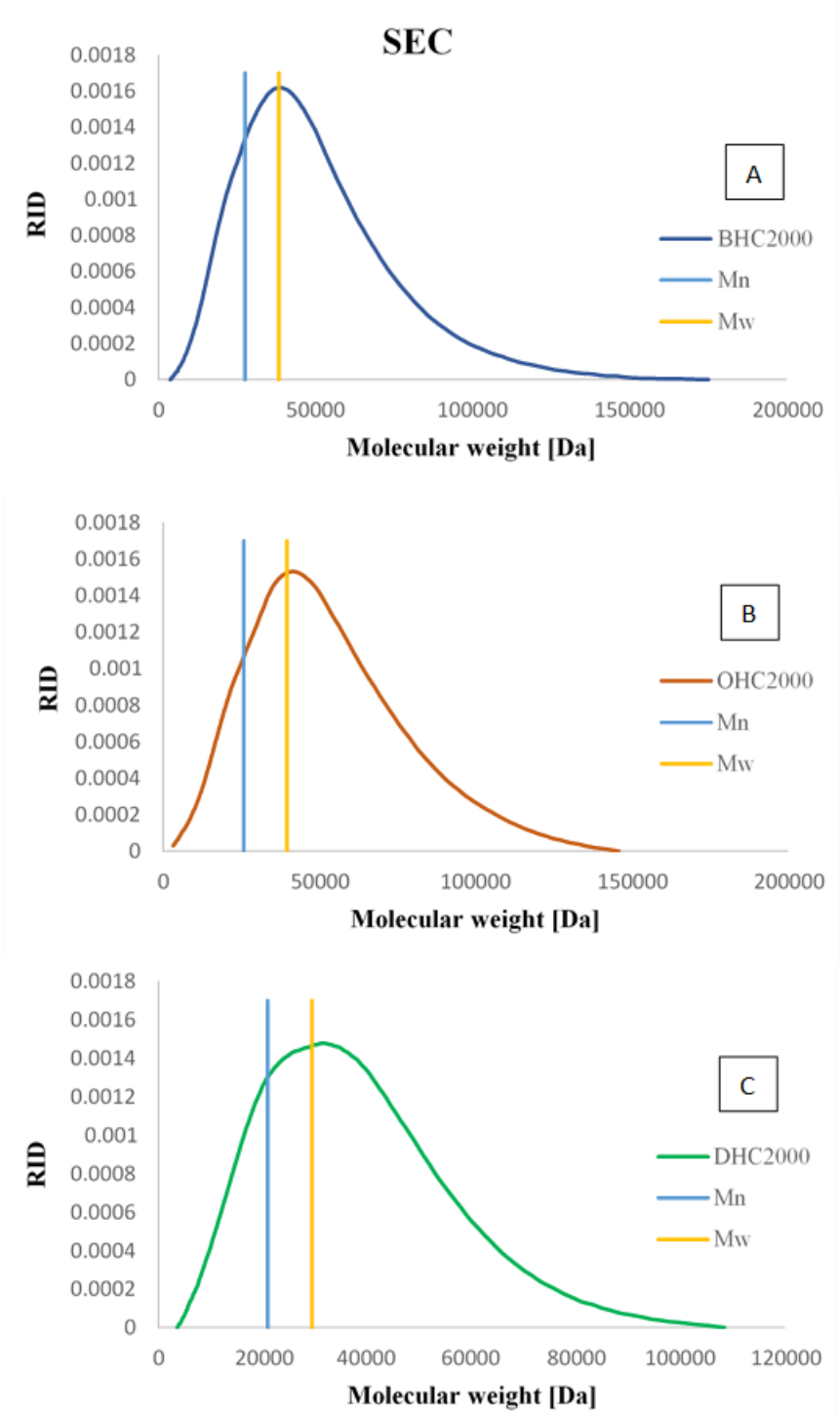

***Figure 32**: Molecular weight distribution profiles (refractive index detector signal vs. molecular weight) of **A**: BHC2000, **B**: OHC2000, **C**: DHC2000*

	BHC2000	OHC2000	DHC2000
Mn	27500	25700	20900
Mw	38300	39600	29400
D	1.4	1.5	1.4

***Table 6**: Values of M_n, M_w and D of the three PUs as obtained by SEC*

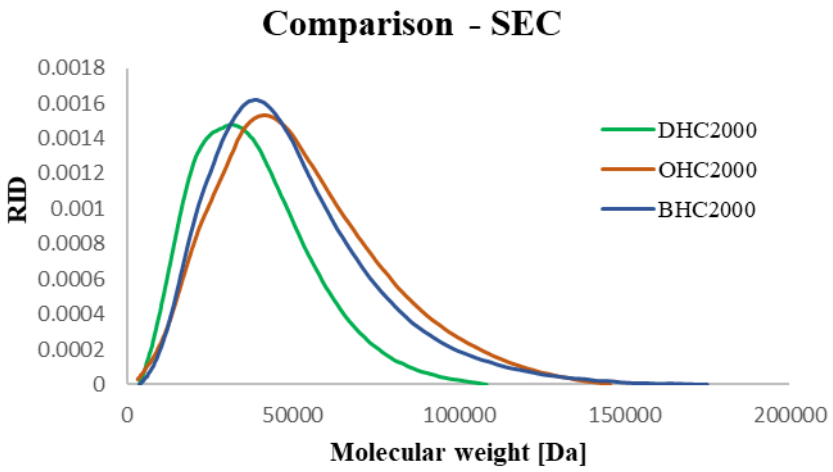

***Figure 33**: Comparison among the molecular weight distribution profiles (refractive index detector signal vs. molecular weight) of BHC2000, OHC2000, and DHC2000*

.

5.1.3 Mechanical characterization

To evaluate the mechanical properties of the three synthesized PUs, tensile tests were performed on an average number of 20 samples for each PU. Results are reported in **Figure 34, Figure 35** and **Table 7**.

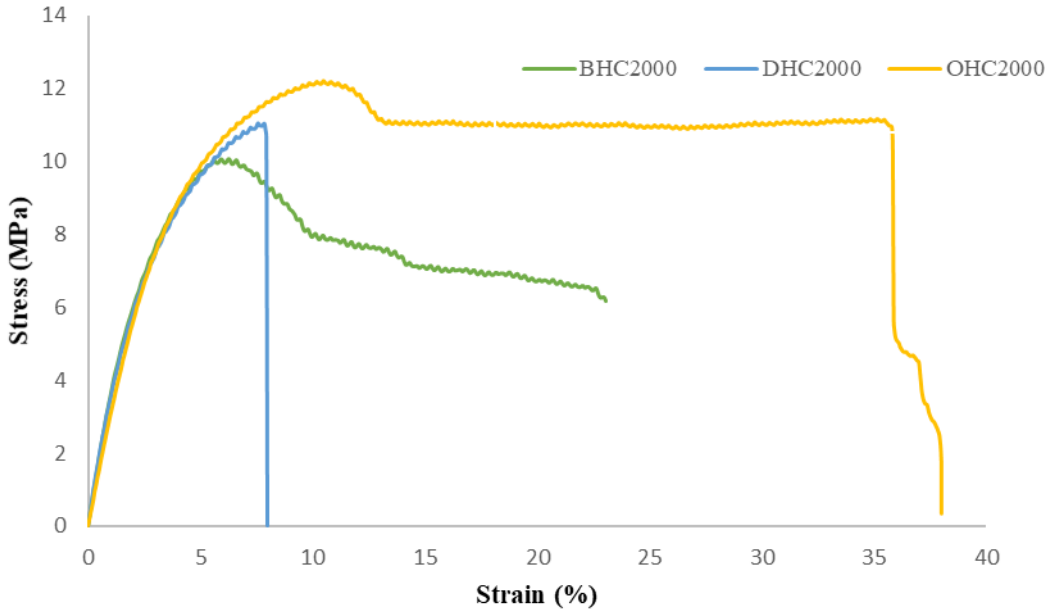

***Figure 34**: Mechanical characterization of PUs*

	E (MPa)		UTS (MPa)		Strain at break (mm)	
	Average	*Dev. STD*	*Average*	*Dev. STD*	*Average*	*Dev. STD*
BHC2000	367	55	10.3	2.8	6.1	1.9
OHC2000	336	60	12.3	3.2	36.9	20.8
DHC2000	368	63	11.8	2.6	8.6	3.8

***Table 7**: Overview of the average values and Dev. STD of Young's Modulus (E), Ultimate Tensile Stress (UTS) and Strain at break of the three PUs*

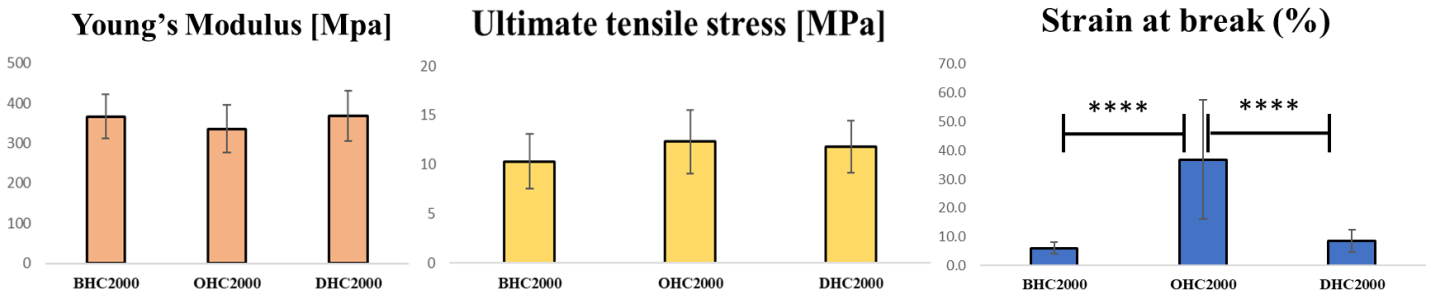

***Figure 35**: Graphicals representations of average values and Dev. STD of E, UTS and strain at break of the three PUs*

On average, the Young's Modulus and Ultimate Tensile Stress (UTS, the maximum value of stress registered before the breakage of the sample) found for the three PUs did not differ significantly. This could probably mean that the mechanical behavior in this sense is mainly due to the macrodiol component of the poly(urethane)s, which is the same in all cases. However, differences could be detected in the macroscopic elongation of the samples and especially regarding the maximum strain that the PUs can withstand before rupture.

BHC2000 samples usually started to show cracking at relatively low stress values, but subsequently the smaller sections formed presented a plastic deformation with considerable elongations, as shown in **Figure 36 A** , that can reach an average value of 6.1 ± 1.9 % of the initial sample length. OHC2000 samples, on the other hand, showed an evident passage from elastic to plastic deformation in the strain range between 5 and 25 % **(Figure 36 B)**, reaching final values that, despite being quite disperse, are significantly higher (36.9 ± 20.8 %) than for the other two PUs. Finally, DHC2000 samples had a fragile behavior, resulting in a net break after a generally small deformation around 8.6 ± 3.8 %.

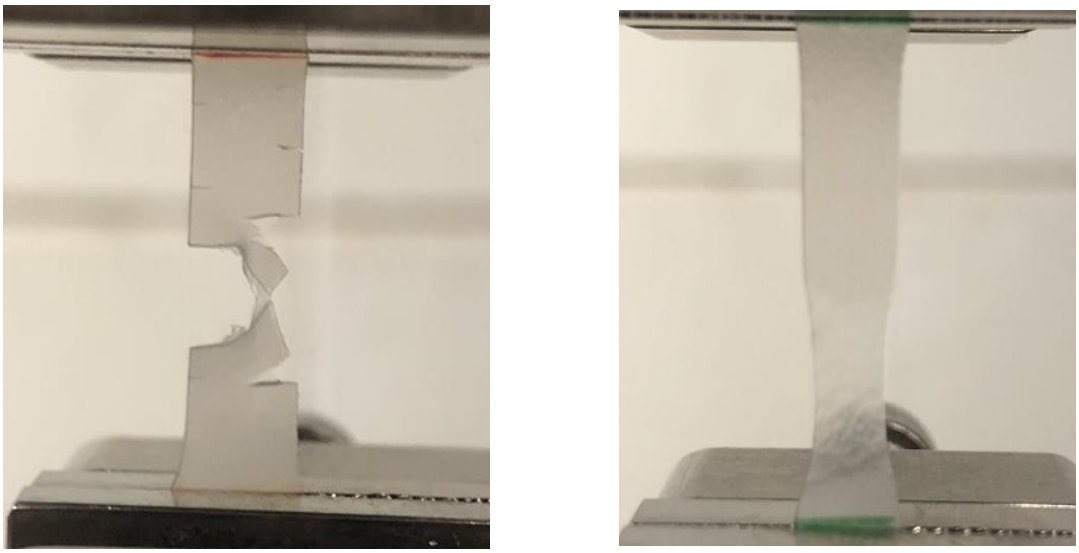

***Figure 36**: Tensile test: differences in sample behavior between, **A:** BHC2000; **B**: OHC2000*

The differences between the ability of these materials to deform when a stress is applied are probably caused by the different chain extenders used for each PU. It has been hypothesized that the chain extender affects the microcrystalline structure of the films used for the mechanical testing, thus influencing their macroscopic behavior. To confirm this supposition, further characterizations by Atomic Force Spectroscopy (AFM) and Scanning Electron Microscopy (SEM) will be performed.

5.1.4 Thermal characterization

The DSC curves obtained for the three PUs are reported in **Figure 37 A-B-C.**

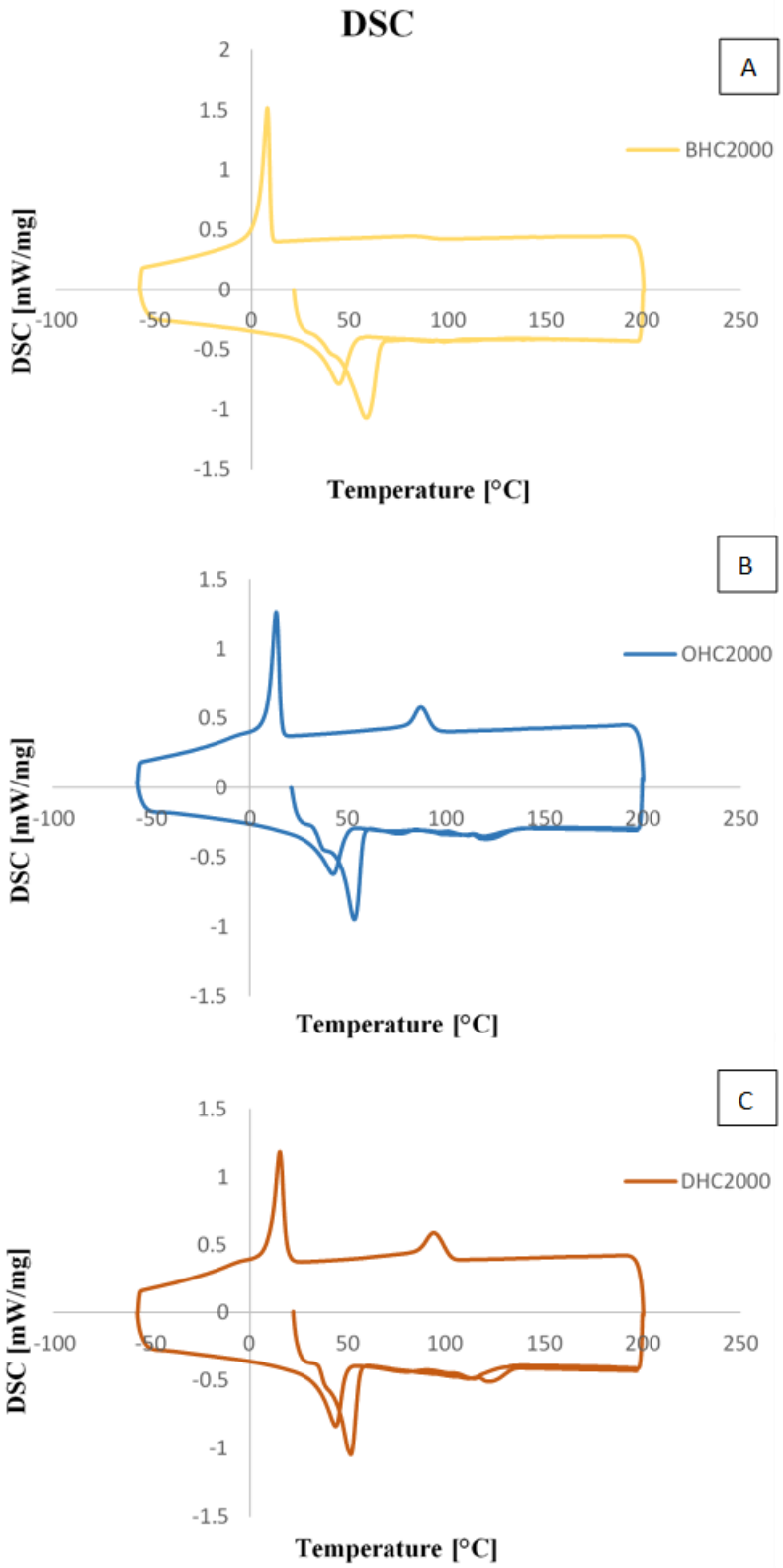

Figure 37*: DSC thermograms of the three heating-cooling-heating cycles for* ***A:*** *BHC2000;* ***B:*** *OHC2000;* ***C:*** *DHC2000*

Figure 38 represents the first heating cycle, from 20 °C to 200 °C. The first endothermic peak present in the thermograms (around 50 °C) is due to the melting of the PCL block, which is the macrodiol used for the synthesis of all PUs. At higher temperatures, up until around 150 °C, for OHC2000 and DHC2000 other peaks are present, although less pronounced, that are due to the melting of the crystalline phases based on the PU hard segment. For BHC2000, on the other hand, no secondary endothermic peaks were clearly identifiable, suggesting a less relevant presence of crystalline structures based on the hard segment. At around 35 °C a glass transition temperature (T_g) can also be identified, that can be ascribed to the PU hard segments. The glass transition temperature of the soft segment, instead, was not visible, as it is expected to appear at around -50 °C. The thermal properties of the synthesized PUs are in agreement with those already reported for a PU with similar composition (i.e., same macrodiol, but different diisocyanate and chain extender)[179].

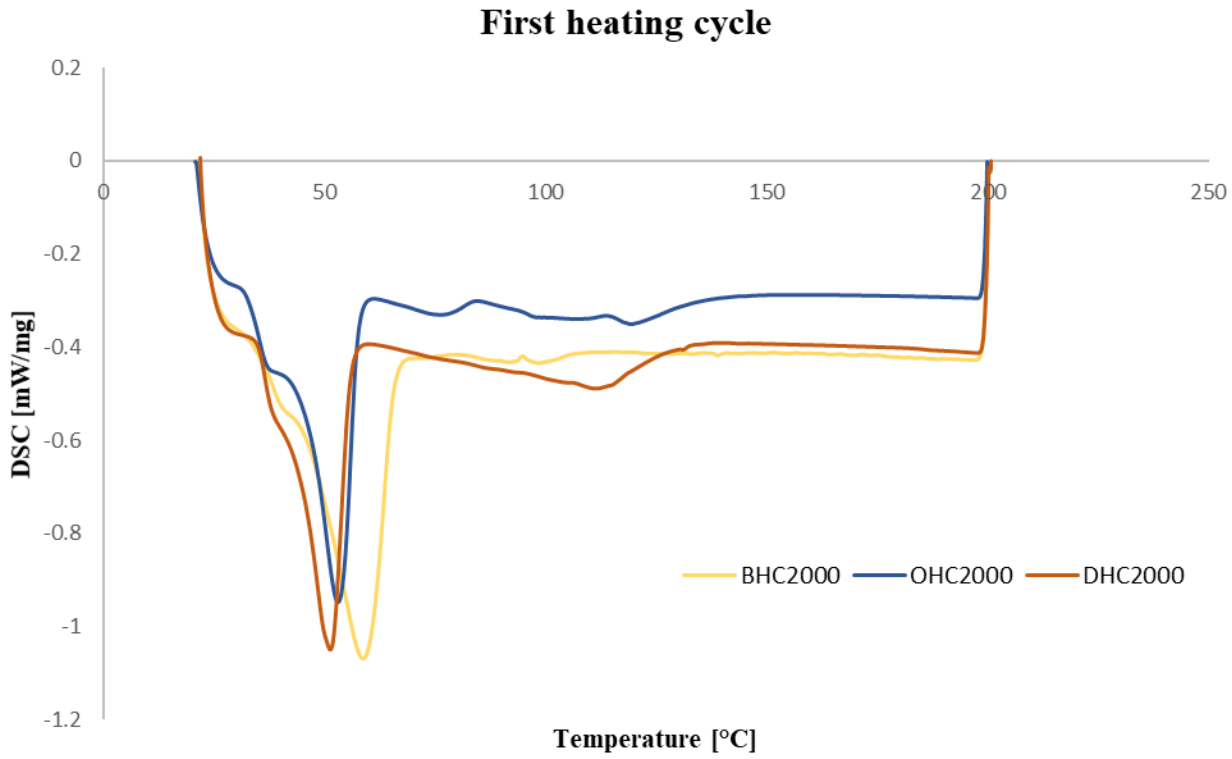

Figure 38: *Thermograms of the first heating cycle of the three PUs.*

Figure 39 represents the cooling cycle, from 200 °C to -60 °C. In accordance with the results obtained from the heating cycle, the main exothermic peak is due to the re-crystallization of the PCL block, in the region between 30 °C and -20 °C; moreover, for OHC2000 and DHC2000 a peak was also present at higher temperatures (around 90 °C), signaling the re-crystallization of the crystalline phases based on the hard segments. These phenomenon agrees to what was observed during the heating phase and confirms the presence of a secondary hard segment-based crystalline phase apart from PCL. For BHC2000, no clear re-crystallization peak was visible apart from the one relative to PCL, which again confirms what was before observed.

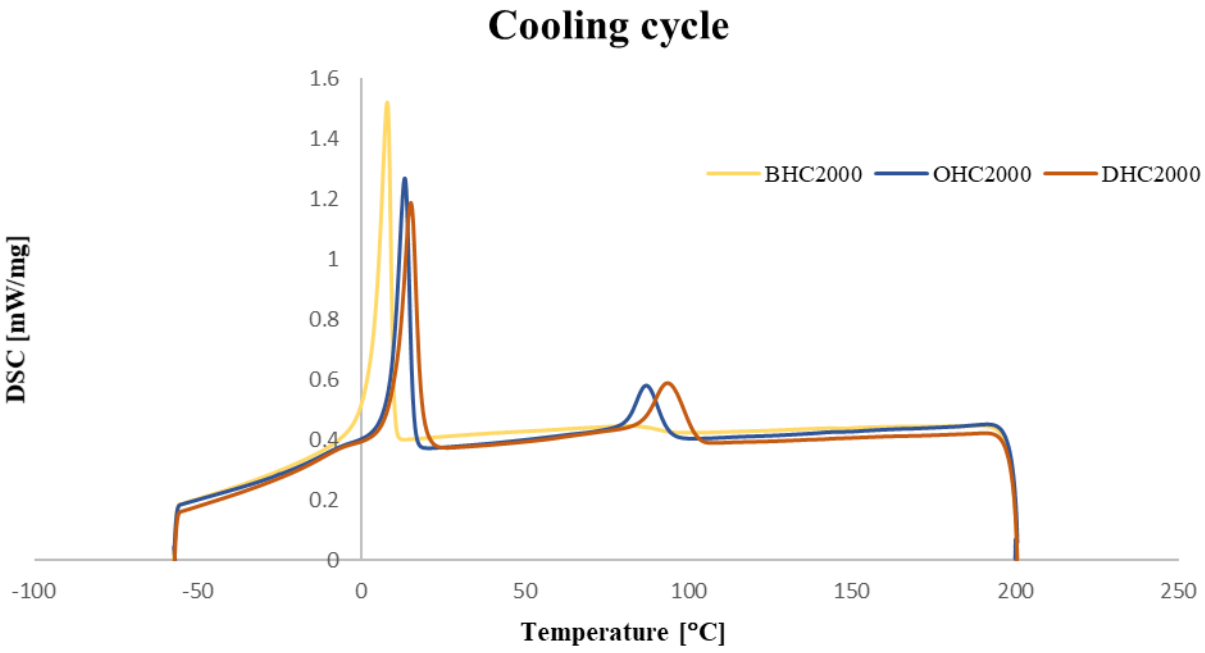

Figure 39: *Thermograms of the first cooling cycle of the three PUs.*

The second heating step, **Figure 40**, from -60 °C to 200 °C, confirmed the previous results. In this case, the curves were not affected by the sample starting condition (i.e., accumulated thermal and mechanical stresses), so the peaks relative to PCL block are almost perfectly aligned around 43 °C. It can also be noted that the secondary peaks present in the OHC2000 and DHC2000 curves are similar, suggesting the formation of similar crystalline structures in both PUs. Again, BHC2000 presents a marked difference, showing a much less pronounced peak.

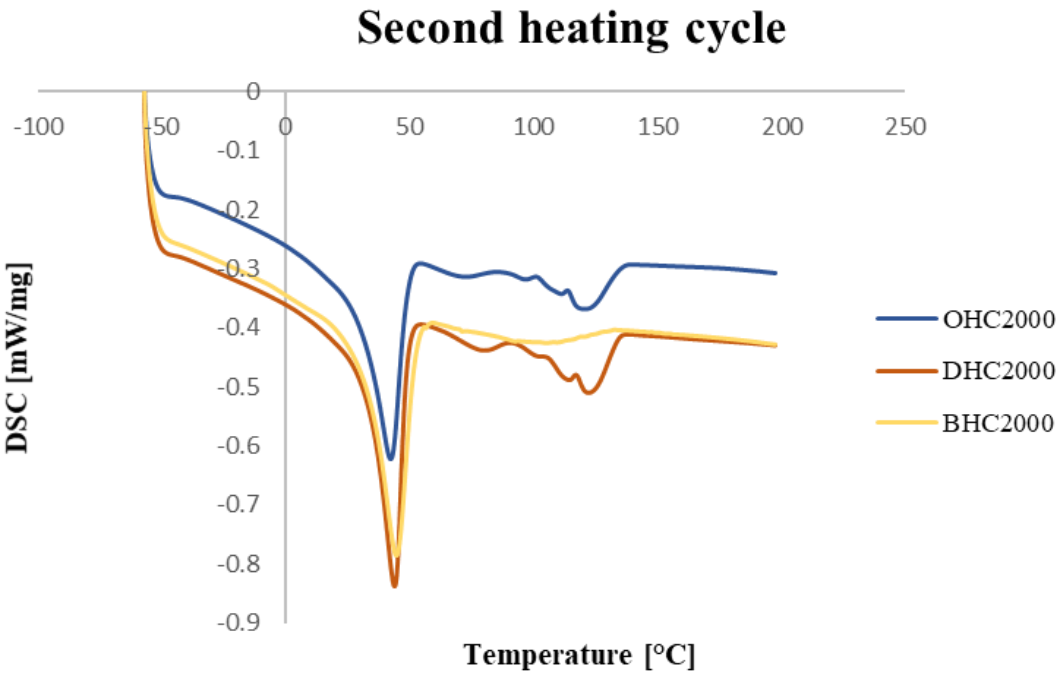

Figure 40: *Thermograms of the second heating cycle of the three PUs.*

Crystallization results are reported in **Table 8**:

	w	ΔH_m(PCL) [mJ/mg]	C %
BHC2000	0.803	41.7	38.3
OHC2000	0.804	34.3	31.5
DHC2000	0.786	38.3	36.0

Table 8*: PCL weight content (w) within PU chemical structure (hypothesis: 100% yield of the synthsis reaction); melting enthalpy (ΔH_m) estimated by integrating the PCL melting peak in the second heating cycle; PCL crystallization percentage (C %) for the three PUs*

A similar evaluation was not possible in the first heating cycle because the inflection due to the glass transition of the hard phases overlapped with the peak of the PCL melting, thus not allowing a correct integration of the melting peak.

As for the mechanical characterization results, further investigations on the microcrystalline structure are needed to completely understand the different behavior of these materials. However, from these tests it is possible to state that all three PUs can be processed at temperatures compatible with common Fused Deposition Modeling (FDM) printers. However, other characterizations need to be performed, such as Thermogravimetric Analysis (TGA), in order to evaluate their thermal stability during the printing process.

5.1.5 Degradation Tests

Degradation tests were conducted to evaluate the behavior of the three synthesized materials in different environments, in view of their application as tissue engineering scaffolds material.

Degradation in both enzymatic and hydrolytic environments was evaluated for all three PUs. A statistical analysis has been carried out as explained in paragraph 4.2.6. In the enzymatic environment, **Figure 41**, a clear increase in degradation over time was observed for BHC2000, reaching up to 88 % after 8 weeks.

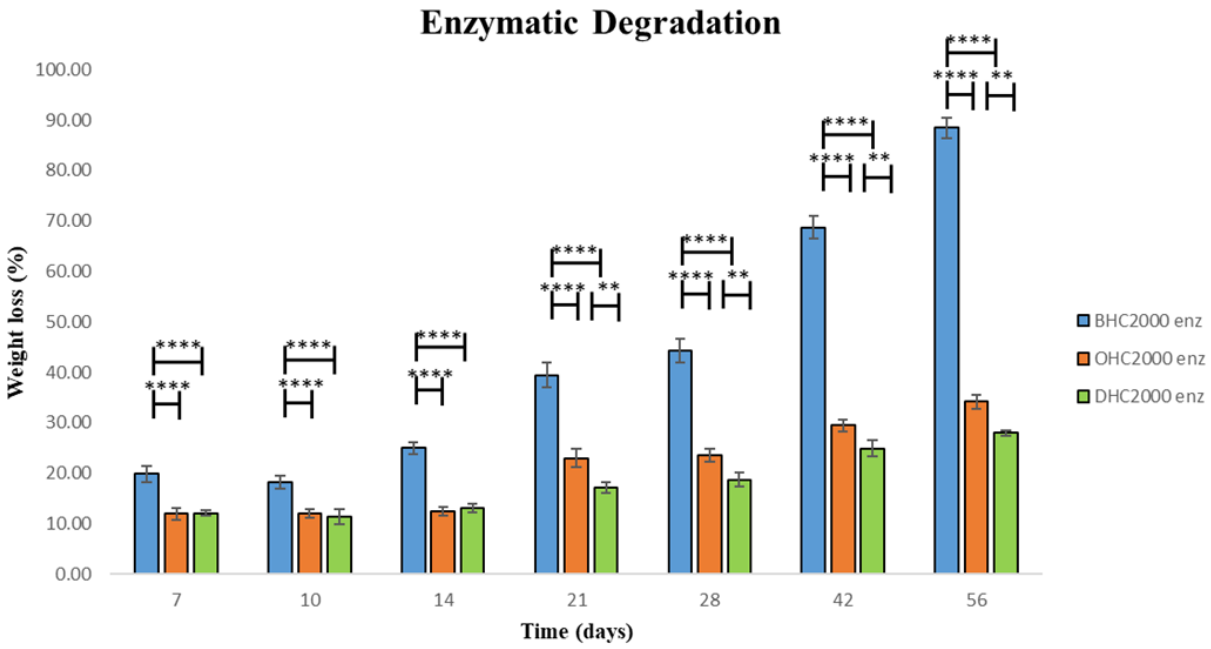

Figure 41: *Enzymatic degradation evaluated for the three PUs*

The other two polymers, instead, showed an increase in weight loss but much less marked than BHC2000 and the differences are already extremely significant after one-week incubation. A possible explanation for this behavior could be the strong influence of PCL in the structure of BHC2000: as already hypothesized, in this case the hard phases are not long enough to crystallize significantly, and the soft phase is much more exposed to the lipase targeting. The presence of crystallized hard phases in OHC2000 and DHC2000, on the other hand, could impair the enzymatic attack toward PCL resulting in a greater degradation resistance. After 3 weeks, the difference in weight loss becomes significant also between these last two PUs, suggesting that the increase in chain length of the chain extender could also correspond to an increased degree of crystallinity of the hard phase.

Hydrolytic degradation, instead (**Figure 42)**, did not significantly differ between the three PUs and remained stable after about 3 weeks, reaching final values around 15% after 8 weeks. This result could be explained by the reduced thickness and small initial weight of the samples, so that even a small weight loss appears high in percentage. Indeed, given the hydrophobicity of these materials, the expected tendency is to be stable in water environments for several years before incurring in hydrolytic degradation.

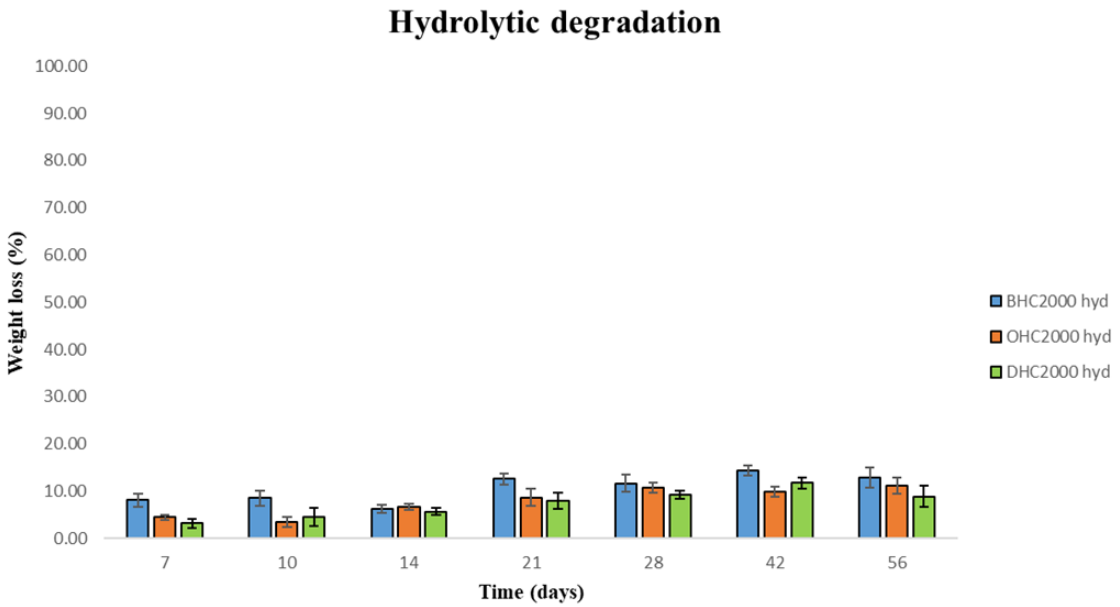

Figure 42: *Hydrolytic degradation evaluated for the three PUs*

5.1.6 Size Exclusion Chromatography (SEC)

SEC analyses were also performed at each time step, to verify a possible change in the molecular weight profile. In **Figure 43** an example is shown for enzymatic and hydrolytic degradation of OHC2000.

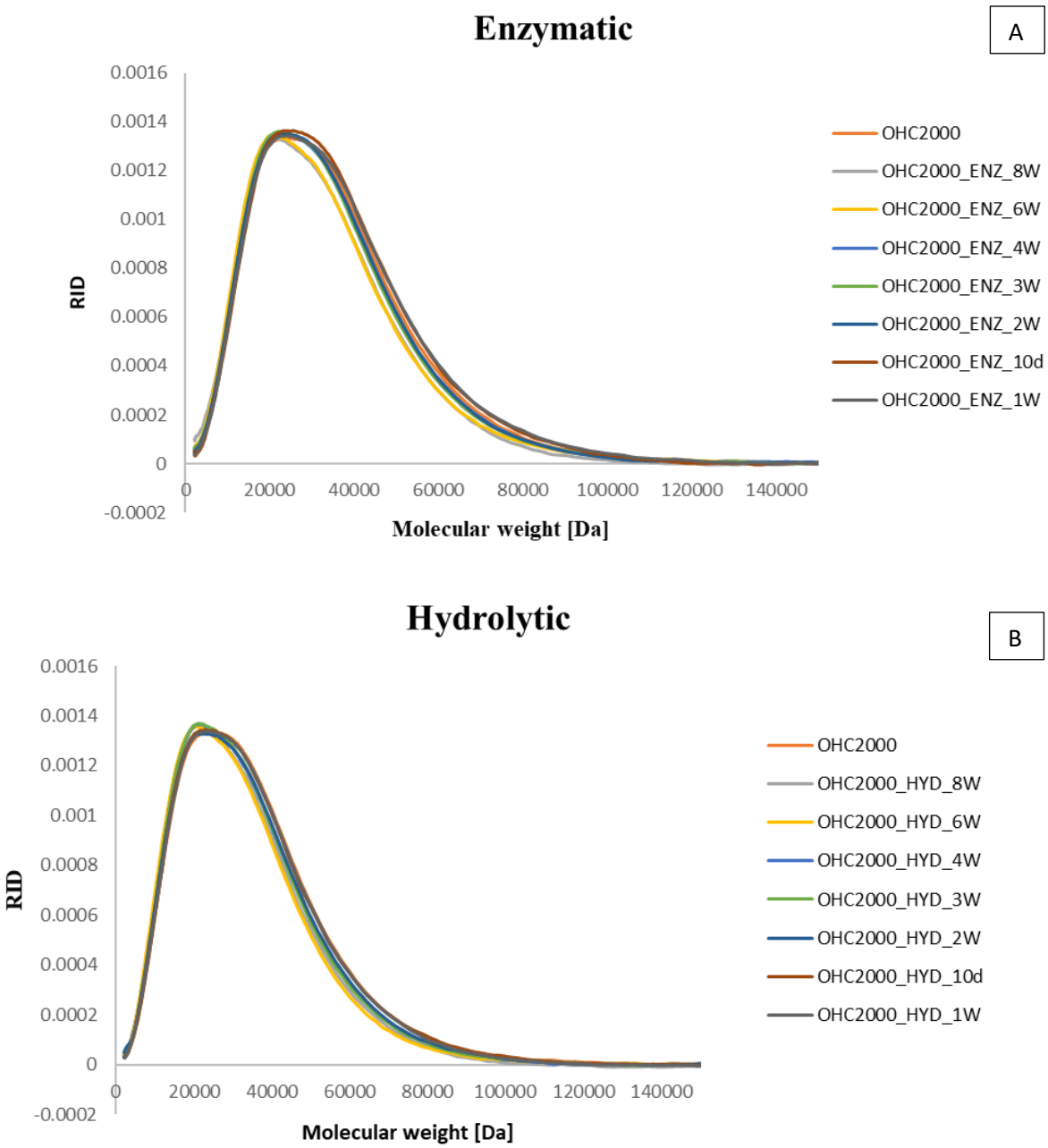

***Figure 43**: Molecular weight distribution of OHC2000 samples subjected to **A**: enzymatic, **B**: hydrolytic degradation*

No relevant differences were detected in the profile shape and thus in molecular weight values for all the three PUs, that showed a similar behavior to the reported OHC2000. Although this result could appear in contrast to the significant differences found regarding weight loss, it could be explained by the fact that degradation is in this case mostly a superficial erosion of the tested films. For this reason, although shorter chains are eliminated in the first steps of the process, their loss did not result in a significant change of the molecular weight distribution.

Anyway, the most evident change between the registered molecular weight profiles was evidenced by comparing the pristine BHC2000 and samples after 8 weeks of enzymatic degradation (**Figure 44**). A reduction in Mn (from 27500 to 17500 Da) and Mw (from 38300 to 29200 Da) values can be detected, with a shift of the peak molecular weight toward smaller values.

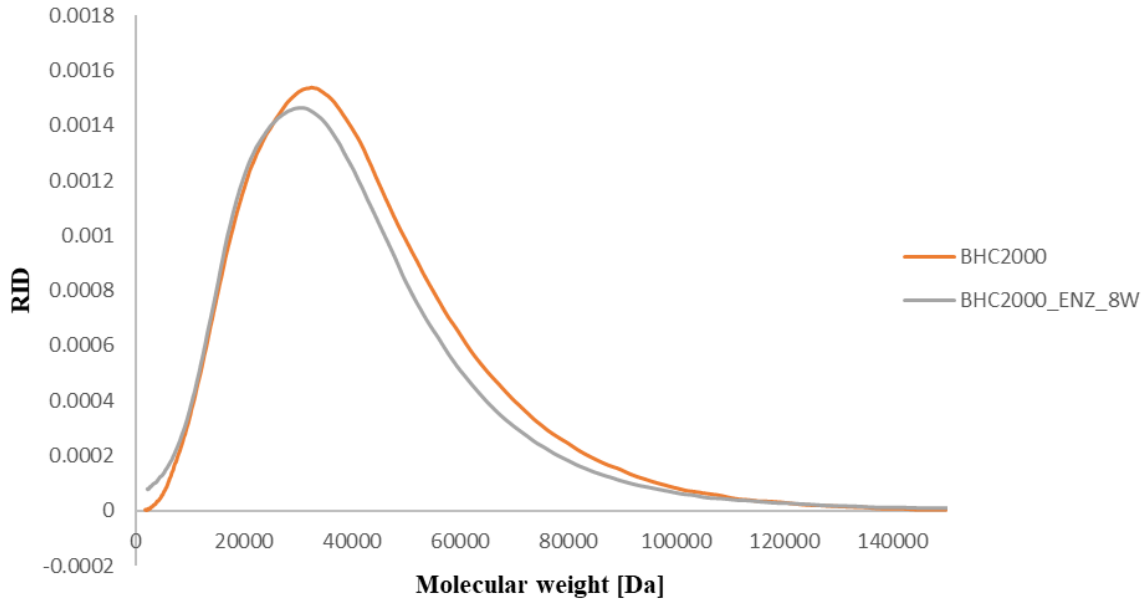

Figure 44: *Molecular weight distribution profiles for BHC2000 before and after 8w enzymatic degradation*

5.2 Surface Modification

5.2.1 Attenuated Total Reflectance Fourier Transform Infrared (ATR-FTIR) spectroscopy

ATR-FTIR analyses were conducted on the PU films as described on paragraph 4.2.1 on both plasma treated and untreated samples. No relevant differences could be detected between the two families of spectra, as reported in **Figure 45**, **46** and **47**. This is due to the fact that the carboxylic acid groups exposed on the surfaces present bonds that are already present in the bulk material in a great amount (i.e. C=O both from the PCL ester group and the urethane linkage). This results in very pronounced peaks already visible in the native spectra, so that the contribution of the newly exposed groups cannot be discriminated.

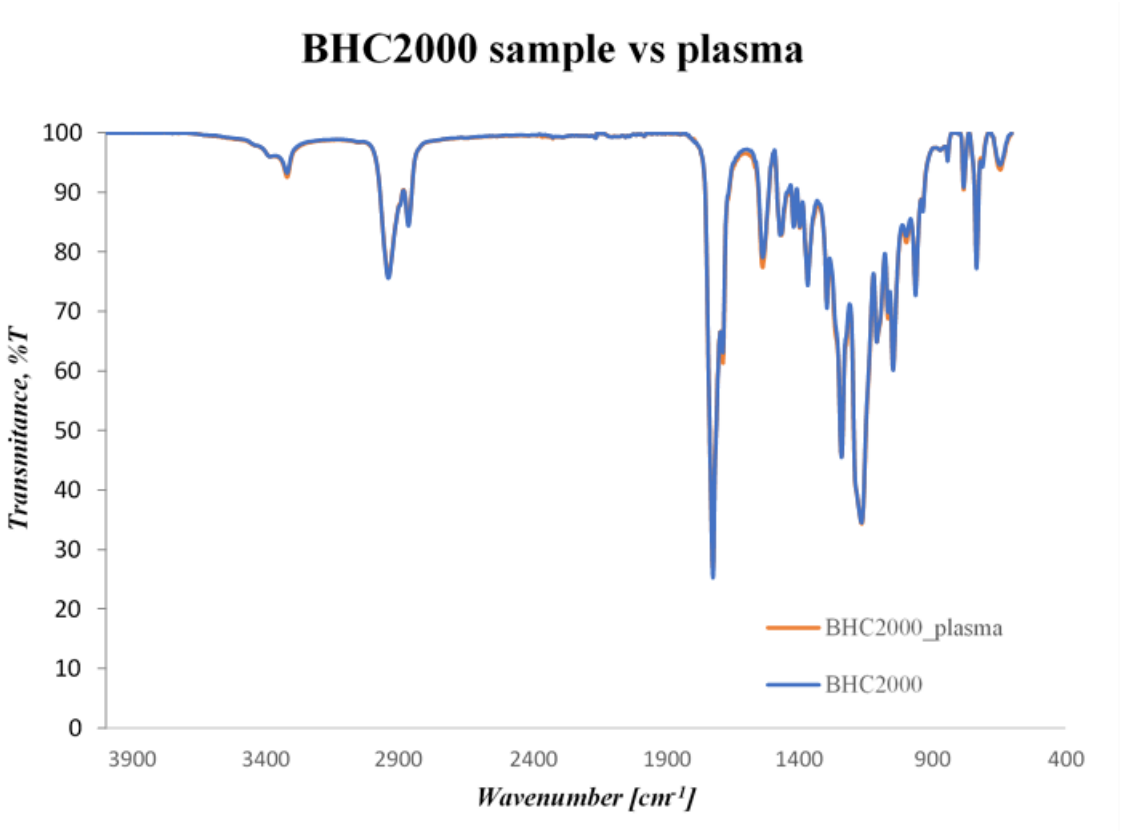

Figure 45: *Comparison between BHC2000 ATR-FTIR spectra before and after plasma treatment.*

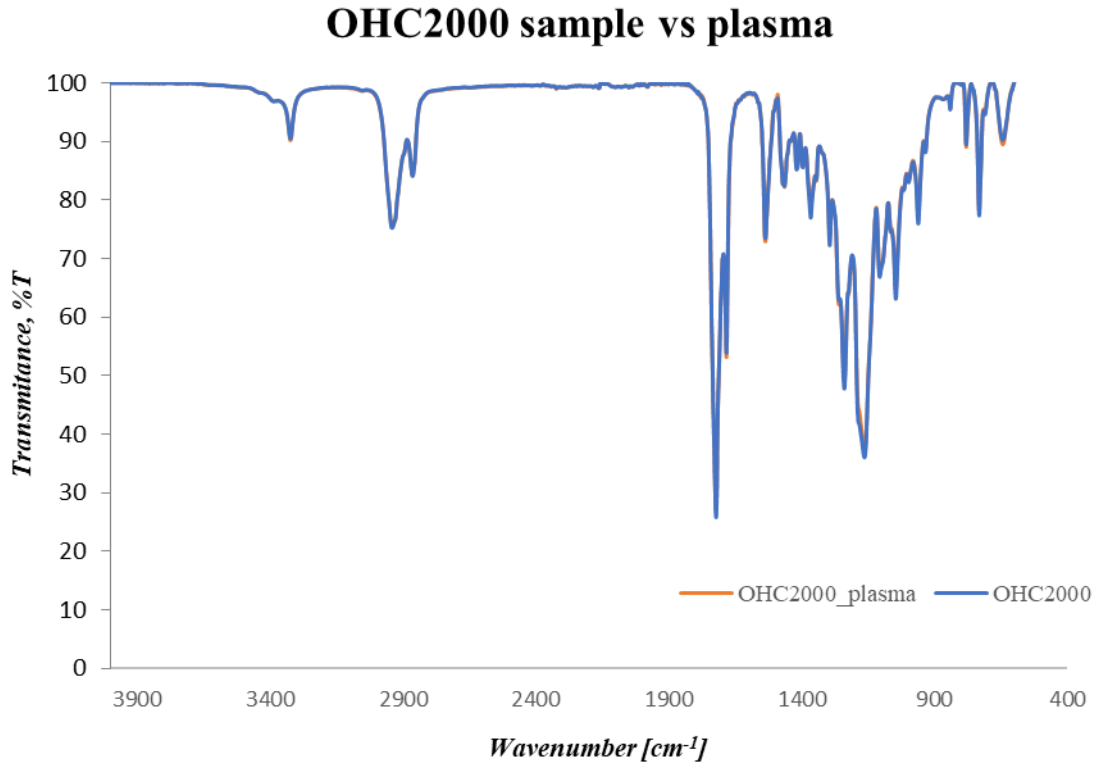

***Figure 46**: Comparison between OHC2000 ATR-FTIR spectra before and after plasma treatment.*

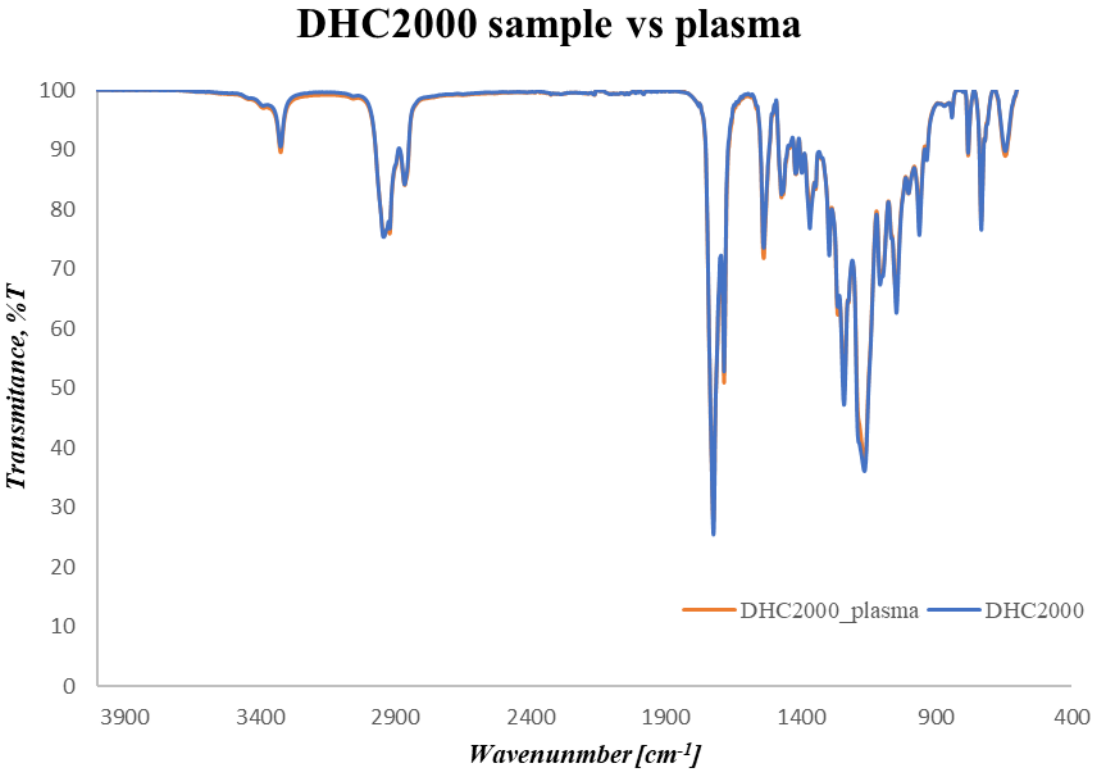

***Figure 47**: Comparison between DHC2000 ATR-FTIR spectra before and after plasma treatment.*

5.2.2. Size Exclusion Chromatography

SEC analyses were performed on PU films after plasma treatment to confirm that no degradation occurred during the process. As an example, **Figure 48** reports the molecular weight distribution obtained for the treated BHC2000 sample compared to the untreated one. No relevant changes were observed in the molecular weight distribution, thus confirming that the surface modification preserves the material properties. Similar results were obtained for OHC2000 and DHC2000.

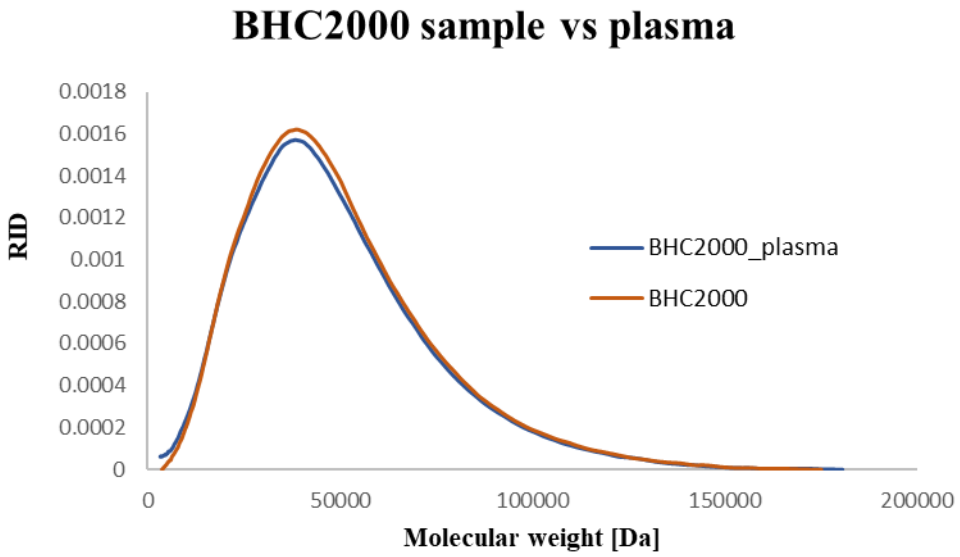

Figure 48: *Comparison between DHC2000 molecular weight distribution before and after plasma treatment.*

5.2.3 Contact Angle Measurements

To assess the success of the plasma treatment, a wettability test was performed through contact angle measurements. The exposed -COOH groups, indeed, have the effect to improve the hydrophilicity of the surface and thus should result in a lowering of the contact angle value. Three different samples were prepared for each material and a total of nine drops were deposited on different areas, in order to evaluate the homogeneity of the surface treatment.

Figure 49 and **Table 9** report the contact angle values for the three PUs before and after plasma treatment. **Figure 50**, moreover, reports an example of a drop deposited on each PU before and after modification.

BHC2000		OHC2000		DHC2000	
Before treat.	*After treat.*	*Before treat.*	*After treat.*	*Before treat.*	*After treat.*
91.56 ± 2.4	58.89 ± 4.1	84.1 ± 1.6	56.5 ± 3.5	88.8 ± 2.6	48.1 ± 3.3

Table 9: *Summary of average values and Dev. STD of PU static contact angle values before and after plasma treatment*

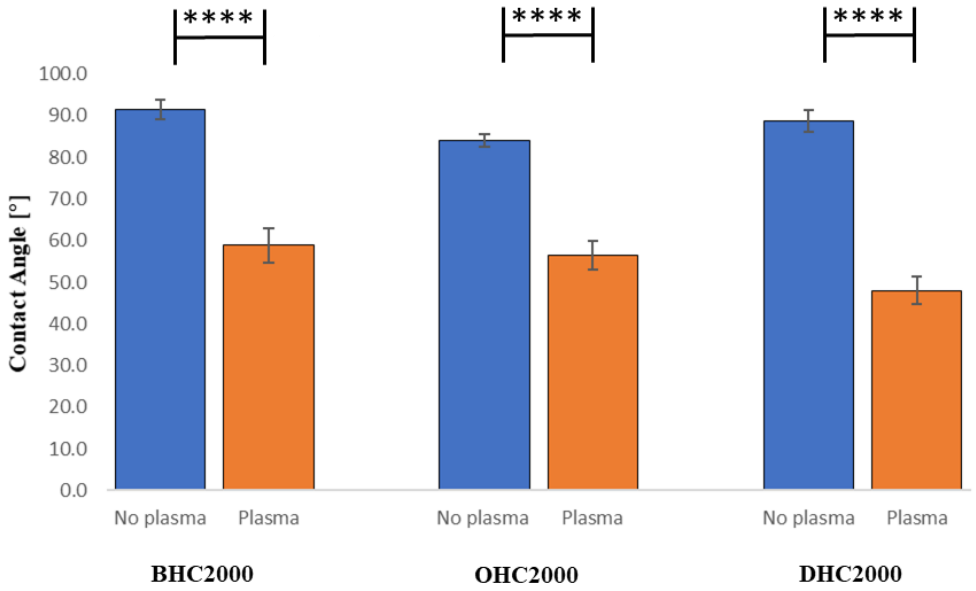

Figura 49: *Static contact angle values before and after plasma treatment for the three PUs*

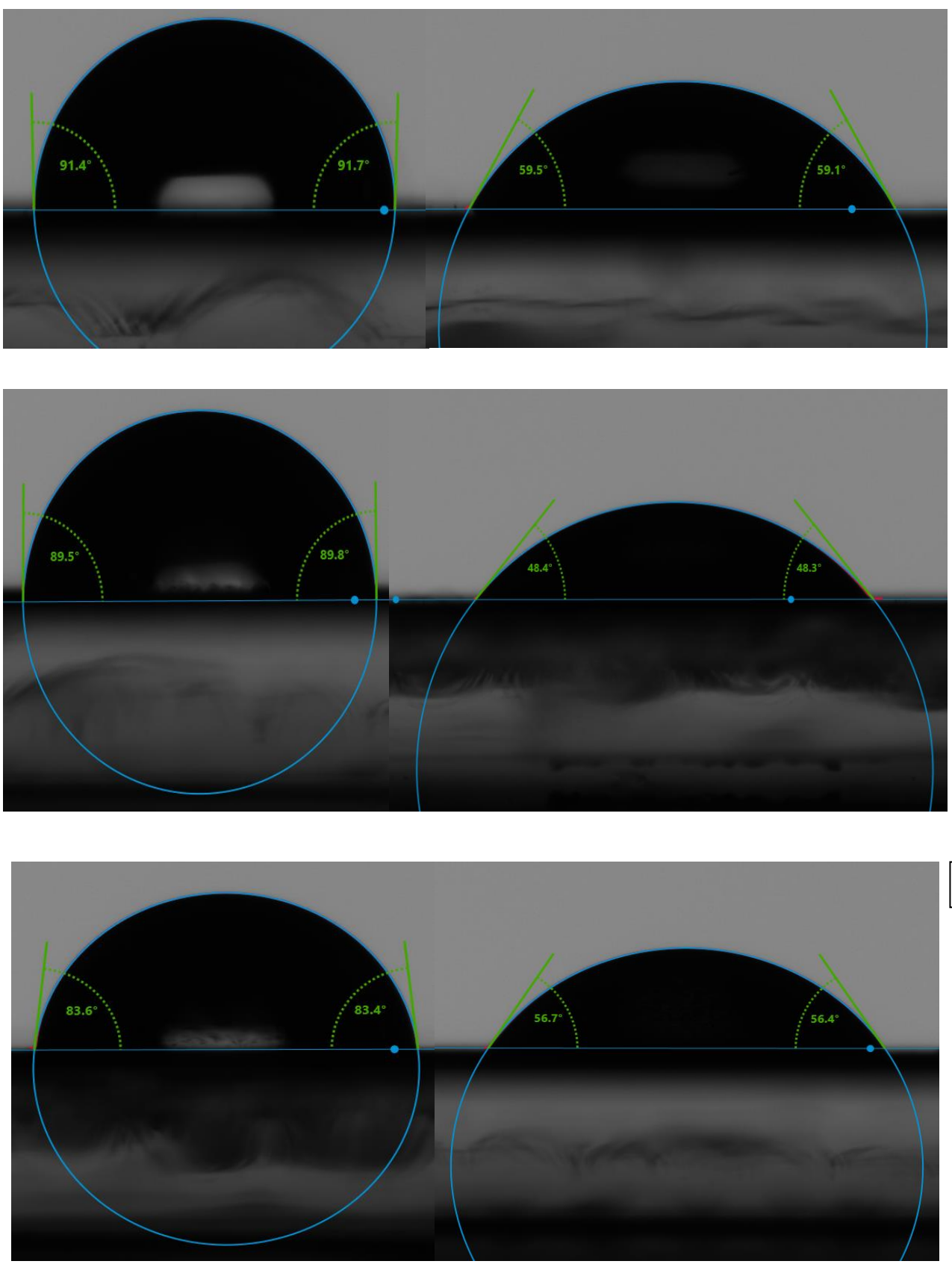

Figure 50: *Drop shape and contact angle values before (left) and after (right) plasma treatment for A: BHC2000, B:OHC2000, C:DHC2000.*

For all the PUs, a significant lowering of the contact angle values was detected, with no relevant differences between the materials. In detail, for all PUs an average variation between 30 and 40% was observed, with values starting from around 90° reaching around 50° after treatment. In this way, the effectiveness of plasma treatment was demonstrated by the substantial improvement in the sample hydrophilicity. Since no significant differences could be found in the superficial response of the three PUs to the plasma treatment, all the subsequent tests were performed only on BHC2000, assuming a similar behavior could be expected also for the other PUs.

5.2.2 Toluidine Blue O (TBO) assay

After the treatment and to optimize a further surface functionalization, the number of carboxylic acid groups present on PU surface was quantified through the colorimetric TBO assay. The TBO assay was performed on both treated and untreated samples. **Figure 51** shows the typical UV-Vis spectra obtained after the test, where 3 samples of pristine BHC2000 (BHC2000_ctrl_n) and 3 samples of BHC2000 treated with plasma (BHC2000_plasma_n) were analyzed.

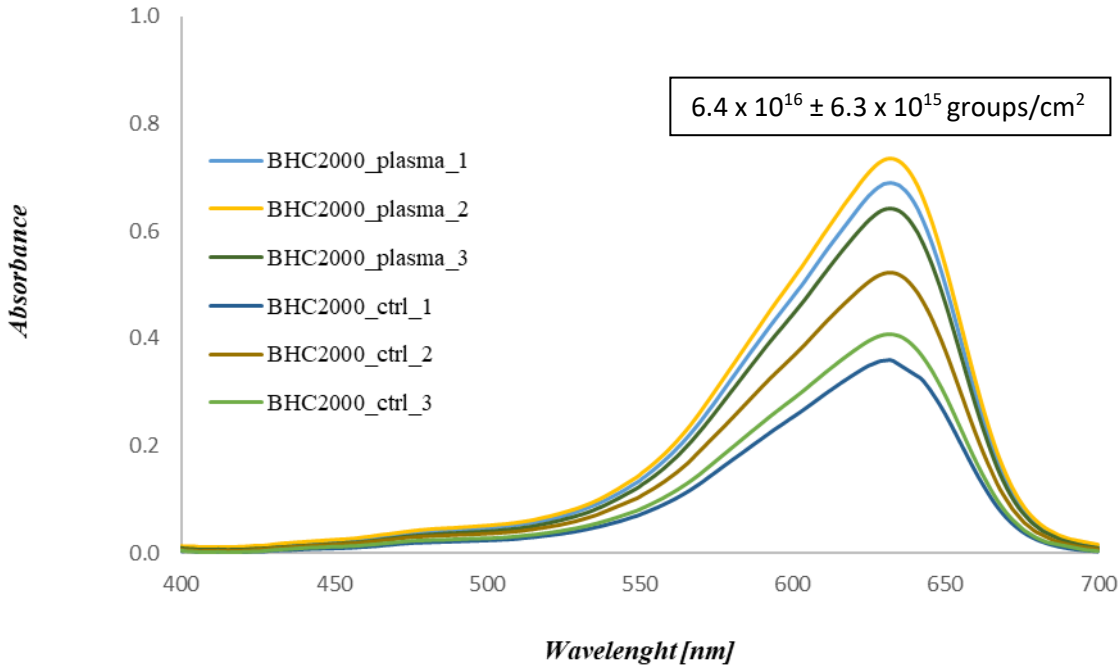

***Figure 51**: UV-Vis spectra obtained for BHC2000 after the TBO assay.*

Taking advantage of the previously constructed calibration line and the absorption values at 632 nm peak, the number of carboxylic acid groups present on the surface could be obtained (considering an area of 1 cm^2, given by the shape of our samples).

The untreated samples serve as control, since an important hydrophobic absorption of the TBO molecules on the surface could be observed also when the -COOH groups were not present. Indeed, when repeating the test, on many occasions absorbance values of the untreated samples resulted almost comparable to the treated ones.

Although this test cannot be considered completely reliable for the aforementioned reasons, by performing the assay several times an average value of 10^{16} -COOH groups/cm^2 could be determined. This value was used as reference in designing the following functionalizations.

5.3 Grafting of biomolecules

5.3.1 Benzylamine grafting

5.3.1.1 Benzylamine quantification

To indirectly evaluate the amount of BA grafted on the PU film surfaces, the incubation solutions were analyzed through UV-Vis spectroscopy, focusing on the peak around 260 nm. In addition, while quantifying the amount of grafted BA we aimed to indirectly quantify also the number of carboxylic acid groups exposed on the surface, taking into account that one molecule of BA reacts with one -COOH group. BA was selected as model molecule because of the presence in its structure of an aromatic ring, which presents a strong absorbance in the UV region and can be easily detected by ^{1}H NMR spectroscopy. **Figure 52** reports the results obtained for 3 plasma-treated BHC2000 samples grafted with BA through carbodiimide chemistry (indicated as BHC2000_PLASMA_BA_n) and three control samples which underwent the same incubation and washing procedures performed for chemically modified samples (indicated as BHC2000_BA_CTRL_n). As a comparison, the stock solution used to incubate the samples was also analyzed.

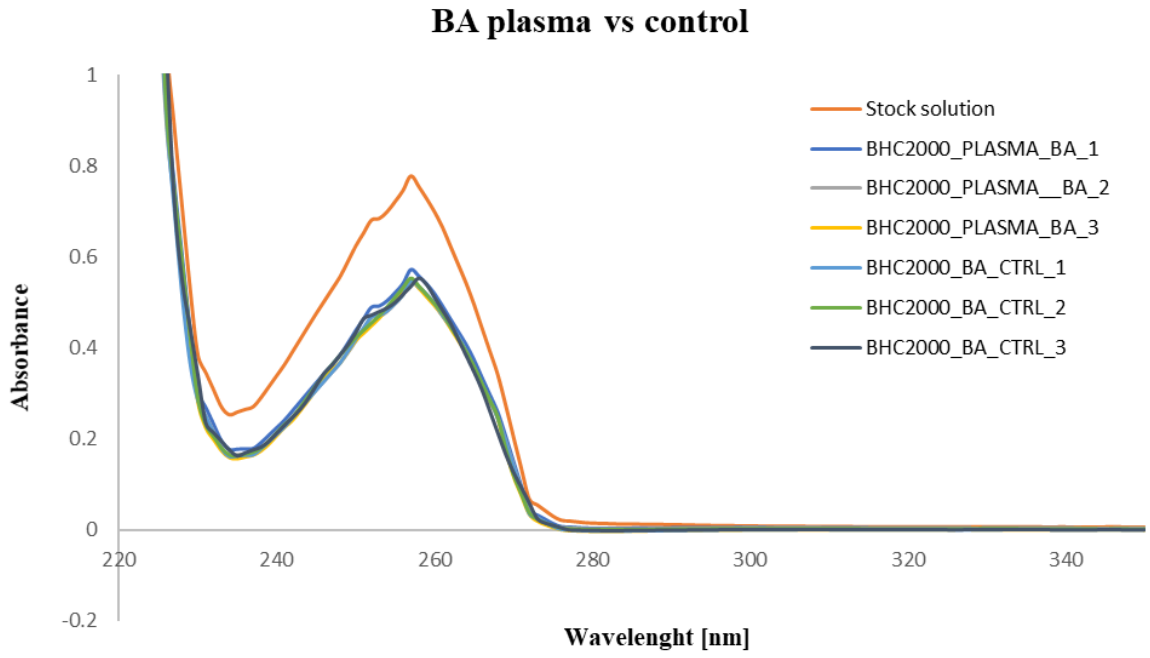

Figure 52: *Comparison in terms of UV-Vis registered spectra between plasma and control samples in contact with BA. The UV-Vis spectrum of the BA stock solution used to incubate the samples is also reported.*

Although a difference can be detected between the stock solution and the samples, absorbance trends from treated samples and controls were comparable. This suggests the occurrence of a relevant BA adsorption on the surface, which was also present in the control samples, thus not allowing the clear discrimination between chemically grafted and adsorbed BA molecules. For this reason, the contribution due to the adsorbed BA is so much higher than the grafted one that the latter component cannot be clearly resolved in the spectrum. This behavior can be due to strong hydrophobic interactions and hydrogen bonds occurring between the PU substrate and benzylamine molecules.

To decrease the effect of adsorption phenomena, a possible solution was to treat both the surfaces of the PU films used during the tests, instead of only one side as usually done for the other experiments. The aim was to improve the PU hydrophilicity on both sides, thus trying to modulate non-covalent interactions. However, also in this case no significant differences was observed, suggesting that complex interactions occur between the biomolecule and the PU, possibly through the formation of hydrogen bonds between the PU chains and the biomolecule in addition to hydrophobic interactions. For these reasons, it was concluded that this method cannot be considered reliable to indirectly quantify the carboxylic acid groups exposed through the plasma treatment.

5.3.1.2 Attenuated Total Reflectance Fourier Transform Infrared (ATR-FTIR) spectroscopy

The efficacy of BA grafting was investigated also by ATR-FTIR. The test was carried out on benzylamine as such (BA), BHC2000, plasma treated BHC2000 chemically grafted with BA (BHC2000_PLASMA_BA), BHC2000 treated with plasma (BHC2000_PLASMA), and an untreated sample that followed the same protocol explained in paragraph 4.4.1 (BHC2000_BA_CTRL). In **Figure 53**, the entire spectrum obtained for all the samples has been reported. In **Figure 54**, some parts have been magnified to better highlight the differences between the samples. The spectrum segment of interest was identified between 2000 and 600 nm, where the presence of peaks due to BA have a noticeable influence on the other samples.

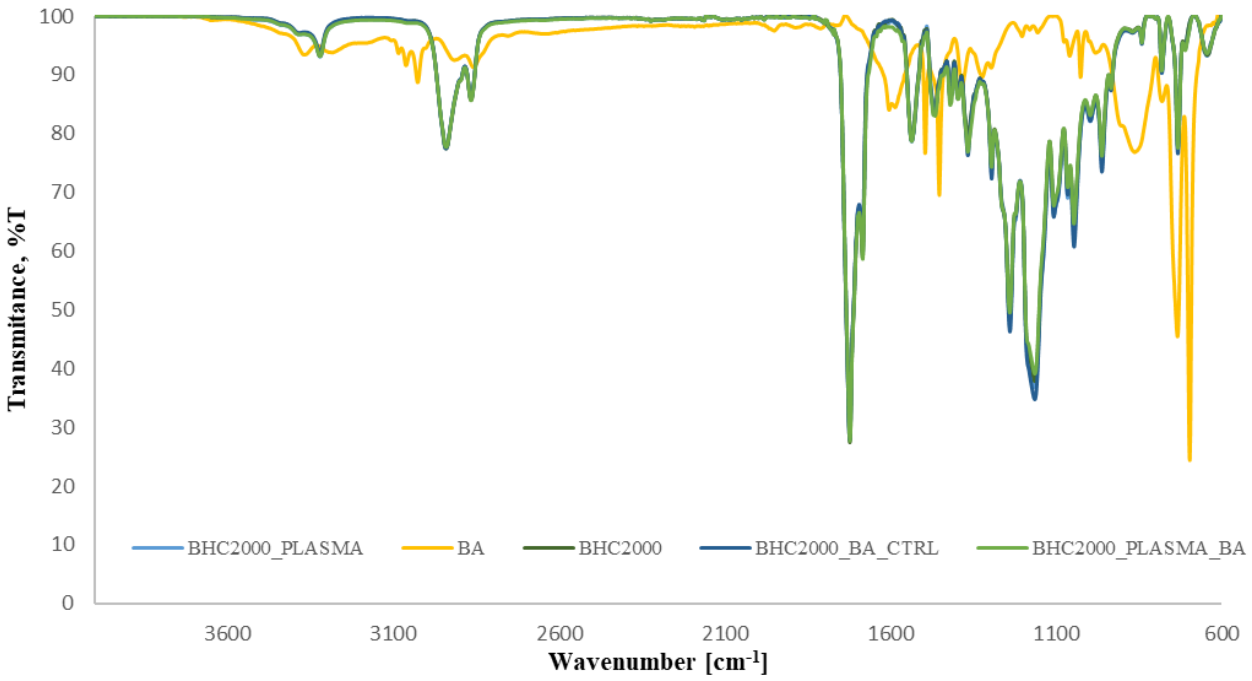

Figure 53: *ATR-FTIR spectra of BHC2000, benzylamine (BA), plasma treated BHC2000, pristine BHC2000 subjected to BA grafting procedure, and plasma treated BCH2000 chemically grafted with BA*

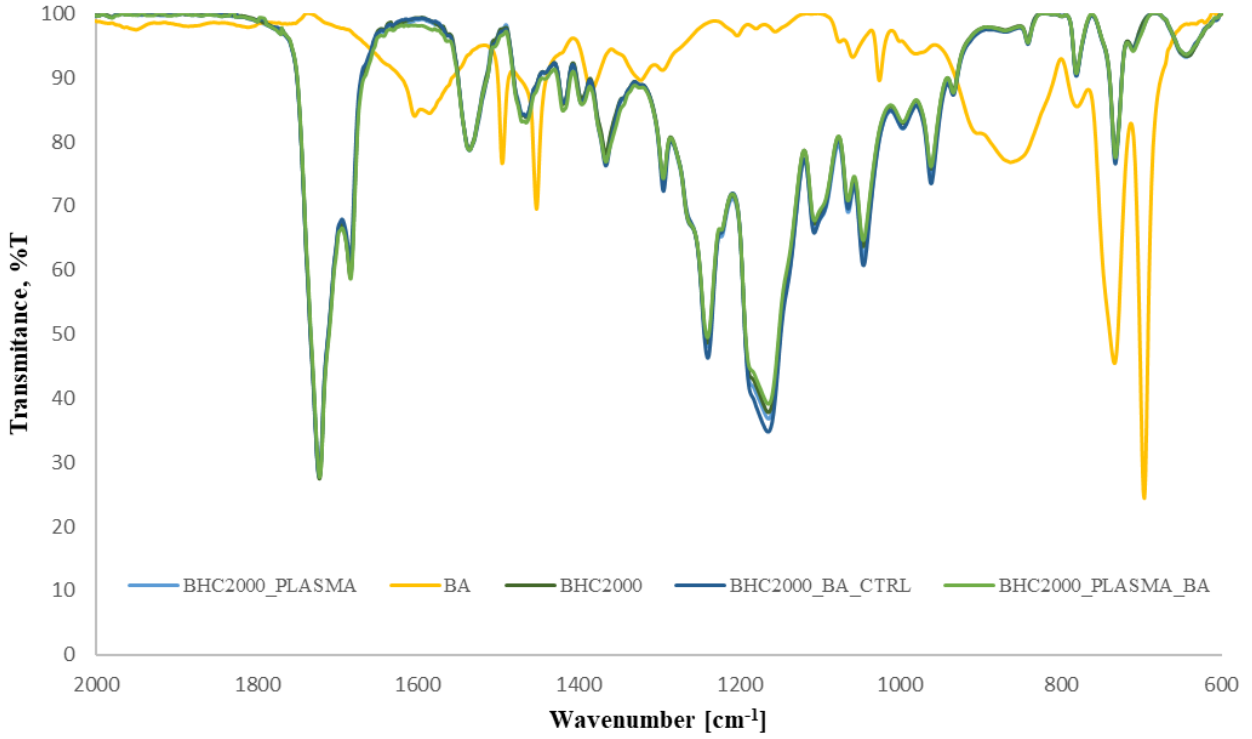

To better visualize the changes in the BHC2000 samples spectra, two other areas have been magnified: around 1600 nm (**Figure 55**) and around 1500 nm (**Figure 56**), which correspond to the main BA peaks that are not completely overlapped with the polyurethane signals. In **Figure 55**, a peak slightly more pronounced can be detected for BHC2000_PLASMA_BA, corresponding to the maximum absorption of benzylamine in that area. Similarly, in **Figure 56**, in correspondence to the BA absorption peaks at 1495 and 1452 nm, a change in the BHC2000_PLASMA_BA can also be noted. Conversely, all other samples did not show relevant differences from the starting control samples, suggesting that in this case it was possible to discriminate the effect of bonded BA from adsorbed one. However, this method is not quantitative; hence it was not possible to quantify the number of grafted BA molecules.

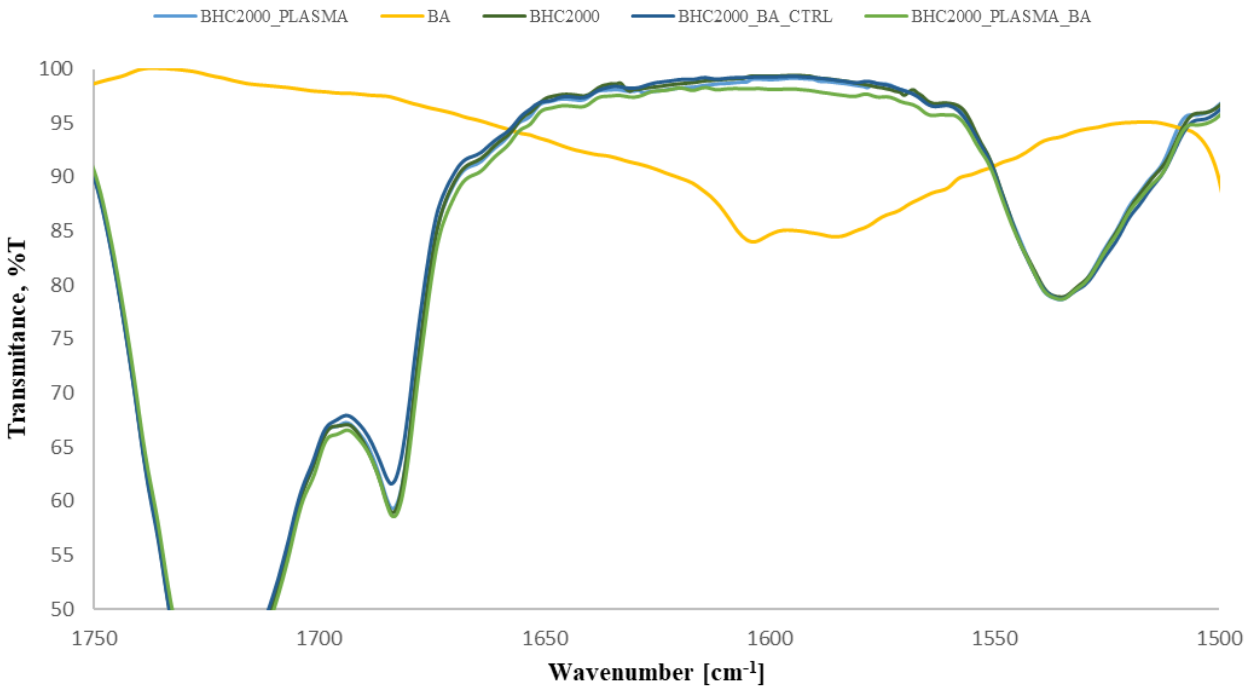

Figure 55: *ATR-FTIR magnification from 1750 nm to 1500 nm for BHC2000, benzylamine (BA), plasma treated BHC2000, pristine BHC2000 subjected to BA grafting procedure, and plasma treated BCH2000 chemically grafted with BA*

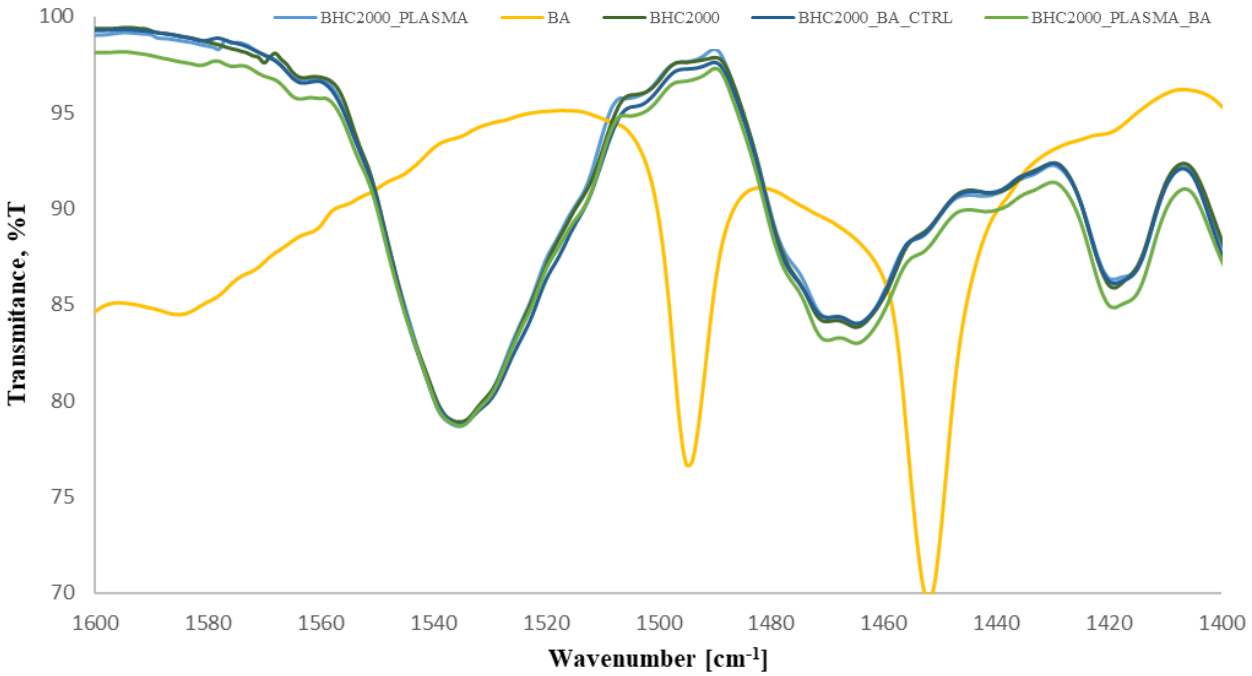

***Figure 56**: ATR-FTIR magnification from 1600 nm to 1400 nm for BHC2000, benzylamine (BA), plasma treated BHC2000, pristine BHC2000 subjected to BA grafting procedure, and plasma treated BCH2000 chemically grafted with BA*

5.3.1.3 Proton Nuclear Magnetic Resonance (^{1}H NMR) Spectroscopy

Finally, to quantify the carboxylic acid groups by mean of benzylamine (**Figure 57**) ^{1}H NMR spectroscopy was attempted, since as previously explained the aromatic ring is expected to be easily visible in the final spectra. **Figure 58** reports the ^{1}H NMR spectra of benzylamine (BA), plasma treated BHC2000 chemically grafted with BA (BHC2000_PLASMA_BA), plasma treated BHC2000 (BHC2000_PLASMA) and an untreated sample that followed the same protocol explained in paragraph 4.4.1.4 (BHC2000_BA_CTRL). As already evidenced by the ATR-FTIR analysis, no relevant difference can be seen between the treated and untreated samples.

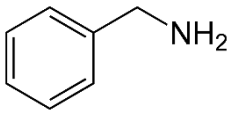

***Figure 57:** Benzylamine chemical structure*

The reference peaks from the BA spectrum can be found in the area between 7.5 and 7 ppm (red square, protons of the aromatic ring); between 2.0 and 1.5 ppm (blue square, proton signal of the terminal -NH_2 groups) and between 4.0 and 3.5 ppm (green square,

proton of the -CH_2 present between the aromatic ring and the terminal -NH_2). The peak at 2.5 ppm (yellow square) is due to the DMSO and used as reference.

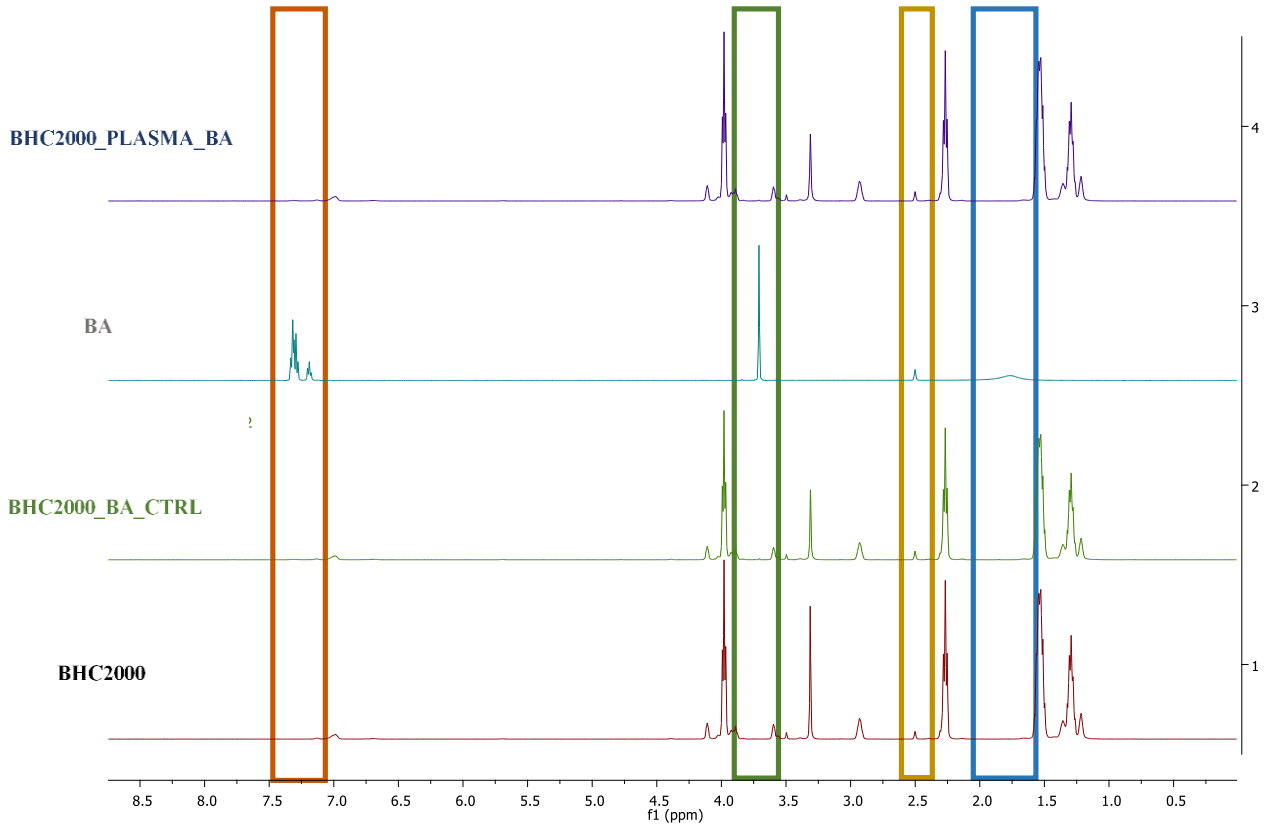

Figure 58: *Proton Nuclear Magnetic Resonance spectra of benzylamine (BA), plasma treated BHC2000 chemically grafted with BA (BHC2000_PLASMA_BA), plasma treated BHC2000 (BHC2000_PLASMA) and an untreated sample that followed the same protocol explained in paragraph 4.4.1.4 (BHC2000_BA_CTRL).*

This test aimed to identify a peak of integration to quantify BA, in a region where the starting material (BHC2000) did not interfere. In this way if in the treated materials a new peak appeared in this region, it means that the material possesses adsorbed or covalently bound BA. The most suitable peak to this aim appeared to be the one at 3.7 ppm (**Figure 59**), since the aromatic carbons resulted in multiple peaks and the -NH_2 proton signal was not visible in the PU samples. However, also in this case a prominent hydrophobic absorption effect could be detected, since no difference can be seen between the treated and untreated samples. Nevertheless, a shift in peak positioning was observed in BHC2000_PLASMA_BA spectrum compared to BA and BHC2000_BA_CTRL spectra, suggesting that chemically grafted BA in BHC2000_PLASMA_BA exhibited a different

chemical environment compared to adsorbed BA in BHC2000_BA_CTRL, which peak appeared at the same chemical shift as in pristine BA. This difference indirectly proved the successful chemical grafting of BA to plasmed treated BHC2000 surfaces. By integrating the peak at 3.7 ppm using the 2.5 ppm peak of DMSO as reference, a final number of 10^{18} BA molecules could be calculated for both kind of samples, probably due to the high tendency of BA due be adsorbed on PU film surfaces.

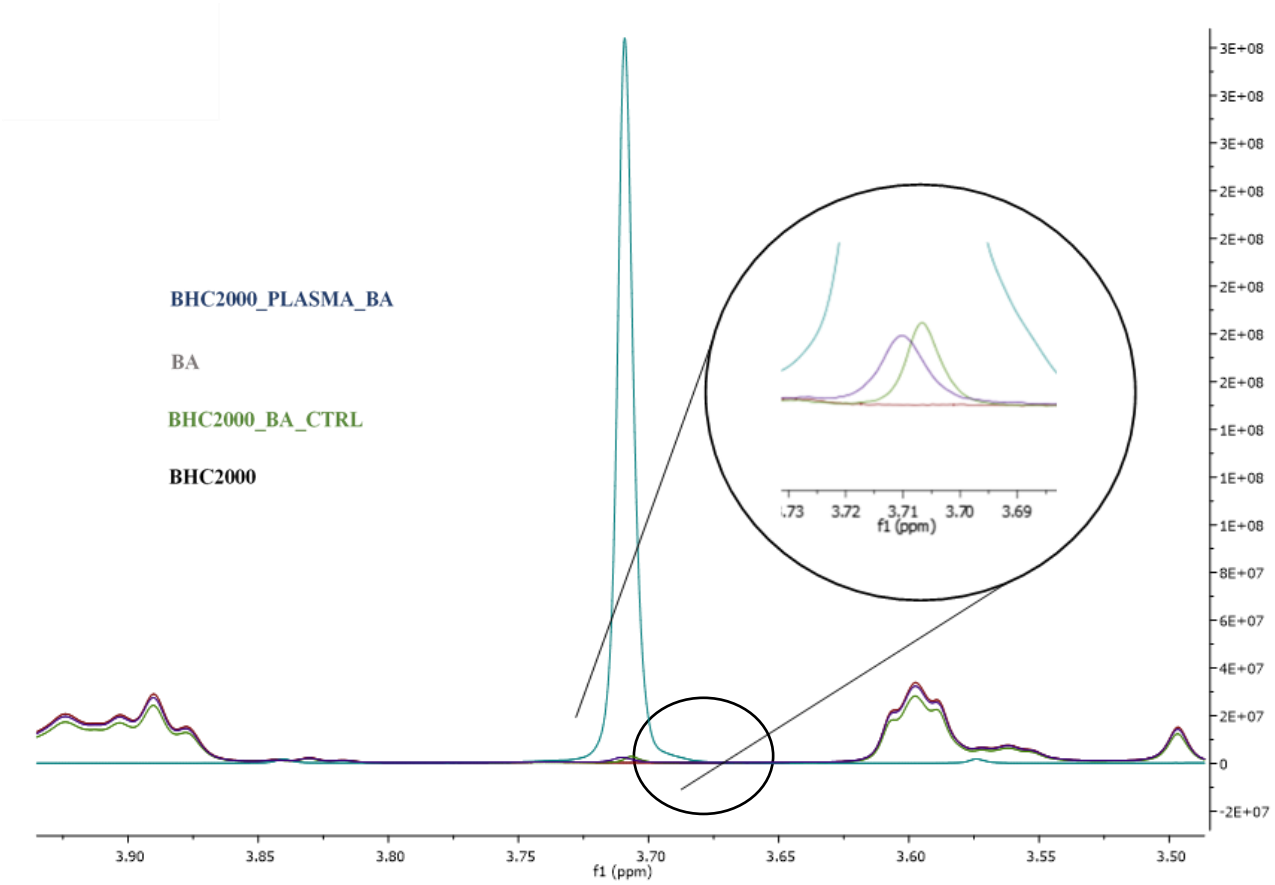

Figure 59: *Magnification of Proton Nuclear Magnetic Resonance spectra of BA, BHC2000_PLASMA_BA, BHC2000_PLASMA and BHC2000_BA_CTRL. around 3.7 ppm*

It can thus be concluded that benzylamine is not suitable as an indirect method to quantify the exposed -COOH groups for this particular polymeric family, due to the prevalence of non-covalent interaction between the hydrophobic molecule and polyurethane chains. However, from the analysis of IR and ^{1}H NMR spectra, it is possible to hypothesize that stronger covalent interactions actually form between the two reagents when carbodiimide chemistry is employed, but their effect is smaller compared to absorption and difficult to detect with standard techniques.

5.3.2 Gelatin grafting

To demonstrate the possibility to graft proteins on the functionalized PUs surfaces, gelatin was used as a proof of concept.

5.3.2.1 Attenuated Total Reflectance Fourier Transform Infrared (ATR-FTIR) spectroscopy

The samples analyzed were: Gelatin (Gel), plasma treated BHC2000 grafted with Gel (BHC2000_PLASMA_Gel), BHC2000 treated with plasma (BHC2000_PLASMA) and BHC2000 treated with plasma and subjected to the grafting procedure in the absence of EDC/NHS (BHC2000_Gel_CTRL). **Figures 60 A,B and C** refer to the three different gelatin concentrations used for the stock solution used during incubation, 0.1%, 0.25% and 0.5% w/v, respectively.

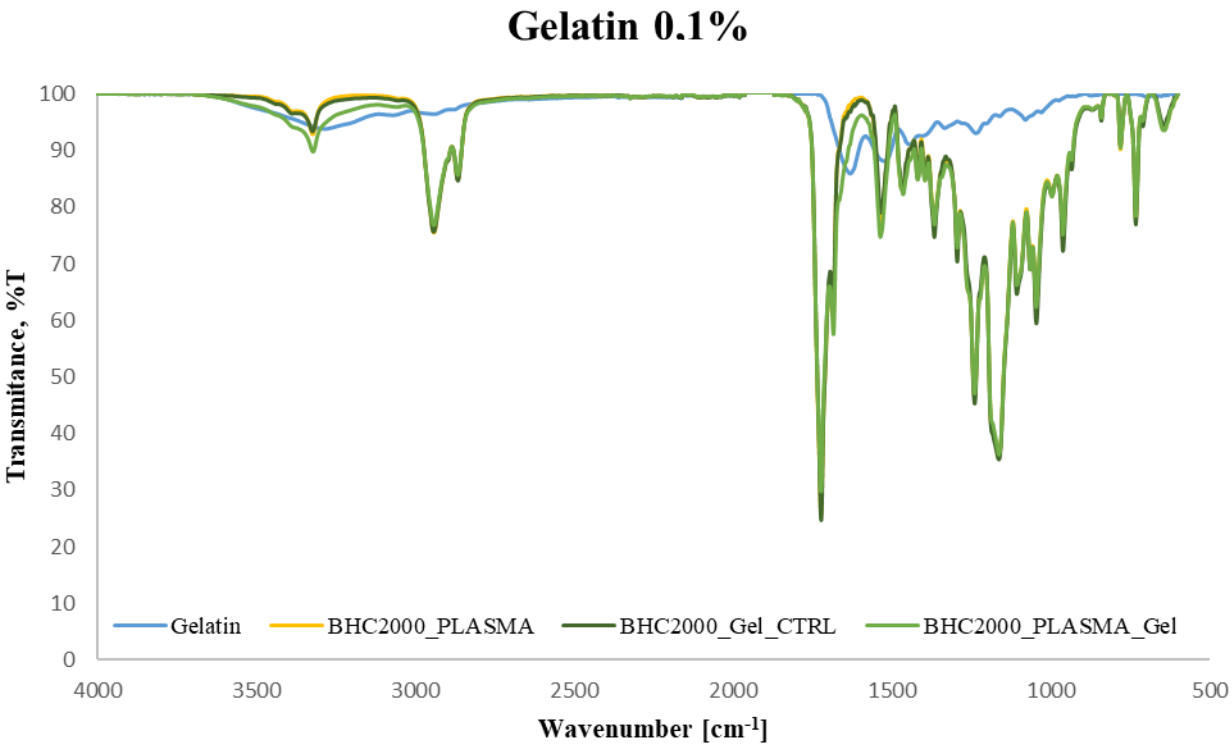

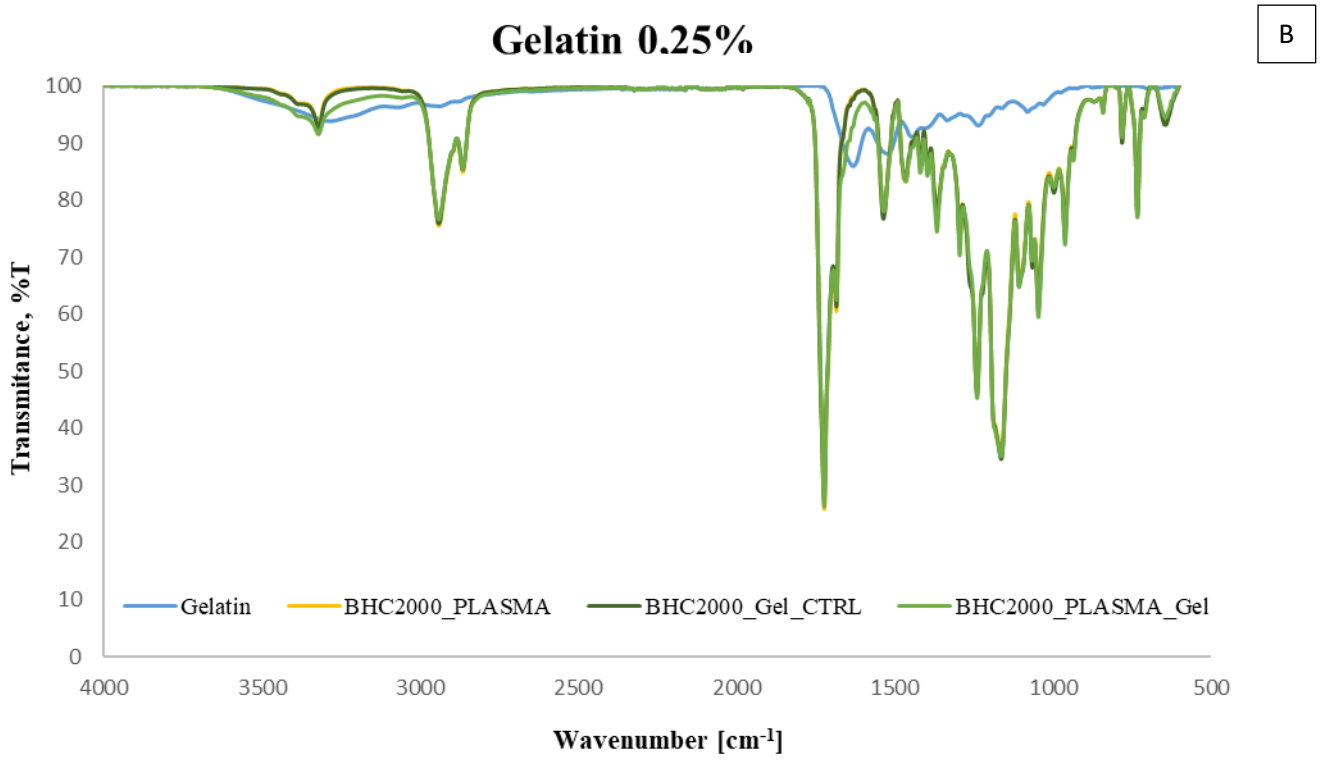

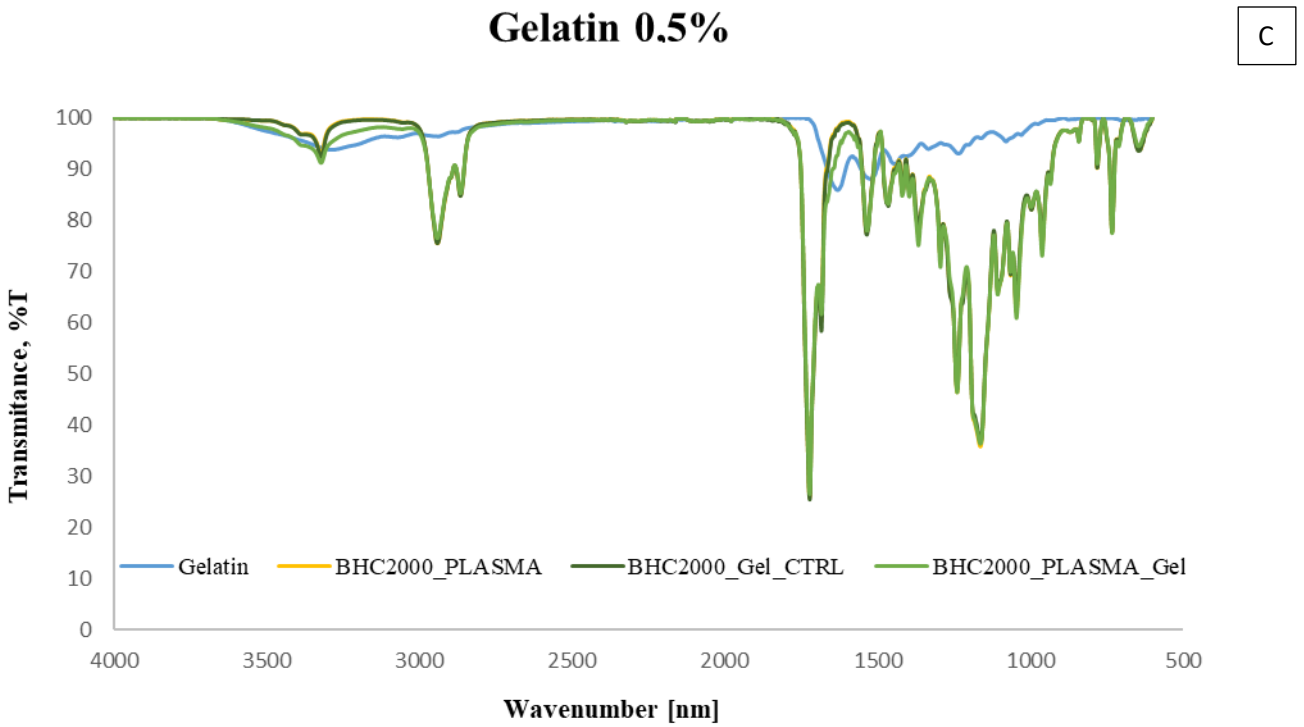

Figure 60: *ATR-FTIR spectra of Gelatin (Gel), plasma treated BHC2000 grafted with Gel (BHC2000_PLASMA_Gel), BHC2000 treated with plasma (BHC2000_PLASMA) and BHC2000 treated with plasma and subjected to the grafting procedure in the absence of EDC/NHS (BHC2000_Gel_CTRL).The grafting was conducted by incubating samples in gelatin solutions at different concentrations:* ***A****: 0,1%,* ***B****: 0,25% and* ***C****: 0,5% w/v*

The two main regions in which the gelatin spectrum differs from the PU one were comprised between 3000 and 3600 cm^{-1} (**Figure 61**) and around 1500 cm^{-1} (**Figure 62**).

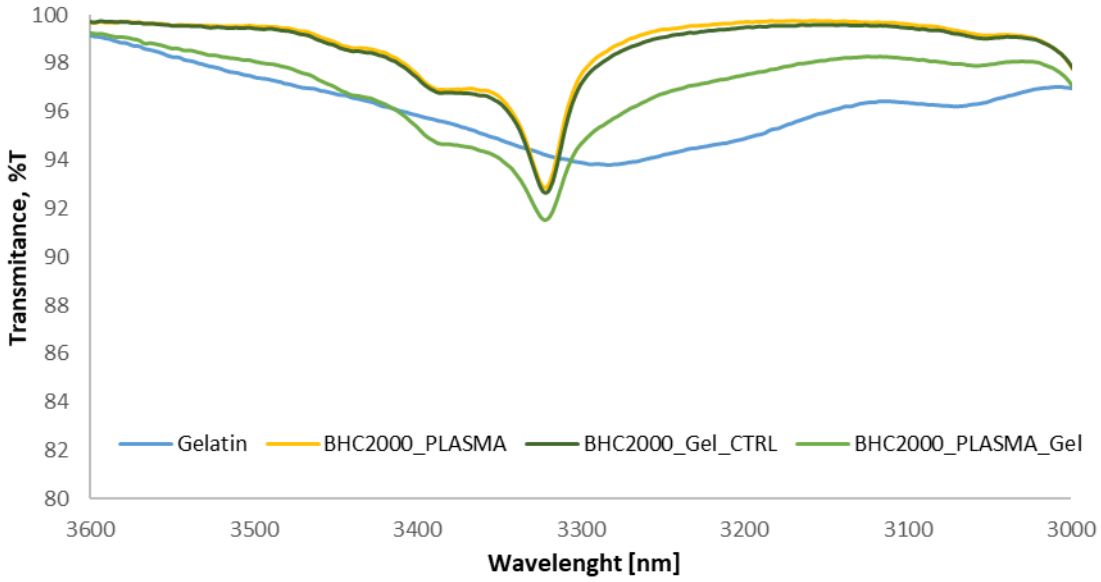

Figure 61: *Magnification from 3600 to 3000 cm^{-1} of ATR-FTIR spectra of Gel, BHC2000_PLASMA_Gel, BHC2000_PLASMA and BHC2000_Gel_CTRL.Gelatin concentration during grafting was fixed at 0.25% w/v*

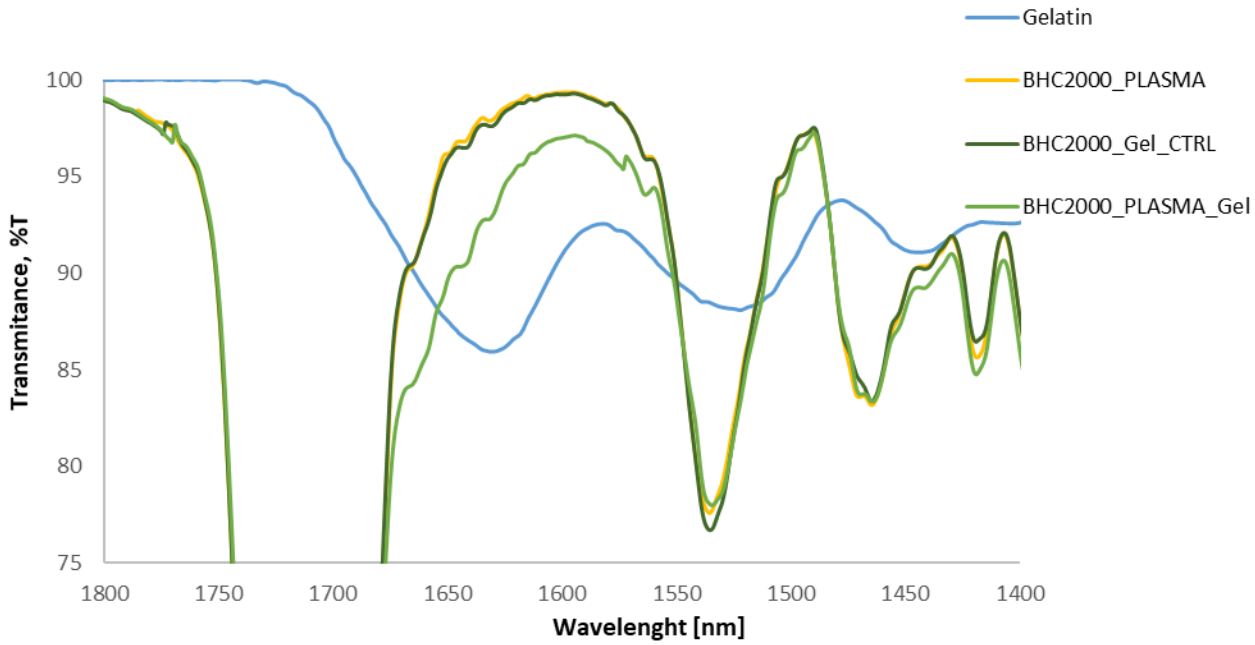

Figure 62: *Magnification from 18000 to 1400 cm^{-1} of ATR-FTIR spectra of Gel, BHC2000_PLASMA_Gel, BHC2000_PLASMA and BHC2000_Gel_CTRL.Gelatin concentration during grafting was fixed at 0.25% w/v*

In both cases, a change in the spectrum trend of the Gel grafted samples was observed, which was not detectable in the controls. This means that differently from BA, for gelatin absorption phenomena are not present in a relevant manner, which is coherent with the different nature of the protein (hydrophilic) and the substrate (hydrophobic). Indeed, by washing the samples with water after the grafting reaction, the adsorbed gelatin in this case was completely washed out and only the molecules covalently bonded to the -COOH groups exposed through plasma were still present. Moreover, no relevant changes were detected by changing the concentration of Gel in the stock solution, suggesting that a saturation effect was already reached with the lowest tested concentration (i.e., 0.1% w/v). However, since the change in the absorption was not directly proportional to the quantity of grafted molecules, this assumption should be verified with other quantitative methods.

5.3.2.2 Bicinchoninic acid assay (BCA)

To quantify the amount of gelatin grafted on the film surfaces, the bicinchoninic acid assay was used. The idea was to quantify the gelatin still present in the incubation solutions after the grafting phase, thus obtaining the amount of grafted protein by subtraction.

However, it was not possible to see any difference in the purple color of stock and incubation solutions after the test was performed and the absorbance measured at 562 nm did not vary even when the gelatin amount was changed. Since gelatin grafting was proved through ATR-FTIR spectroscopy, it can be hypothesized that the amount of gelatin actually grafted on the surface is too small compared to the initial one inserted. For this reason, due to the sensitivity of the test it was not possible to discriminate the differences between the two absorbance values.

To confirm the effective covalent grafting of gelatin to the PU surface, X-ray photoelectron spectroscopy (XPS) will be performed in the future. Moreover, the testing of cell cytocompatibility and viability upon seeding over functionalized surfaces would indirectly prove the successful surface functionalization, as the gelatin coating should improve cell behavior compared to pristine PU samples.

6. Conclusions and future developments

The use of biomaterials has become increasingly interesting in the last decades because it has allowed to overcome the inadequacy of traditional materials in addressing the complexity of therapeutic approaches typical of tissue engineering. Polymeric materials, in particular, are experiencing the greatest increase in use, thanks to their excellent mechanical properties, good biocompatibility and biodegradability.

In this work, new poly(ester urethane)s have been designed and characterized; their properties have then been studied and changes due to surface modification processes (i.e. plasma treatment) have been analyzed. The chemistry of carbodiimides has then been exploited to bind two model biomolecules (benzylamine and gelatin) with different properties to prove the feasibility of biofunctionalization.

Three poly (ester urethane)s, (PUs), have been synthetized using polycaprolactone diol (PCL), 1,6-diisocyanatoexane (HDI) and three different chain extenders, 1,4-butanediol, 1,8-octanediol, 1,12-dodecanediol. The obtained polymers have been named BHC2000, OHC2000 and DHC2000, respectively, and synthesis success has been confirmed by ATR-FTIR spectroscopy. Moreover, by size exclusion chromatography (SEC) an adequate degree of polymerization was observed for all the PUs, with a similar molecular weight distribution for the three materials (Mw 30-40 kDa, polydispersity index around 1,4).

Tensile tests were then carried out to observe any differences in the mechanical properties of the three PUs. The use of different chain extenders determined different mechanical behaviors, in particular regarding the ability to undergo a plastic deformation. Indeed, OHC2000 presented strain at break values reaching 36.9 ± 20.8% , significantly higher than the other two PUs, that present a more fragile behavior, though BHC2000 showed some deformation tendency when smaller sections formed after crack formation.

A thermal characterization of the samples was also carried out using Differential Scanning Calorimetry (DSC). All the PUs presented a prominent exothermic peak around 43-44°C due to the PCL soft phase; however, for OHC2000 and DHC2000 also less

pronounced peaks could be detected, due to crystalline phases that melt above 100°C. These observations were confirmed during the cooling cycle, where re-crystallization peaks of the hard phases are visible only for OHC2000 and DHC2000.

Degradation tests have also been performed to evaluate the resistance of the PUs in a simulated biological environment. Both hydrolytic (PBS) and enzymatic (0.5 mg/ml lipase solution) degradation conditions have been tested. After 8 weeks of incubation, weight loss and molecular weight distribution profile changes were small when only hydrolytic degradation was involved and comparable for all three PUs. On the other hand, enzymatic degradation had a significantly higher impact on BHC2000: samples lost approx. 90% of the initial weight after 8 weeks, while the other two PUs maintained about 70% of their weight.

By comparing the results of all the previously mentioned characterizations, it can be concluded that increasing the chain length of the chain extender used during the PU synthesis has an effect on the ability of the hard phase to crystallize. For this reason, BHC2000 behavior seems to be dominated by the PCL soft phase (no secondary peaks present on DSC thermograms and higher susceptibility to enzymatic degradation by lipase), while DHC2000 resulted a more fragile material, probably due to more developed hard phase crystalline structures.

The second part of this work concentrated on surface functionalization of the PUs, to improve hydrophilicity and allow biofunctionalization. The surface of the samples was treated with Ar plasma in presence of acrylic acid vapors to expose carboxylic groups. After demonstrating that the treatment did not damage the PUs through ATR-FTIR and SEC analysis, wettability measurements were carried out to verify the success of the treatment. The untreated samples showed an hydrophobic character, with contact angle values around 90°; however, after plasma treatment the contact angle values decreased of about 30-40%, thus demonstrating the presence of the more hydrophilic -COOH groups. Then, Toluidine Blue O (TBO) assay was carried out to try to quantify the number of functional groups present on the surface. However, even if an order of magnitude (10^{16} groups/cm^2) could be estimated, the test results were not consistent and showed poor repeatability, so this method could not be considered reliable for -COOH quantification on these materials.

The exposed carboxylic groups were then exploited to graft two molecules on the PUs surface, using carbodiimide chemistry. At first, benzylamine (BA) was used also to try to better quantify the -COOH groups thanks to the aromatic ring present in the molecule. However, both with UV-VIS and ^{1}H Nuclear Magnetic Resonance (NMR) spectroscopy it was not possible to discriminate the absorbed and covalently bonded BA on the different samples, probably due to strong hydrophobic interactions between the molecule and the PU surface. Only by ATR-FTIR a slight difference in transmittance could be detected. On the other hand, by grafting gelatin, a more hydrophilic molecule, more clear differences can be detected with ATR-FTIR spectroscopy, from which no absorbed but only grafted gelatin could be seen. An attempt was also made to indirectly quantify grafted gelatin using the bicinchoninic acid (BCA) assay, but the actual amount of grafted protein was probably too small for the sensitivity of the test.

Further tests are needed to better understand both the PUs characteristics and their surface functionalization. Regarding the PUs bulk characteristics, it could be useful to perform mechanical tests also in wet conditions, to better simulate a biological environment. Moreover, although thermal and mechanical tests already performed showed the suitability of these materials for Fused Deposition Modeling (FDM) applications, deeper analysis still need to be performed to better understand their behavior, for example Thermogravimetric Analysis (TGA) and rheological characterizations. To correlate the macroscopic characteristic observed with mechanical testing and DSC, microstructural analysis will also be carried out, in particular Atomic Force Spectroscopy (AFM) and Scanning Electron Microscopy (SEM). To confirm the effective covalent grafting of gelatin to the PU surface X-ray photoelectron spectroscopy (XPS) will be performed.

For the surface functionalization, it would instead be interesting to observe wettability changes after functionalization with the biomolecules, as a further proof of the success of the grafting; moreover, cytocompatibility tests are needed to demonstrate the efficacy of the coating in improving cell adhesion, viability and eventually proliferation on the functionalized PUs surfaces, in view of tissue engineering applications of these polymers.

7. Bibliography

1. Malafaya PB, Silva GA, Reis RL. Natural-origin polymers as carriers and scaffolds for biomolecules and cell delivery in tissue engineering applications. *Adv Drug Deliv Rev*. 2007;59(4-5):207-233. doi:10.1016/j.addr.2007.03.012

2. Langer R, Vacanti JP. Tissue engineering. *Science (80-)*. 1993;260(5110):920 LP - 926. doi:10.1126/science.8493529

3. Samadian H, Maleki H, Allahyari Z, Jaymand M. Natural polymers-based light-induced hydrogels: Promising biomaterials for biomedical applications. *Coord Chem Rev*. 2020;420. doi:10.1016/j.ccr.2020.213432

4. Dhandayuthapani B, Yoshida Y, Maekawa T, Kumar DS. Polymeric scaffolds in tissue engineering application: A review. *Int J Polym Sci*. 2011;2011(ii). doi:10.1155/2011/290602

5. Geyer R, Jambeck JR, Law KL. Production, use, and fate of all plastics ever made. *Sci Adv*. 2017;3(7):25-29. doi:10.1126/sciadv.1700782

6. Global plastics industry growing 4-5 percent annually. https://www.plasticsnews.com/article/20190501/NEWS/190509992/global-plastics-industry-growing-4-5-percent-annually#:~%7B%7D:text=Theglobalplasticsandrubber,withtheAsia-Pacificregion

7. Khan A, Ahmed N, Rabnawaz M. Covalent adaptable network and self-healingmaterials: Current trends and future prospectsin sustainability. *Polymers (Basel)*. 2020;12(9). doi:10.3390/POLYM12092027

8. Danso D, Chow J, Streita WR. Plastics: Environmental and biotechnological perspectives on microbial degradation. *Appl Environ Microbiol*. 2019;85(19):1-14. doi:10.1128/AEM.01095-19

9. Biomaterials Market Size, Share & Trends Analysis Report By Product (Natural, Metallic, Polymer), By Application (Cardiovascular, Orthopedics, Plastic Surgery), By Region, And Segment Forecasts, 2020 - 2027. https://www.grandviewresearch.com/industry-analysis/biomaterials-industry

10. Polymeric Biomaterials Market - Growth, Trends, COVID-19 Impact, and Forecasts (2021 - 2026). https://www.mordorintelligence.com/industry-reports/polymeric-biomaterials-market

11. Yadav S, Gangwar S. An Overview on Recent progresses and future perspective of biomaterials. *IOP Conf Ser Mater Sci Eng*. 2018;404(1). doi:10.1088/1757-899X/404/1/012013

12. Cook AD, Hrkach JS, Gao NN, et al. Characterization and development of RGD-peptide-modified poly(lactic acid-co-lysine) as an interactive, resorbable biomaterial. *J Biomed Mater Res*. 1997;35(4):513-523. doi:10.1002/(SICI)1097-4636(19970615)35:4<513::AID-JBM11>3.0.CO;2-C

13. Massoumi B, Hatamzadeh M, Firouzi N, Jaymand M. Electrically conductive nanofibrous scaffold composed of poly(ethylene glycol)-modified polypyrrole and poly(ε-caprolactone) for tissue engineering applications. *Mater Sci Eng C*. 2019;98:300-310. doi:https://doi.org/10.1016/j.msec.2018.12.114

14. Abbasian M, Massoumi B, Mohammad-Rezaei R, Samadian H, Jaymand M. Scaffolding polymeric biomaterials: Are naturally occurring biological macromolecules more appropriate for tissue engineering? *Int J Biol Macromol*. 2019;134:673-694. doi:https://doi.org/10.1016/j.ijbiomac.2019.04.197

15. Armentano I, Dottori M, Fortunati E, Mattioli S, Kenny JM. Biodegradable polymer matrix nanocomposites for tissue engineering: A review. *Polym Degrad Stab*. 2010;95(11):2126-2146. doi:https://doi.org/10.1016/j.polymdegradstab.2010.06.007

16. Bonani W, Singhatanadgige W, Pornanong A, Motta A. Natural Origin Materials for Osteochondral Tissue Engineering BT - Osteochondral Tissue Engineering: Nanotechnology, Scaffolding-Related Developments and Translation. In: Oliveira JM, Pina S, Reis RL, San Roman J, eds. Springer International Publishing; 2018:3-30. doi:10.1007/978-3-319-76711-6_1

17. Ullah S, Chen X. Fabrication, applications and challenges of natural biomaterials in tissue engineering. *Appl Mater Today*. 2020;20. doi:10.1016/j.apmt.2020.100656

18. Wasyłeczko M, Sikorska W, Chwojnowski A. Review of synthetic and hybrid

scaffolds in cartilage tissue engineering. *Membranes (Basel)*. 2020;10(11):1-28. doi:10.3390/membranes10110348

19. Abbasian M, Massoumi B, Mohammad-Rezaei R, Samadian H, Jaymand M. Scaffolding polymeric biomaterials: Are naturally occurring biological macromolecules more appropriate for tissue engineering? *Int J Biol Macromol*. 2019;134:673-694. doi:10.1016/j.ijbiomac.2019.04.197

20. Chocholata P, Kulda V, Babuska V. Fabrication of Scaffolds for Bone-Tissue Regeneration. *Materials (Basel)*. 2019;12(4):568. doi:10.3390/ma12040568

21. Zhang J, Feng Y, Zhou X, Shi Y, Wang L. Research status of artificial bone materials. *Int J Polym Mater Polym Biomater*. 2021;70(1):37-53. doi:10.1080/00914037.2019.1685518

22. Irvine SA, Venkatraman SS. Bioprinting and differentiation of stem cells. *Molecules*. 2016;21(9). doi:10.3390/molecules21091188

23. Zhang R. 3D Printing, Filament Winding Forming and Performance Analysis of Skeleton Biological Scaffold. Published online 2016.

24. Long L yu, Wu C, Hu X feng, Wang Y bing. Biodegradable synthetic polymeric composite scaffold-based tissue engineered heart valve with minimally invasive transcatheter implantation. *Polym Adv Technol*. 2020;31(11):2422-2432. doi:10.1002/pat.5012

25. Eltom A, Zhong G, Muhammad A. Scaffold Techniques and Designs in Tissue Engineering Functions and Purposes: A Review. Dong M, ed. *Adv Mater Sci Eng*. 2019;2019:3429527. doi:10.1155/2019/3429527

26. Irawan V, Sung T-C, Higuchi A, Ikoma T. Collagen Scaffolds in Cartilage Tissue Engineering and Relevant Approaches for Future Development. *Tissue Eng Regen Med*. 2018;15(6):673-697. doi:10.1007/s13770-018-0135-9

27. Jiang L, Xu L, Ma B, et al. Effect of component and surface structure on poly(l-lactide-co-ε- caprolactone) (PLCA)-based composite membrane. *Compos Part B Eng*. 2019;174:107031. doi:https://doi.org/10.1016/j.compositesb.2019.107031

28. Katti DS, Lakshmi S, Langer R, Laurencin CT. Toxicity, biodegradation and elimination of polyanhydrides. *Adv Drug Deliv Rev*. 2002;54(7):933-961.

doi:10.1016/s0169-409x(02)00052-2

29. Nair LS, Laurencin CT. Biodegradable polymers as biomaterials. *Prog Polym Sci*. 2007;32(8-9):762-798. doi:10.1016/j.progpolymsci.2007.05.017

30. Guvendiren M, Burdick JA. Engineering synthetic hydrogel microenvironments to instruct stem cells. *Curr Opin Biotechnol*. 2013;24(5):841-846. doi:https://doi.org/10.1016/j.copbio.2013.03.009

31. Bedell ML, Navara AM, Du Y, Zhang S, Mikos AG. Polymeric Systems for Bioprinting. *Chem Rev*. 2020;120(19):10744-10792. doi:10.1021/acs.chemrev.9b00834

32. Panadero JA, Lanceros-Mendez S, Ribelles JLG. Differentiation of mesenchymal stem cells for cartilage tissue engineering: Individual and synergetic effects of three-dimensional environment and mechanical loading. *Acta Biomater*. 2016;33:1-12. doi:https://doi.org/10.1016/j.actbio.2016.01.037

33. Setayeshmehr M, Esfandiari E, Rafieinia M, et al. Hybrid and composite scaffolds based on extracellular matrices for cartilage tissue engineering. *Tissue Eng - Part B Rev*. 2019;25(3):202-224. doi:10.1089/ten.teb.2018.0245

34. Roam JL, Yan Y, Nguyen PK, et al. A modular, plasmin-sensitive, clickable poly(ethylene glycol)-heparin-laminin microsphere system for establishing growth factor gradients in nerve guidance conduits. *Biomaterials*. 2015;72:112-124. doi:https://doi.org/10.1016/j.biomaterials.2015.08.054

35. Annabi N, Fathi A, Mithieux SM, Martens P, Weiss AS, Dehghani F. The effect of elastin on chondrocyte adhesion and proliferation on poly (ε-caprolactone)/elastin composites. *Biomaterials*. 2011;32(6):1517-1525. doi:https://doi.org/10.1016/j.biomaterials.2010.10.024

36. Medvedeva E, Grebenik E, Gornostaeva S, et al. Repair of Damaged Articular Cartilage: Current Approaches and Future Directions. *Int J Mol Sci*. 2018;19(8):2366. doi:10.3390/ijms19082366

37. Polymers Termination. https://en.wikipedia.org/wiki/Radical_polymerization#Termination

38. Basic Polymer Structure. https://www.e-education.psu.edu/matse81/node/2210

39. Polymers: an overview. https://www.essentialchemicalindustry.org/polymers/polymers-an-overview.html

40. Brannigan RP, Dove AP. Synthesis, properties and biomedical applications of hydrolytically degradable materials based on aliphatic polyesters and polycarbonates. *Biomater Sci*. 2017;5(1):9-21. doi:10.1039/c6bm00584e

41. Mogosanu D, Giol E, Vandenhaute M, Dragusin D, Samal SK, Dubruel P. CHAPTER 6. 2021;1(2014):155-197.

42. Zhang C. Biodegradable Polyesters: Synthesis, Properties, Applications. *Biodegrad Polyesters*. Published online 2015:1-24. doi:10.1002/9783527656950.ch1

43. Woodruff MA, Hutmacher DW. The return of a forgotten polymer—Polycaprolactone in the 21st century. *Prog Polym Sci*. 2010;35(10):1217-1256. doi:https://doi.org/10.1016/j.progpolymsci.2010.04.002

44. Christen MO, Vercesi F. Polycaprolactone: How a well-known and futuristic polymer has become an innovative collagen-stimulator in esthetics. *Clin Cosmet Investig Dermatol*. 2020;13:31-48. doi:10.2147/CCID.S229054

45. Kricheldorf HR, Berl M, Scharnagl N. Poly(lactones). 9. Polymerization mechanism of metal alkoxide initiated polymerizations of lactide and various lactones. *Macromolecules*. 1988;21(2):286-293. doi:10.1021/ma00180a002

46. Limwanich W, Meepowpan P, Nalampang K, Kungwan N, Molloy R, Punyodom W. Kinetics and thermodynamics analysis for ring-opening polymerization of ε-caprolactone initiated by tributyltin n-butoxide using differential scanning calorimetry. *J Therm Anal Calorim*. 2015;119(1):567-579. doi:10.1007/s10973-014-4111-x

47. Labet M, Thielemans W. Synthesis of polycaprolactone: a review. *Chem Soc Rev*. 2009;38(12):3484-3504. doi:10.1039/B820162P

48. Chang H-M, Prasannan A, Tsai H-C, Jhu J-J. Ex vivo evaluation of biodegradable poly(ε-caprolactone) films in digestive fluids. *Appl Surf Sci*. 2014;313:828-833. doi:https://doi.org/10.1016/j.apsusc.2014.06.082

49. Mohamed RM, Yusoh K. A Review on the Recent Research of Polycaprolactone

(PCL). *Adv Mater Res*. 2016;1134:249-255. doi:10.4028/www.scientific.net/AMR.1134.249

50. Delgado-Aguilar M, Puig R, Sazdovski I, Fullana-i-Palmer P. Polylactic acid/polycaprolactone blends: On the path to circular economy, substituting single-use commodity plastic products. *Materials (Basel)*. 2020;13(11):1-18. doi:10.3390/ma13112655

51. Zhang L, Xiong C, Deng X. Biodegradable polyester blends for biomedical application. *J Appl Polym Sci*. 1995;56(1):103-112. doi:https://doi.org/10.1002/app.1995.070560114

52. Mandal P, Shunmugam R. Polycaprolactone: a biodegradable polymer with its application in the field of self-assembly study. *J Macromol Sci Part A Pure Appl Chem*. 2020;0(0):1-19. doi:10.1080/10601325.2020.1831392

53. Ali SAM, Zhong S-P, Doherty PJ, Williams DF. Mechanisms of polymer degradation in implantable devices: I. Poly(caprolactone). *Biomaterials*. 1993;14(9):648-656. doi:https://doi.org/10.1016/0142-9612(93)90063-8

54. Shih C. Chain-end scission in acid catalyzed hydrolysis of poly (d,l-lactide) in solution. *J Control Release*. 1995;34(1):9-15. doi:https://doi.org/10.1016/0168-3659(94)00100-9

55. Bartnikowski M, Dargaville TR, Hutmacher DW. Progress in Polymer Science Degradation mechanisms of polycaprolactone in the context of chemistry , geometry and environment. 2019;96:1-20. doi:10.1016/j.progpolymsci.2019.05.004

56. Borkar T, Goenka V, Jaiswal AK. Application of poly-ε-caprolactone in extrusion-based bioprinting. *Bioprinting*. 2021;21(November 2020):e00111. doi:10.1016/j.bprint.2020.e00111

57. Malikmammadov E, Tanir TE, Kiziltay A, Hasirci V, Hasirci N. PCL and PCL-based materials in biomedical applications. *J Biomater Sci Polym Ed*. 2018;29(7-9):863-893. doi:10.1080/09205063.2017.1394711

58. Valčić MD, Cakić SM, Ristić IS, Cakić JD, Cvetinov MJ, János CJ. Polycaprolactone-based biodegradable acrylated polyurethanes: Influence of

nanosilica amount on functional properties. *Int J Adhes Adhes*. 2021;104. doi:10.1016/j.ijadhadh.2020.102738

59. Sartori S, Boffito M, Serafini P, et al. Synthesis and structure-property relationship of polyester-urethanes and their evaluation for the regeneration of contractile tissues. *React Funct Polym*. 2013;73(10):1366-1376. doi:10.1016/j.reactfunctpolym.2013.01.006

60. Vermette P, Griesser HJ, Laroche G, Guidoin R. Biomedical applications of polyurethanes. *Tiss Eng Intellig Unit*. Published online January 1, 2001.

61. Guelcher SA. Biodegradable Polyurethanes: Synthesis and Applications in Regenerative Medicine. *Tissue Eng Part B Rev*. 2008;14(1):3-17. doi:10.1089/teb.2007.0133

62. Howard GT. Biodegradation of polyurethane: A review. *Int Biodeterior Biodegrad*. 2002;49(4):245-252. doi:10.1016/S0964-8305(02)00051-3

63. Lamba NMK, Woodhouse KA, Cooper SL. *Polyurethanes in Biomedical Applications*. 1st ed. Bosa Roca: CRC Press; 1998. doi:10.1201/9780203742785

64. Naureen B, Haseeb ASMA, Basirun WJ, Muhamad F. Recent advances in tissue engineering scaffolds based on polyurethane and modified polyurethane. *Mater Sci Eng C*. 2021;118(February 2020):111228. doi:10.1016/j.msec.2020.111228

65. Pistillo BR, Detomaso L, Sardella E, Favia P, d'Agostino R. RF-plasma deposition and surface characterization of stable (COOH)-rich thin films from cyclic L-lactide. *Plasma Process Polym*. 2007;4(SUPPL.1):817-820. doi:10.1002/ppap.200731912

66. Szycher M. Basic Concepts in Polyurethane Chemistry and Technology. *Szychers Handb Polyurethanes, Second Ed*. 2012;(2012):13-36.

67. Szycher M. Isocyanate chemistry. *Szychers Handb Polyurethanes, Second Ed*. 2012;(2012):87-133. doi:10.1201/b12343

68. Gunatillake PA, Adhikari R. Biodegradable synthetic polymers for tissue engineering. *Eur Cell Mater*. 2003;5:1-16.

69. Grivet Brancot A. Novel thermo-sensitive and photo-curable hydrogels as

potential bioinks in regenerative medicine. 2017;(December).

70. Szycher M. 5. Polyols. 2021;(2012):135-154.

71. Fink JK. Chapter 2 - Poly(urethane)s. In: Fink JKBT-RPF and A (Second E, ed. *Plastics Design Library*. William Andrew Publishing; 2013:49-93. doi:https://doi.org/10.1016/B978-1-4557-3149-7.00002-4

72. Szycher M. Chain extenders. *Szychers Handb Polyurethanes, Second Ed*. 2012;(2012):155-180. doi:10.1201/b12343

73. Ryszkowska J, Waśniewski B. Quantitative description of the morphology of polyurethane nanocomposites for medical applications. *WIT Trans Eng Sci*. 2011;72:377-386. doi:10.2495/MC110331

74. Samarth N, Kamble V, Rane A V, Abitha VK, Gohatre O, Kanny K. Chapter 16 - Mechanical and Dynamic Mechanical Properties of Polyurethane Blends and Interpenetrating Polymer Networks. Published online 2017:377-397. doi:10.1016/B978-0-12-804039-3.00016-6

75. Szycher M. Structure–Property Relations in Polyurethanes. *Szychers Handb Polyurethanes, Second Ed*. 2012;(2012):41-85.

76. Marois Y GR. Biocompatibility of Polyurethanes. *Madame Curie Biosci Database [Internet]; Austin Landes Biosci 2000-2013*.

77. Spilezewski KL, Anderson JM, Schaap RN, Solomon DD. In vivo biocompatibility of catheter materials. *Biomaterials*. 1988;9(3):253-256. doi:10.1016/0142-9612(88)90093-2

78. Lee PC, Huang LL, Chen LW, Hsieh KH, Tsai CL. Effect of forms of collagen linked to polyurethane on endothelial cell growth. *J Biomed Mater Res*. 1996;32(4):645-653. doi:10.1002/(SICI)1097-4636(199612)32:4<645::AID-JBM18>3.0.CO;2-C

79. Noishiki Y. Application of immunoperoxidase method to electron microscopic observation of plasma protein on polymer surface. *J Biomed Mater Res*. 1982;16(4):359-367. doi:10.1002/jbm.820160405

80. Horbett TA, Weathersby PK. Adsorption of proteins from plasma to a series of

hydrophilic-hydrophobic copolymers. I. Analysis with the in situ radioiodination technique. *J Biomed Mater Res*. 1981;15(3):403-423. doi:10.1002/jbm.820150311

81. Baumgartner JN, Cooper SL. Influence of thrombus components in mediating Staphylococcus aureus adhesion to polyurethane surfaces. *J Biomed Mater Res*. 1998;40(4):660-670. doi:10.1002/(sici)1097-4636(19980615)40:4<660::aid-jbm18>3.0.co;2-j

82. Ishihara K, Shibata N, Tanaka S, Iwasaki Y, Kurosaki T, Nakabayashi N. Improved blood compatibility of segmented polyurethane by polymeric additives having phospholipid polar group. II. Dispersion state of the polymeric additive and protein adsorption on the surface. *J Biomed Mater Res*. 1996;32(3):401-408. doi:10.1002/(SICI)1097-4636(199611)32:3<401::AID-JBM13>3.0.CO;2-J

83. Juan V. Cauich-Rodríguez, Lerma H. Chan-Chan FH-S and JMC-U. Degradation of Polyurethanes for Cardiovascular Applications. doi:10.5772/53681

84. Fromstein JD, Woodhouse KA. Elastomeric biodegradable polyurethane blends for soft tissue applications. *J Biomater Sci Polym Ed*. 2002;13(4):391-406. doi:10.1163/156856202320253929

85. Guelcher SA, Srinivasan A, Dumas JE, Didier JE, McBride S, Hollinger JO. Synthesis, mechanical properties, biocompatibility, and biodegradation of polyurethane networks from lysine polyisocyanates. *Biomaterials*. 2008;29(12):1762-1775. doi:https://doi.org/10.1016/j.biomaterials.2007.12.046

86. Guelcher S, Srinivasan A, Hafeman A, et al. Synthesis, in vitro degradation, and mechanical properties of two-component poly (ester urethane)urea scaffolds: Effects of water and polyol composition. *Tissue Eng*. 2007;13(9):2321-2333. doi:10.1089/ten.2006.0395

87. Wang W, Jin Y, Ping P, Chen X, Jing X, Su Z. Structure evolution in segmented poly(ester urethane) in shape-memory process. *Macromolecules*. 2010;43(6):2942-2947. doi:10.1021/ma902781e

88. Żółtowska K, Piotrowska U, Oledzka E, Kuras M, Zgadzaj A, Sobczak M. Biodegradable Poly(ester-urethane) Carriers Exhibiting Controlled Release of Epirubicin. *Pharm Res*. 2017;34(4):780-792. doi:10.1007/s11095-017-2105-7

89. Camarero-Espinosa S, Calore A, Wilbers A, Harings J, Moroni L. Additive manufacturing of an elastic poly(ester)urethane for cartilage tissue engineering. *Acta Biomater*. 2020;102:192-204. doi:10.1016/j.actbio.2019.11.041

90. Chiono V, Sartori S, Rechichi A, et al. Poly(ester urethane) guides for peripheral nerve regeneration. *Macromol Biosci*. 2011;11(2):245-256. doi:10.1002/mabi.201000354

91. Takahara A, Coury AJ, Hergenrother RW, Cooper SL. Effect of soft segment chemistry on the biostability of segmented polyurethanes. I. In vitro oxidation. *J Biomed Mater Res*. 1991;25(3):341-356. doi:10.1002/jbm.820250306

92. Kylmä J, Seppälä J V. Synthesis and characterization of a biodegradable thermoplastic poly (ester− urethane) elastomer. *Macromolecules*. 1997;30(10):2876-2882.

93. Guan J, Sacks MS, Beckman EJ, Wagner WR. Synthesis, characterization, and cytocompatibility of elastomeric, biodegradable poly(ester-urethane)ureas based on poly(caprolactone) and putrescine. *J Biomed Mater Res*. 2002;61(3):493-503. doi:https://doi.org/10.1002/jbm.10204

94. Saad B, Hirt TD, Welti M, Uhlschmid GK, Neuenschwander P, Suter UW. Development of degradable polyesterurethanes for medical applications: in vitro and in vivo evaluations. *J Biomed Mater Res*. 1997;36(1):65-74. doi:10.1002/(sici)1097-4636(199707)36:1<65::aid-jbm8>3.0.co;2-j

95. Umare SS, Chandure AS. Synthesis, characterization and biodegradation studies of poly(ester urethane)s. *Chem Eng J*. 2008;142(1):65-77. doi:10.1016/j.cej.2007.11.017

96. Kim YD, Kim SC. Effect of chemical structure on the biodegradation of polyurethanes under composting conditions. *Polym Degrad Stab*. 1998;62(2):343-352. doi:10.1016/S0141-3910(98)00017-2

97. Rozynek Z, Castberg R, Kalicka A, Jankowski P, Garstecki P. Electric field manipulation of particles in leaky dielectric liquids. *Arch Mech*. 2015;67(5):385-399. doi:10.24423/aom.1969

98. Ambekar RS, Kandasubramanian B. Progress in the Advancement of Porous

Biopolymer Scaffold: Tissue Engineering Application. *Ind Eng Chem Res*. 2019;58(16):6163-6194. doi:10.1021/acs.iecr.8b05334

99. Naveena N, Venugopal J, Rajeswari R, et al. Biomimetic composites and stem cells interaction for bone and cartilage tissue regeneration. *J Mater Chem*. 2012;22(12):5239-5253. doi:10.1039/C1JM14401D

100. Zhang Z, Gupte MJ, Jin X, Ma PX. Injectable Peptide Decorated Functional Nanofibrous Hollow Microspheres to Direct Stem Cell Differentiation and Tissue Regeneration. *Adv Funct Mater*. 2015;25(3):350-360. doi:10.1002/adfm.201402618

101. Hernandez-Gordillo V, Chmielewski J. Mimicking the extracellular matrix with functionalized, metal-assembled collagen peptide scaffolds. *Biomaterials*. 2014;35(26):7363-7373. doi:10.1016/j.biomaterials.2014.05.019

102. Tocchio A, Tamplenizza M, Martello F, et al. Versatile fabrication of vascularizable scaffolds for large tissue engineering in bioreactor. *Biomaterials*. 2015;45:124-131. doi:https://doi.org/10.1016/j.biomaterials.2014.12.031

103. Blaker JJ, Maquet V, Jérôme R, Boccaccini AR, Nazhat SN. Mechanical properties of highly porous PDLLA/Bioglass composite foams as scaffolds for bone tissue engineering. *Acta Biomater*. 2005;1(6):643-652. doi:10.1016/j.actbio.2005.07.003

104. Ohtsuki C, Kamitakahara M, Miyazaki T. Bioactive ceramic-based materials with designed reactivity for bone tissue regeneration. *J R Soc Interface*. 2009;6 Suppl 3:S349-60. doi:10.1098/rsif.2008.0419.focus

105. Dhivya S, Ajita J, Selvamurugan N. Metallic Nanomaterials for Bone Tissue Engineering. *J Biomed Nanotechnol*. 2015;11(10):1675-1700. doi:10.1166/jbn.2015.2115

106. Eglin D, Alini M. Degradable polymeric materials for osteosynthesis: tutorial. *Eur Cell Mater*. 2008;16:80-91. doi:10.22203/ecm.v016a09

107. Serrano-aroca Á. Enhancement of Hydrogels ' Properties for Biomedical Applications : Latest Achievements Enhancement of Hydrogels ' Properties for Biomedical Applications : Latest Achievements Serrano-Aroca. 2018;(August).

doi:10.5772/intechopen.71671

108. Profile SEE. Interaction between Water and Polymer Chains in Poly (Hydroxyethyl Acrylate) Interaction between water and polymer chains in poly (hydroxyethyl acrylate) hydrogels. 2001;(February 2015). doi:10.1007/s003960000426

109. Aroca AS, Pradas MM, Ribelles JLG. Effect of crosslinking on porous poly(methyl methacrylate) produced by phase separation. *Colloid Polym Sci*. 2008;286(2):209-216. doi:10.1007/s00396-007-1755-0

110. Sachlos E, Czernuszka JT, Gogolewski S, Dalby M. Making tissue engineering scaffolds work. Review on the application ofsolid freeform fabrication technology to the production of tissue engineeringscaffolds. *Eur Cells Mater*. 2003;5:29-40. doi:10.22203/ecm.v005a03

111. Kundu J, Pati F, Shim J-H, Cho D-W. 10 - Rapid prototyping technology for bone regeneration. In: Narayan RBT-RP of B, ed. Woodhead Publishing; 2014:254-284. doi:https://doi.org/10.1533/9780857097217.254

112. Fereshteh Z, Fathi M, Bagri A, Boccaccini AR. Preparation and characterization of aligned porous PCL/zein scaffolds as drug delivery systems via improved unidirectional freeze-drying method. *Mater Sci Eng C Mater Biol Appl*. 2016;68:613-622. doi:10.1016/j.msec.2016.06.009

113. Hou Q, Grijpma DW, Feijen J. Porous polymeric structures for tissue engineering prepared by a coagulation, compression moulding and salt leaching technique. *Biomaterials*. 2003;24(11):1937-1947. doi:10.1016/s0142-9612(02)00562-8

114. Kasoju N, Bhonde RR, Bora U. Fabrication of a novel micro–nano fibrous nonwoven scaffold with Antheraea assama silk fibroin for use in tissue engineering. *Mater Lett*. 2009;63(28):2466-2469. doi:10.1016/j.matlet.2009.08.037

115. Kucharska M, Walenko K, Butruk B, Brynk T, Heljak M, Ciach T. Fabrication and characterization of chitosan microspheres agglomerated scaffolds for bone tissue engineering. *Mater Lett*. 2010;64(9):1059-1062. doi:10.1016/j.matlet.2010.02.012

116. Di Martino A, Liverani L, Rainer A, Salvatore G, Trombetta M, Denaro V. Electrospun scaffolds for bone tissue engineering. *Musculoskelet Surg*. 2011;95(2):69-80. doi:10.1007/s12306-011-0097-8

117. CAPITO RM, SPECTOR M. Collagen scaffolds for nonviral IGF-1 gene delivery in articular cartilage tissue engineering. *Gene Ther*. 2007;14(9):721-732. doi:10.1038/sj.gt.3302918

118. Wu X, Liu Y, Li X, et al. Preparation of aligned porous gelatin scaffolds by unidirectional freeze-drying method. *Acta Biomater*. 2010;6(3):1167-1177. doi:10.1016/j.actbio.2009.08.041

119. Salmoria G V, Klauss P, Paggi RA, Kanis LA, Lago A. Structure and mechanical properties of cellulose based scaffolds fabricated by selective laser sintering. *Polym Test*. 2009;28(6):648-652. doi:10.1016/j.polymertesting.2009.05.008

120. Boffito M, Sartori S, Ciardelli G. Polymeric scaffolds for cardiac tissue engineering: Requirements and fabrication technologies. *Polym Int*. 2014;63(1):2-11. doi:10.1002/pi.4608

121. Subia B, Kundu J, C. S. Biomaterial Scaffold Fabrication Techniques for Potential Tissue Engineering Applications. *Tissue Eng*. 2010;(3). doi:10.5772/8581

122. A. C, Olivas-Armendariz I, S. J, E. P. Scaffolds for Tissue Engineering Via Thermally Induced Phase Separation. *Adv Regen Med*. Published online 2011. doi:10.5772/25476

123. Lloyd DR, Kim SS, Kinzer KE. Microporous membrane formation via thermally-induced phase separation. II. Liquid-liquid phase separation. *J Memb Sci*. 1991;64(1-2):1-11. doi:10.1016/0376-7388(91)80073-F

124. Lloyd DR, Tseng HS, Kinzer KE. Microporous membrane formation via thermally-induced phase separation. I. Solid-liquid phase separation. *J Memb Sci*. 1990;52:239-261.

125. Gore PM, Gore PM, Khurana L, et al. Ion-imprinted electrospun nanofibers of chitosan/1-butyl-3-methylimidazolium tetrafluoroborate for the dynamic expulsion of thorium (IV) ions from mimicked effluents. *Environ Sci Pollut Res*

Int. 2018;25(4):3320-3334. doi:10.1007/s11356-017-0618-6

126. De Mulder ELW, Buma P, Hannink G. Anisotropic Porous Biodegradable Scaffolds for Musculoskeletal Tissue Engineering. *Mater* . 2009;2(4). doi:10.3390/ma2041674

127. Lendlein A, Behl M, Hiebl B, Wischke C. Shape-memory polymers as a technology platform for biomedical applications. *Expert Rev Med Devices*. 2010;7(3):357-379. doi:10.1586/erd.10.8

128. de Mulder ELW, Buma P, Hannink G. Anisotropic porous biodegradable scaffolds for musculoskeletal tissue engineering. *Materials (Basel)*. 2009;2(4):1674-1696. doi:10.3390/ma2041674

129. Patel H, Bonde M, Srinivasan G. Biodegradable polymer scaffold for tissue engineering. *Trends Biomater Artif Organs*. 2011;25(1):20-29.

130. Short-Term Degradation of Bi-Component Electrospun Fibers: Qualitative and Quantitative Evaluations via AFM Analysis. *J Funct Biomater*. 2018;9(2):27. doi:10.3390/jfb9020027

131. Spadaccio C, Rainer A, Trombetta M, et al. A G-CSF functionalized scaffold for stem cells seeding: a differentiating device for cardiac purposes. *J Cell Mol Med*. 2011;15(5):1096-1108. doi:10.1111/j.1582-4934.2010.01100.x

132. Yeong WY, Sudarmadji N, Yu HY, et al. Porous polycaprolactone scaffold for cardiac tissue engineering fabricated by selective laser sintering. *Acta Biomater*. 2010;6(6):2028-2034. doi:10.1016/j.actbio.2009.12.033

133. Liang S-L, Cook WD, Thouas GA, Chen Q-Z. The mechanical characteristics and in vitro biocompatibility of poly(glycerol sebacate)-bioglass elastomeric composites. *Biomaterials*. 2010;31(33):8516—8529. doi:10.1016/j.biomaterials.2010.07.105

134. Rastogi P, Kandasubramanian B. Breakthrough in the printing tactics for stimuli-responsive materials: 4D printing. *Chem Eng J*. 2019;366:264-304.

135. Tada K, Kudo T, Kishimoto Y. Effects of L-dopa or dopamine on human decidual prostaglandin synthesis. *Acta Med Okayama*. 1991;45(5):333-338. doi:10.18926/AMO/32193

136. Shie MY, Shen YF, Astuti SD, et al. Review of polymeric materials in 4D printing biomedical applications. *Polymers (Basel)*. 2019;11(11):1-17. doi:10.3390/polym11111864

137. Momeni F, Liu X, Ni J. A review of 4D printing. *Mater Des*. 2017;122:42-79.

138. Gao B, Yang Q, Zhao X, Jin G, Ma Y, Xu F. 4D Bioprinting for Biomedical Applications. *Trends Biotechnol*. 2016;34(9):746-756. doi:10.1016/j.tibtech.2016.03.004

139. Makamba H, Kim JH, Lim K, Park N, Hahn JH. Surface modification of poly(dimethylsiloxane) microchannels. *Electrophoresis*. 2003;24(21):3607-3619. doi:10.1002/elps.200305627

140. Alves P, Coelho JFJ, Haack J, Rota A, Bruinink A, Gil MH. Surface modification and characterization of thermoplastic polyurethane. *Eur Polym J*. 2009;45(5):1412-1419. doi:10.1016/j.eurpolymj.2009.02.011

141. Anselme K, Ploux L, Ponche A. Cell/Material Interfaces: Influence of Surface Chemistry and Surface Topography on Cell Adhesion. *J Adhes Sci Technol*. 2010;24(5):831-852. doi:10.1163/016942409X12598231568186

142. Wilson CJ, Clegg RE, Leavesley DI, Pearcy MJ. Mediation of biomaterial-cell interactions by adsorbed proteins: a review. *Tissue Eng*. 2005;11(1-2):1-18. doi:10.1089/ten.2005.11.1

143. Castner DG, Ratner BD. Biomedical surface science: Foundations to frontiers. *Surf Sci*. 2002;500(1):28-60. doi:https://doi.org/10.1016/S0039-6028(01)01587-4

144. Zimmerman E, Geiger B, Addadi L. Initial stages of cell-matrix adhesion can be mediated and modulated by cell-surface hyaluronan. *Biophys J*. 2002;82(4):1848-1857. doi:10.1016/S0006-3495(02)75535-5

145. Schuler M, Owen GR, Hamilton DW, et al. Biomimetic modification of titanium dental implant model surfaces using the RGDSP-peptide sequence: a cell morphology study. *Biomaterials*. 2006;27(21):4003-4015. doi:10.1016/j.biomaterials.2006.03.009

146. Mantz A, Pannier AK. Biomaterial substrate modifications that influence cell-material interactions to prime cellular responses to nonviral gene delivery. *Exp*

Biol Med. 2019;244(2):100-113. doi:10.1177/1535370218821060

147. Formoso P, Pantuso E, De Filpo G, Nicoletta FP. Electro-Conductive Membranes for Permeation Enhancement and Fouling Mitigation: A Short Review. *Membr* . 2017;7(3). doi:10.3390/membranes7030039

148. Hunger K, Schmeling N, Jeazet HBT, Janiak C, Staudt C, Kleinermanns K. Investigation of Cross-Linked and Additive Containing Polymer Materials for Membranes with Improved Performance in Pervaporation and Gas Separation. *Membr* . 2012;2(4). doi:10.3390/membranes2040727

149. Alves P, Coelho JFJ, Haack J, Rota A, Bruinink A, Gil MH. Surface modification and characterization of thermoplastic polyurethane. *Eur Polym J*. 2009;45(5):1412-1419. doi:10.1016/j.eurpolymj.2009.02.011

150. Zinger O, Anselme K, Denzer A, et al. Time-dependent morphology and adhesion of osteoblastic cells on titanium model surfaces featuring scale-resolved topography. *Biomaterials*. 2004;25(14):2695-2711. doi:10.1016/j.biomaterials.2003.09.111

151. Lipski AM, Pino CJ, Haselton FR, Chen I-W, Shastri VP. The effect of silica nanoparticle-modified surfaces on cell morphology, cytoskeletal organization and function. *Biomaterials*. 2008;29(28):3836-3846. doi:10.1016/j.biomaterials.2008.06.002

152. Nguyen T, Roddick FA, Fan L. Biofouling of Water Treatment Membranes: A Review of the Underlying Causes, Monitoring Techniques and Control Measures. *Membr* . 2012;2(4). doi:10.3390/membranes2040804

153. Jacobs T, Morent R, De Geyter N, Dubruel P, Leys C. Plasma Surface Modification of Biomedical Polymers: Influence on Cell-Material Interaction. *Plasma Chem Plasma Process*. 2012;32(5):1039-1073. doi:10.1007/s11090-012-9394-8

154. Vandencasteele N, Reniers F. Plasma-modified polymer surfaces: Characterization using XPS. *J Electron Spectros Relat Phenomena*. 2010;178-179:394-408. doi:https://doi.org/10.1016/j.elspec.2009.12.003

155. Rosenfeld L. General introduction. *Niels Bohr Collect Work*. 1972;1(C):1-8.

doi:10.1016/S1876-0503(08)70003-3

156. Asadian M, Chan KV, Norouzi M, et al. Fabrication and plasma modification of nanofibrous tissue engineering scaffolds. *Nanomaterials*. 2020;10(1). doi:10.3390/nano10010119

157. Yan D, Jones J, Yuan XY, et al. Plasma treatment of electrospun PCL random nanofiber meshes (NFMs) for biological property improvement. *J Biomed Mater Res A*. 2013;101(4):963-972. doi:10.1002/jbm.a.34398

158. Bax D V, McKenzie DR, Weiss AS, Bilek MMM. The linker-free covalent attachment of collagen to plasma immersion ion implantation treated polytetrafluoroethylene and subsequent cell-binding activity. *Biomaterials*. 2010;31(9):2526-2534. doi:10.1016/j.biomaterials.2009.12.009

159. Meng F, Chae S-R, Drews A, Kraume M, Shin H-S, Yang F. Recent advances in membrane bioreactors (MBRs): Membrane fouling and membrane material. *Water Res*. 2009;43(6):1489-1512. doi:https://doi.org/10.1016/j.watres.2008.12.044

160. Al-Jumaili A, Bazaka K, Jacob M V. Retention of Antibacterial Activity in Geranium Plasma Polymer Thin Films. *Nanomater* . 2017;7(9). doi:10.3390/nano7090270

161. Kochkodan VM, Sharma VK. Graft polymerization and plasma treatment of polymer membranes for fouling reduction: A review. *J Environ Sci Heal Part A*. 2012;47(12):1713-1727. doi:10.1080/10934529.2012.689183

162. Laurano R, Boffito M, Torchio A, Cassino C, Chiono V, Ciardelli G. Plasma treatment of polymer powder as an eective tool to functionalize polymers: Case study application on an amphiphilic polyurethane. *Polymers (Basel)*. 2019;11(12). doi:10.3390/polym11122109

163. Ricciardi S, Castagna R, Severino SM, et al. Surface functionalization by poly-acrylic acid plasma-polymerized films for microarray DNA diagnostics. *Surf Coatings Technol*. 2012;207:389-399. doi:10.1016/j.surfcoat.2012.07.026

164. Chang Y, Cheng T-Y, Shih Y-J, Lee K-R, Lai J-Y. Biofouling-resistance expanded poly(tetrafluoroethylene) membrane with a hydrogel-like layer of

surface-immobilized poly(ethylene glycol) methacrylate for human plasma protein repulsions. *J Memb Sci*. 2008;323(1):77-84. doi:https://doi.org/10.1016/j.memsci.2008.06.023

165. Jhong J-F, Venault A, Hou C-C, et al. Surface Zwitterionization of Expanded Poly(tetrafluoroethylene) Membranes via Atmospheric Plasma-Induced Polymerization for Enhanced Skin Wound Healing. *ACS Appl Mater Interfaces*. 2013;5(14):6732-6742. doi:10.1021/am401669q

166. Venault A, Wei T-C, Shih H-L, et al. Antifouling pseudo-zwitterionic poly(vinylidene fluoride) membranes with efficient mixed-charge surface grafting via glow dielectric barrier discharge plasma-induced copolymerization. *J Memb Sci*. 2016;516:13-25. doi:https://doi.org/10.1016/j.memsci.2016.05.044

167. Macchione MA, Biglione C, Strumia M. Design, synthesis and architectures of hybrid nanomaterials for therapy and diagnosis applications. *Polymers (Basel)*. 2018;10(5):1-34. doi:10.3390/polym10050527

168. Mazur J, Roy K, Kanwar JR. Recent advances in nanomedicine and survivin targeting in brain cancers. *Nanomedicine (Lond)*. 2018;13(1):105-137. doi:10.2217/nnm-2017-0286

169. Nedela O, Slepicka P, Švorcík V. Surface modification of polymer substrates for biomedical applications. *Materials (Basel)*. 2017;10(10). doi:10.3390/ma10101115

170. Ruckenstein E, Li ZF. Surface modification and functionalization through the self-assembled monolayer and graft polymerization. *Adv Colloid Interface Sci*. 2005;113(1):43-63. doi:10.1016/j.cis.2004.07.009

171. Trizio I, Trulli MG, Lo Porto C, et al. *Plasma Processes for Life Sciences*. Elsevier Inc.; 2018. doi:10.1016/b978-0-12-409547-2.12271-1

172. Vartiainen J, Rättö M, Paulussen S. Antimicrobial activity of glucose oxidase-immobilized plasma-activated polypropylene films. *Packag Technol Sci*. 2005;18(5):243-251. doi:10.1002/pts.695

173. Bax D V., Davidenko N, Gullberg D, et al. Fundamental insight into the effect of carbodiimide crosslinking on cellular recognition of collagen-based scaffolds.

Acta Biomater. 2017;49:218-234. doi:10.1016/j.actbio.2016.11.059

174. Carbodiimide Crosslinker Chemistry. https://www.thermofisher.com/it/en/home/life-science/protein-biology/protein-biology-learning-center/protein-biology-resource-library/pierce-protein-methods/carbodiimide-crosslinker-chemistry.html

175. Grover CN, Cameron RE, Best SM. Investigating the morphological, mechanical and degradation properties of scaffolds comprising collagen, gelatin and elastin for use in soft tissue engineering. *J Mech Behav Biomed Mater*. 2012;10:62-74. doi:https://doi.org/10.1016/j.jmbbm.2012.02.028

176. Pawelec KM, Husmann A, Best SM, Cameron RE. Altering crystal growth and annealing in ice-templated scaffolds. *J Mater Sci*. 2015;50(23):7537-7543. doi:10.1007/s10853-015-9343-z

177. Pawelec KM, Husmann A, Best SM, Cameron RE. A design protocol for tailoring ice-templated scaffold structure. *J R Soc Interface*. 2014;11(92):20130958.

178. Ashworth JC, Mehr M, Buxton PG, Best SM, Cameron RE. Parameterizing the Transport Pathways for Cell Invasion in Complex Scaffold Architectures. *Tissue Eng - Part C Methods*. 2016;22(5):409-417. doi:10.1089/ten.tec.2015.0483

179. Chiono V, Mozetic P, Boffito M, et al. Polyurethane-based scaffolds for myocardial tissue engineering. *Interface Focus*. 2014;4(1):20130045. doi:10.1098/rsfs.2013.0045

180. Contact Angle Measurement. https://www.biolinscientific.com/measurements/contact-angle

181. Sartori S, Boffito M, Serafini P, et al. Synthesis and structure-property relationship of polyester-urethanes and their evaluation for the regeneration of contractile tissues. *React Funct Polym*. 2013;73(10):1366-1376. doi:10.1016/j.reactfunctpolym.2013.01.006